博士論文

Quantitative evaluation of barrier properties of ultra-thin PVD-Co(W) diffusion barrier layer in Cu interconnects by developing a new method

（新規手法開発による Cu 多層配線用極薄 PVD-Co(W)膜の拡散バリア性の定量的評価）

金　泰雄

Quantitative evaluation of barrier properties of ultra-thin PVD-Co(W) diffusion barrier layer in Cu interconnects by developing a new method

（新規手法開発による Cu 多層配線用極薄 PVD-Co(W)膜の拡散バリア性の定量的評価）

KIM, TAEWOONG

A dissertation submitted to the Graduate School of

The University of Tokyo

In partial fulfillment of the requirements for the degree of

DOCTOR OF PHILOSOPHY

(Materials Engineering)

2022. 02

Abstract（要旨）

Quantitative evaluation of barrier properties of ultra-thin PVD-Co(W) diffusion barrier layer in Cu interconnects by developing a new method

（新規手法開発による Cu 多層配線用極薄 PVD-Co(W)膜の拡散バリア性の定量的評価）

金　泰雄

This dissertation focused on the development of a new method for the quantitative evaluation of barrier properties for continuously miniaturized Cu interconnect in ultra-large-scale integration (ULSI) devices. Quantitative evaluation of barrier properties is essential to make an effective barrier layer in Cu interconnects. This will help us understand the diffusion phenomenon of future Cu interconnects.

In chapter 1, I summarized the issues arising from the miniaturized Cu interconnects so far and discussed the solution. Cu generally diffuses into Si in the semiconductor manufacturing process, creating an active deep level. Therefore, the development of effective diffusion barriers for Cu interconnects is the most important issue. Cu interconnects generally have Cu/liner/barrier/low-k structures. The latest ULSI device needs to have a thinner liner/barrier layer in order to maintain the cross-sectional area of Cu. However, there are some difficulties when technology node is extremely miniaturized; (1) resistance-capacitive (RC) signal delay, (2) electro-migration (EM) and stress-induced voiding (SIV). Subsequently, specific requirements to solve the issues were summarized from the viewpoints of material, structural, and manufacturing. The liner/barrier layer should not to react chemically with Cu and should not to dissolve Cu. In order to satisfy these requirements, I proposed amorphous Co(W) single layer made by physical vapor deposition (PVD).

In addition, the methods of evaluating barrier properties for Cu diffusion have been systematically organized; (1) qualitative, (2) semi-quantitative, and (3) qualitative evaluation. (1) The method in which any

numerical discussion cannot be made from the measurement results is called a qualitative evaluation method. The qualitative evaluation method only evaluates whether the barrier layer prevents diffusion or whether the barrier layer has lost its barrier properties due to diffusion. (2) The semi-quantitative evaluation method can numerically evaluate the change in barrier properties to some extent. If the results of changes in measurement conditions can be compared numerically, at least the superiority and inferiority of the barrier properties will be masked. (3) A method capable of directly measuring the quantity of diffused Cu is called a quantitative evaluation method. Since the quantity of diffused Cu is directly used, the barrier properties can be evaluated most accurately. Finally, the importance of quantitative evaluation of Cu diffusion represented by diffusion coefficient (*D*) was explained.

In Chapter 2, the quantitative evaluation of the barrier properties of 20-nm-thick PVD-Co(W) for Cu was covered. Its principles and experimental methods was also explained. Samples of the stacked structure [100-nm-thick Cu / 20-nm-thick PVD-Co(W) / 100-nm-thick SiO_2 / Si wafer] were annealed by rapid thermal anneal (RTA). After annealing, the concentration profile of Cu diffused into PVD-Co(W) was obtained by X-ray photoelectron spectroscopy (XPS). At this time, for the first time, the back-side depth profile method was applied. The experimental concentration profile of Cu obtained by XPS was then fitted to a theoretical profile based on Fick's second law and *D* was determined. Changes in barrier properties according to W concentration changes were investigated using samples of six different Co and W composition. For the Arrhenius plot of PVD-Co(W) film with six different W concentrations, the logarithm of *D* varied linearly against reciprocal of temperature in the range of 500 to 700ºC. This means that the diffusion mechanism of Cu in Co(W) was unchanged in this temperature range. *D* at 500°C was compared with ALD-Co(W) with W 20 at. % and PVD-TaN, because it was the closest to the temperature used in the back end of line (BEOL) manufacturing. Of the W concentrations tested, PVD-Co(W) with W 43 at. % showed the lowest *D*, and thus expecting better Cu diffusion barrier properties than PVD-Ta/TaN and ALD-Co(W). Therefore, PVD-Co(W) with W 43 at. % was considered to be optimal for BEOL manufacturing. Crystallinity and resistivity results were also measured to find the optimal composition of PVD-Co(W) single layer. From the results of crystallinity, the cause of the excellent barrier properties of PVD-Co(W) was predicted. Thanks to the amorphous-like structure containing trace quantity of Co crystals, fast diffusion paths

such as grain boundaries did not occur, as a result, excellent barrier properties seem to be maintained. The significance of this chapter is that it is a starting point for quantitative evaluation of the barrier properties of PVD-Co(W) single layer. If quantitative evaluation is successfully introduced, it will be possible to predict what will happen in the initial stage of thin film growth. The adhesion was also additionally discussed. To evaluate adhesion, the contact angle of the cross-sectional image of SEM were used. From the results, the dependence of the adhesion on the change of the W concentration was investigated. The excellent adhesion of PVD-Co(W) was confirmed through comparison with the results of ALD-Co(W).

Chapter 3 deals with the process of establishing a quantitative evaluation method of barrier properties for thinned PVD-Co(W). A quantitative evaluation of the barrier properties using the depth profile method has already been completed in previous chapter. However, the depth profile method is difficult to apply to ultra-thin films such as 1 or 2 nm. This is because, in the depth profile method, a barrier layer having a certain thickness is essential for the concentration profile of diffused Cu. Therefore, it is essential to develop a method capable of quantitative evaluation of ultra-thin films. First of all, quantitative evaluation using atomic probe tomography (APT) was attempted. Then, considering the reason why the APT measurement failed, I could obtain the experimental results using inductively coupled plasma-optical emission spectrometry (ICP-OES). For this, I developed the modified time-lag method to measure the trace quantity of Cu passing through the Co(W) barrier. The sample was [Cu/Co(W)/sputtered SiO_2/Ti/Co(W)/SiO_2/Si substrate]. The whole procedure of the modified time-lag method after annealing was as follows. (1) The Cu and Co(W) were etched by $FeCl_3$ solution. (2) The diffused Cu in the SiO_2/Ti/Co(W) structure was dissolved with 1HF (5%) + 1HNO_3 (5%) mixed solution. (3) The Cu concentration [ppb] in the mixed solution was measured using ICP-OES. (4) It was converted Cu concentration [ppb] into the quantity of Cu atoms per unit area passing through the barrier layer [mol/cm^2]. By repeating these procedures at various annealing temperatures, *D* was obtained. I can obtain Q-t plot from the x-axis represents annealing time (t) and the y-axis represents the number of diffused Cu moles per unit area (Q). The slope in Q-t plot denotes a flux of the substance passing through the barrier. The x-intercept in Q-t plot is called "time-lag". According to the analytical solution of the diffusion equation, relations between *D* and x-intercept or slope are

given by,

$$\text{(x intercept, i.e. time-lag)} = \frac{L^2}{6D} \quad (1),$$

$$\text{(slope, i.e. flux)} = \frac{DC_0}{L} \quad (2),$$

where C_0 is the concentration of diffused substance at the upstream interface of the barrier, and L is a thickness of the barrier. D is, therefore, obtained from the time-lag using equation (1), since L is known in general prior to the measurement. D is also obtained from the slope using equation (2), since C_0 is the experimental condition. To prove the validity of the modified time-lag method, two D values obtained using the x-intercept and slope from the Q-t plot were compared. It was confirmed that the results obtained from the modified time-lag method are valid. Through comparison with the result of 20-nm-thick PVD-Co(W), it was possible to predict the change in barrier properties according to the change in the thickness of the thin film. The barrier properties of PVD-Co(W) were quantitatively evaluated using the modified time-lag method, and the reliability of the results was also secured. Using this method, D can be obtained theoretically no matter how thin the barrier layer is. It is meaningful that it is possible to quantitatively evaluate the barrier properties even in miniaturized Cu interconnects.

Chapter 4 mainly deals with the quantitative evaluation of the barrier properties of thinned PVD-Co(W). The modified time-lag method was used to discuss the thickness dependence and temperature dependence of the barrier properties of PVD-Co(W) layer. The thickness dependence of barrier properties is important because the starting point for miniaturization of Cu interconnects is the thickness dependence of the barrier layer. It would be desirable if the barrier properties are improved as the thickness of the barrier layer became thinner. On the contrary, if the barrier properties decrease as the thickness of the barrier layer becomes thinner, the cause should be investigated. However, it is not known whether or not the barrier properties change depending on the thickness of the barrier layer.

The barrier properties were quantitatively evaluated by experimentally estimating the D of Cu for 8, 10, 12-nm-thick PVD-Co(W) layer in the 780, 830, and 855°C. D increases as the annealing temperature increases. At the same annealing temperature, D tends to decrease slightly as the PVD-Co(W) barrier becomes thinner. The activation energy (E_a) for Cu diffusion in the 780, 830, and 855°C was obtained to explain the diffusion behavior

from the nanostructure point of view. From the results, it was confirmed that the thinned PVD-Co(W) has excellent barrier properties. When the thickness of PVD-Co(W) layer changes, the change in D is important for understanding the barrier properties. The reason why the barrier properties of the thinned barrier are further improved is that the thinner the barrier, the stronger the amorphous structure of the barrier. Basically, as the thin film becomes thinner, the probability of nucleation required for crystallization decreases. Therefore, the thinner the thin film, the more improved the amorphous state could exist. In addition, it is also an important data to understand the diffusion phenomenon occurring in the initial stage of thin film growth.

In addition to the barrier properties of thinned PVD-Co(W) thin films, I further discussed crystallinity. From the result of XRD, it was confirmed that crystallization of Co and W did not occur. The reason for the superiority of the barrier properties was proved by combining the crystallinity results and the barrier properties results.

In Chapter 5, I organized the contents of achievements through my research. (1) The quantitative barrier properties of PVD-Co(W) were evaluated using the back-side depth profile method. (2) For the first time, modified time-lag method for Cu interconnects has established to quantitatively measure the barrier properties of the thinned barrier layer. (3) The modified time-lag method was used to find out whether the barrier properties change according to the thickness of the barrier layer. Based on the research results, several proposals were made for the diffusion field of Cu interconnects; (1) Optimal thin film conditions for using PVD-Co(W) as a single liner/barrier layer, (2) A single layer incorporating barrier properties and adhesion properties, (3) The need for a metal liner/barrier layer, (4) Application to dual damascene trench structure, and (5) The possibility of PVD in the fabrication of extremely thin barrier layers such as 1 nm. Finally, the remaining tasks were arranged; (1) Possibility for quantitative evaluation of barrier properties even for 1 nm barrier layers, (2) Investigating how the D and E_a vary according to the change in the composition of ultra-thin Co(W) film, (3) Applicability to quantitative evaluation of barrier properties of oxygen or moisture barrier, (4) Applicability to trench structures.

Table of contents

List of tables

Chapter 1

Chapter 2

Chapter 3

Chapter 4

List of figures

Chapter 1

Chapter 2

Chapter 3

Chapter 4

Chapter 5

Chapter 1

Introduction

1.1 Trend & current issues of Cu interconnect in ULSI

Ultra-large scale integration (ULSI) is a technology that integrates approximately 40 billion transistors (as of 2020) into a single chip[1)]. ULSI manufacturing process is divided into front end of line (FEOL) process and back end of line (BEOL) process. The FEOL process is the stage of fabricating transistors on silicon wafer, and the BEOL process is the stage of making metal wiring for copper (Cu) interconnects between transistors[1)]. Cu is an attractive material for interconnection due to its low electrical resistivity and superior electro-migration resistance compared to Al-based alloys[2)]. However, Cu generally diffuses into silicon (Si) as an impurity in the semiconductor manufacturing process, creating an active deep level[3)]. In addition, Cu diffuses into the SiO_2 based dielectric material, causing electrical shorts between adjacent interconnect lines[4)]. Therefore, the development of effective diffusion barriers for Cu interconnects is the most important issue for realizing Cu interconnects in Si-based devices. As the manufacturing technology is miniaturized as shown in Figure 1, more transistors are integrated in the same area, resulting in lower process cost, reduced power consumption, and improved device performance. According to the International Roadmap for Devices and Systems (IRDS), the latest ULSI devices are manufactured based on 7 nm design rules[1)]. Cu interconnects in ULSI devices generally have Cu/liner/barrier/low-k structures[5)]. The purpose of the liner/barrier in the Cu interconnects system is as follows. (1) The USLI devices must be protected from diffused Cu. (2) In Cu metallization, liner/barrier layer should be usable as a path through which current flows. (3) The liner acts to improve the adhesion strength between the Cu and the barrier, and the barrier prevents diffusion of Cu outside of the Cu lines, in turn preventing damage to Si-based devices. It also prevents moisture and oxygen diffusion into the Cu lines, which would cause oxidization. That is, in order to successfully integrate Cu interconnects, an appropriate diffusion barrier layer to prevent diffusion of Cu into the Si and SiO_2 layers, and a liner layer that improves adhesion between the two is required.

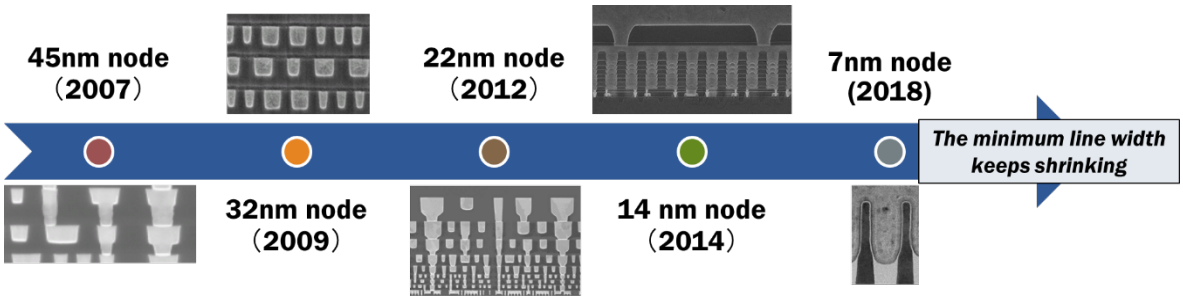

Fig 1. The evolution of the miniaturization [6].

The latest ULSI device needs to have a thinner liner/barrier layer in order to maintain the cross-sectional area of Cu even in miniaturized situations. However, there are some difficulties in continuously improving the performance of ULSI devices in a situation where manufacturing technology is extremely miniaturized. Figure 2 shows the phenomenon that occurs in Cu interconnects due to miniaturization and the resulting problems.

Effects of miniaturization	Effective resistivity ↑	Current density ↑	Reduced spacing bet ween Cu wiring	The more complex manufacturing process
Problems	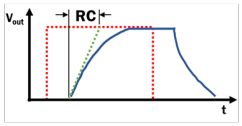 R/C delay	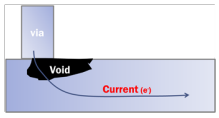 EM & SIV	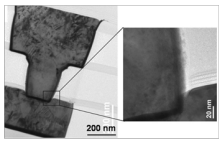 Electric short & Unwanted current	Semiconductor manufacturing cost ↑

Fig 2. The effect of miniaturization and its problems [7].

(1) As Cu interconnects become thinner, electrical resistance and capacitance increase, resulting in resistance-capacitive (RC) signal delay[8]. In particular, electrical resistance increases for the following reasons. First, the effective resistivity of Cu is increased by the size effects. Second, the ratio of resistance by liner/barrier increases in total resistance of Cu interconnects. Until now, since the resistance of Cu itself was sufficiently low, the total resistance of the Cu interconnects was low even when the resistance of the liner/barrier was considered. However, if it is further miniaturized in the future, the resistance of the

liner/barrier cannot be ignored. In Figure 3, Lo et al. investigated the relationship between barrier thickness and resistance, barrier thickness and cross-sectional area of Cu in various Half Pitch (HP) [9]. It can be seen that the more the miniaturized, the more the barrier occupies the more cross-sectional area, and the total resistance increases further.

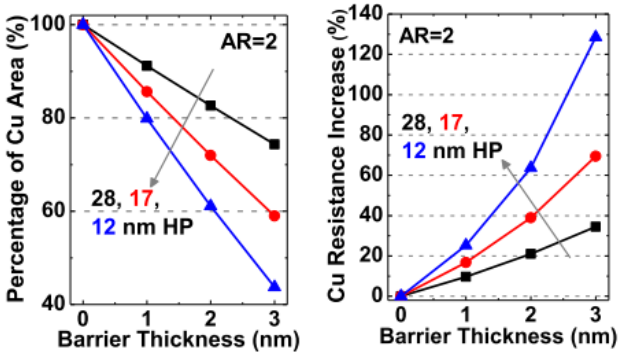

Fig 3. Percentage of Cu area and increase in Cu resistance with various barrier thicknesses in 12, 17, 28 nm Half Pitch(HP) [9].

(2) As miniaturization proceeds, the current density also increases. This problem is related to the electromigration (EM) and stress-induced voiding (SIV) of Cu at the interface between the Cu and the liner/barrier[4)10)11)].

(3) The reduced spacing between Cu wiring is also a problem. The current flowing through the Cu interconnects creates a magnetic field around it. If two Cu interconnects through which current flows close together, unwanted current changes may occur due to a change in the magnetic field.

(4) Miniaturization dramatically increases semiconductor manufacturing costs. In order to create an extremely miniaturized manufacturing process, additional manufacturing equipment is required, and the manufacturing process becomes more complex. That is, the cost reduction effect obtained by making the semiconductor smaller is reduced.

As mentioned earlier, the most important challenge in future Cu interconnects is to introduce a material that satisfies reliability while lowering R and C. Table 1 shows the latest IRDS Cu interconnect

roadmap[1)]. First of all, the aspect ratio of Cu interconnects is expected to remain between 1.5 and 2.5. In addition, there seems to be a possibility that Co and Ru other than Cu may be used in the metallization material. The design rule of Cu interconnects will continue to be thinner to 3 nm in 2022, and accordingly, the liner/barrier layer will also be thinner to 1 nm and 0.5 nm. Therefore, a new liner/barrier layer with a 1-nm-thickness and an aspect ratio of 2.5 is required. In addition, IRDS proposed TaNRuCo and TaNCo as candidate materials for future barrier materials. Probably, it seems that the existing TaN is used to maintain the barrier properties and to improve the adhesion by adding Ru and Co having excellent adhesion to Cu. However, the problem with this method is TaN. No matter how excellent the barrier properties are, metal nitrides have weak electrical properties such as relatively high resistivity.

Table 1. Interconnect roadmap [1)].

YEAR OF PRODUCTION	2020	2022	2025	2028	2031	2034
	G48M36	G45M24	G42M20	G40M16	G38M16T2	G38M16T4
Logic industry "Node Range" Labeling (nm)	"5"	"3"	"2.1"	"1.5"	"1.0 eq"	"0.7 eq"
IDM-Foundry node labeling	i7-f5	i5-f3	i3-f2.1	i2.1-f1.5	i1.5e-f1.0e	i1.0e-f0.7e
Logic device structure options	FinFET	finFET LGAA	LGAA	LGAA	LGAA-3D	LGAA-3D
Mainstream device for logic	finFET	finFET	LGAA	LGAA	LGAA-3D	LGAA-3D
INTERCONNECT TECHNOLOGY						
Number of Mx layers	3	3	3	3	2	2
Number of P80 layers	12	14	14	15	17	17
Number of P720 layers	2	2	2	2	2	2
Routing resources - Mx+P80+P720 - relative	1.00	1.00	0.98	0.98	1.00	1.00
Number of wiring layers - M1+Mx+P80+P720	18	20	20	21	22	22
Mx - tight-pitch interconnect resistance (Ohms/um)	133	301	474	920	1447	1447
Mx - tight-pitch interconnect capacitance (aF/um)	208	208	208	208	208	208
Vx - tight-pitch interconnect via resistance (Ohms/via)	28.4	50.0	52.8	38.3	63.9	63.9
MP80 - 80nm pitch interconnect resistance (Ohms/um)	13.3	13.3	13.3	13.3	13.3	13.3
MP80 - 80nm pitch interconnect capacitance (aF/um)	198	198	198	198	198	198
VP80 - 80nm pitch interconnect via resistance (Ohms/via)	5.0	5.0	5.0	5.0	5.0	5.0
Aspect ratio - M0, M1, Mx, MP80, MP720	1.5-2.5	1.5-2.5	1.5-2.5	1.5-2.5	1.5-2.5	1.5-2.5
Metallization - M0	Co, Cu	Co, Ru	Co, Ru	Co, Ru	Co, Ru	Co, Ru
Barrier - Cu M0	2.0nm TaNRuCo, TaNCo					
Barrier - Non-Cu M0	1.0nm TiN+WC	0.5nm TiN+WC	0.5nm TiN+WC	0.5nm TiN+WC	0.5nm TiN+WC	0.5nm TiN+WC
Di-electrics k value - M0,M1,Mx	SiCOH (2.70-3.20)	SiCOH (2.70-3.20)	SiCOH (2.70-3.20)	SiCOH (2.70-3.20)	SiCOH (2.70-3.20)	SiCOH (2.70-3.20)
Metallization - M1, Mx	Cu	Cu	Cu, Co, Ru	Cu, Co, Ru	Cu, Co, Ru	Cu, Co, Ru
Barrier metal - M1,Mx	2.0nm TaNRuCo, TaNCo	1.5nm TaNRuCo, TaNCo	0.5nm TiN+WC	0.5nm TiN+WC	0.5nm TiN+WC	0.5nm TiN+WC
Di-electrics k value - M0,M1,Mx	SiCOH (2.70-3.20)	SiCOH (2.70-3.20)	SiCOH (2.70-3.20)	SiCOH (2.70-3.20)	SiCOH (2.70-3.20)	SiCOH (2.70-3.20)
Metallization - MP80, MP720	Cu	Cu	Cu	Cu	Cu	Cu
Barrier metal - M1,Mx	2.5nm TaNRuCo, TaNCo	2.5nm TaNRuCo, TaNCo	2.5nm TaNRuCo, TaNCo	2.5nm TaNRuCo, TaNCo	2.5nm TaNRuCo, TaNCo	2.5nm TaNRuCo, TaNCo
Di-electrics k value - MP80	SiCOH (2.40-2.55) Airgap (1.0)	SiCOH (2.40-2.55) Airgap (1.0)	SiCOH (2.20-2.55) Airgap (1.0)	SiCOH (2.20-2.55) Airgap (1.0)	SiCOH (2.20-2.55) Airgap (1.0)	SiCOH (2.20-2.55) Airgap (1.0)
TDDB (MV/cm) - M0,M1,Mx						
Jmax (MA/cm2 at 105C) - M0,M1,Mx						

1.2 Requirement to solve issues in the Cu interconnects from a material, structural, and manufacturing perspective

To solve the problems mentioned in Chapter 1.1, the Cu interconnects require a liner/barrier layer with lower resistance, thinner thickness, better barrier properties, and higher adhesion to Cu than conventional materials. Especially, to decrease the resistance, the resistance of the liner/barrier itself should be decreased by using a material with a lower resistivity. Increasing the volume of Cu by replacing the liner/barrier with a thinner single layer is also effective in lowering the resistance. To solve these problems, it is necessary to approach them from both metallurgical and structural viewpoints. First, it is necessary to consider which materials have excellent barrier properties. M.A. Nicolet proposed the following conditions for ideal diffusion barriers[12]:

(1) The diffusion rate across the barrier should be small.

(2) The barrier must be thermodynamically stable.

(3) The barrier must have strong adhesion.

(4) The barrier should be uniform.

(5) The barrier must be able to withstand mechanical stress.

(6) The barrier must be resistant to thermal stress.

(7) The barrier should have high thermal conductivity.

(8) The barrier must have high electrical conductivity.

All of these requirements are hard to be met simultaneously in reality. Among them, leading two requirements are not to react chemically with Cu and not to dissolve Cu.

In order to satisfy these requirements, various materials have been proposed for Cu interconnects. First, various pure metal barriers were investigated[13][14]. Pure metal barrier has extremely low mutual solid solubility with Cu and no intermediate compound is formed. Papers on various materials have been published. Among them Ti, Ta, W, and Co received attention. (1) As a barrier material, Ti shows that the barrier properties are maintained up to around 400°C[15]. (2) Electrical tests have demonstrated the stability of the

Cu/Ta/Si structure up to 550°C. However, above this temperature, Ta reacted with Si to form $TaSi_2$ and Cu diffused[16]. (3) The W barrier layer that prevents Cu diffusion up to 650°C has been reported[17]. (4) The Cu/Co system was found to be stable up to 400°C, and Co showed some mutual solubility at temperatures above 400°C[13]. The negligible solubility of these metals has the advantage of suppressing the increase in resistivity of Cu interconnects.

The barrier properties of pure metal barriers are further improved with metal nitrides. High melting point materials fulfill both requirements due to their high binding energies [18]. Accordingly, the nitrides of some transition metals, such as titanium nitride (TiN)[19][20], tantalum nitride (TaN)[21], molybdenum nitride (MoN)[22],[23], and tungsten nitride (WN)[17],[24]–[26], are considered as barrier metals because they are conductive and have high melting points. TiN showed better barrier properties than Ti. TiN is a diffusion barrier that has been widely studied among various metals used in the manufacture of ULSI, showing low resistivity and excellent step coverage. TaN showed excellent EM performance and high E_a for Cu diffusion. As a result of studying the barrier properties between TiN and TaN, it was found that TaN remained stable even at higher temperatures. WN was confirmed to have high stability in RBS measurement. These excellent barrier properties are related to the melting point of the material. A good diffusion barrier has a high melting point. High melting point materials are appropriate barrier materials due to their high binding energies. Currently, Ta is used as a liner and TaN is used as a barrier[27][28][29][30][31][32]. However, for high electrical conductivity, metallic compounds are more appropriate Cu diffusion barriers than nitrides of transition metals[33].

In fact, TaN is commercially used as a barrier [27]–[32]. However, studies have been conducted to improve barrier properties by alloying barrier materials. Metallic compounds are more appropriate than nitrides of transition metals due to low electrical resistivity [33]. Many metallic compounds, e.g. Cu-Ag [34]–[36], Cu-Al [37],[38], and Cu(Mn) [39],[40] have been studied, because they are more thermodynamically stable than pure metals due to the formation of negative free energy, ensuring them not to react with Cu. This stability ensures that the barrier does not react with Cu. As a material other than metal, graphene is attracting attention as a barrier layer because of its small resistivity (1 μΩ-cm), high melting point (3652°C), and the ability to make

thin film (~ 1 nm) [41)42)].

A study on the single liner/barrier layer that added barrier properties to the adhesion properties was also conducted. Shimizu et al. proposed a metallic compound consisting of Co (adhesion) and W (diffusion barrier for Cu) that acts both as a liner and as a Cu diffusion barrier, based on metallurgical principles[43)]. Metallurgical analysis suggests that the addition of W could improve barrier properties by changing the nanostructure of the Co thin film.

Next, I determine which structures have superior barrier properties. The nanostructure of the barrier layer is important, which is categorized into three groups; single crystal, polycrystalline, and amorphous as shown in Figure 4. A single crystal has excellent barrier properties due to lack of grain boundaries that provide fast diffusion paths, but obtainable under only extremely limited conditions. Most of metal thin films used for Cu interconnects have polycrystalline structures. As they include grain boundaries, stuffing the grain boundary by some material was proposed for slowing down the grain boundary diffusion of Cu [44),45)]. Subsequently, use of an amorphous structure was proposed [11)]. Amorphous structures are expected to have better barrier properties than grain boundary stuffing structures due to inexistence of grain boundary [46)]. Amorphous structure is likely to be formed for metal compounds, i.e. adding an nonmetal to a pure metal; for example TaN_x [28)–30)] and ruthenium phosphide (RuP_x) [47),48)]. However, adding such nonmetal to improve the barrier property adversely increase the resistivity and decrease the adhesion to Cu line. In addition, high-entropy alloy (HEA) is also attracting attention as an amorphous metal [49)50)]. HEA composed of multiple elements (typically five or more) with similar mole fractions has a low diffusivity due to structural stability by lattice distortion [50)]. For a typical alloy with the main element plus small quantity of the other element, as the number or amount of elements increases, intermetallic compounds are formed, which weakens the mechanical properties of the material. However, HEA has potential as a barrier material because its solid solution phase is more stable than intermetallic compounds due to its high entropy of mixing [50)]. From this point of view, amorphous metal alloys expect high barrier property while suppressing the resistivity increase [51)]. Therefore, our group previously screened W as an adding metal to Co based on metallurgical principles,

and proposed Co(W) alloy [43),52),53)].

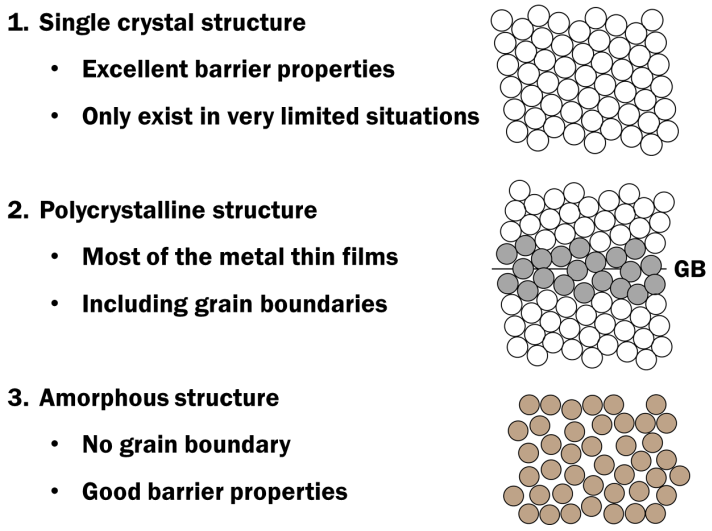

Fig 4. Thin film structure: single crystal, polycrystalline, and amorphous structure.

Based on the two perspectives (material perspective and structural perspective) mentioned above, I looked for the feasibility of Co(W) to solve the RC delay, EM, and SIV problems. The Co(W) single liner/barrier is advantageous for RC delay against Ta/TaN doubled layer because it can lower the total resistance of Cu interconnects. It is enabled by three factors. 1) Co(W) itself has a lower resistivity than Ta/TaN [52)]. 2) Thinness of the single liner/barrier layer compared with the double layer allows more volume for Cu, thereby reducing the effective resistivity of Cu. Note that effective resistivity increases for films narrower than 100 nm due to the thin film effect [54)]. For example, when the Cu line width reduced from 10 nm to 5 nm, the effective resistivity increases from 4.2 to 6.7 μΩ-cm [55)]. 3) Large volume of Cu contributes lower total resistance. Therefore, Co(W) enables to solve RC delay due to smaller total resistance of Cu interconnect.

In addition to the barrier property, Co(W) also has potential to act as a liner. Functions of the liner is to solve the EM and SIV problems by improving adhesion to the Cu line. EM and SIV have a large influence on the reliability of Cu interconnects. The adhesion strength depends on both mismatch of crystal lattice and

crystal structure [56]. Ru and Co have superior adhesion to Cu compared to current Ta [57–59] because Cu (fcc) and Ru (hcp) or Co (hcp) have lattice mismatch of approximately 2.5% and structurally consistent, while Cu (fcc) and Ta (bcc) have mismatch of 10.5% and structurally non-consistent. Longer EM lifetime was demonstrated for Ru and Co than Ta [60]. However, the barrier layer is still needed underneath liner layer because they do not have barrier properties [57–59,61–64]. It is therefore necessary to add materials that can improve their barrier properties. Addition of P [47,48], W [65], and Mn [66] was attempted. Alternatively, approaches to enhance adhesion strength on conventional barrier materials such as Ru-doped TaN have also been studied [67]. Similar research has been conducted for Co, which is about 250 times cheaper than Ru [68]. Accordingly, for Co(W), Co ensures adhesion while W offers barrier, and thus Co(W) film is expected to work as liner and barrier simultaneously [43], i.e. single liner/barrier to improve EM and SIV.

Cu interacts with various materials including Si and SiO_2. Various research has been done to determine the applicability of various metals as liner/barrier materials. Cu generally has poor adhesion to SiO_2. To solve this, some studies have been conducted. (1) Cu deposition using sputtering under extremely high purity conditions, (2) a heating process to desorb water molecules on the SiO_2 surface. When Cu is clean and there is no moisture, the adhesion is increased. However, this does not guarantee adhesion under high stress conditions that occur during Cu annealing. Therefore, there is a need for other technologies to improve the adhesion between SiO_2 and Cu; (1) Using adhesion layer, (2) increasing deposition temperature, (3) ionization of deposition materials, (4) surface pretreatment (ion implantation of metal surfaces, etc.). Among them, the adhesion layer induces a chemical bond between the diffusion barrier and Cu with high adhesive strength. However, as the miniaturization progressed, there were no longer areas where the liner layer and the barrier layer could be separately deposited. Therefore, a single layer that integrates the liner/barrier double layer into one is desirable. Shimizu et al. propose a Co thin film containing W [Co(W)] for the first time as a liner/barrier single layer.

Previously, Shimizu et al. demonstrated that chemical vapor deposition/atomic layer deposition (CVD/ALD)-Co(W) could be used to fabricate a continuous thin film with a thickness of 20 nm and evaluated

its properties as a Cu diffusion barrier[52),69),70)]. However, due to the characteristics of the island-shape nucleation, formation of a continuous 1-nm-thick film is difficult. Therefore, other deposition methods are required. I chose physical vapor deposition(PVD) for the following reasons. (1) Since PVD theoretically has a sticking probability of almost 1, the atoms once attached to the substrate are not desorbed. As a result, a thin and uniform film can be formed. (2) PVD is also expected to be excellent in terms of barrier properties because it does not require enough thermal energy to cause crystallization during deposition. (3) As mentioned in Chapter 1.1, since the aspect ratio of Cu interconnects still stays between 1.5 and 2.5, a sufficiently uniform deposition is possible even with PVD, which is somewhat inferior in uniformity. (4) Finally, PVD is superior to CVD/ALD in terms of impurities. Therefore, in my work, PVD-Co(W) thin films were prepared and evaluated in the same manner as CVD/ALD-Co(W) thin films.

1.3 Understanding the diffusion mechanism for evaluating barrier properties

In order to quantitatively evaluate the barrier properties, an understanding of the diffusion mechanism is essential. The barrier properties depend on how well it blocks the diffusion of atoms. Diffusion is a phenomenon in which atoms or molecules move from one point to another by thermal motion. Therefore, to obtain a deeper knowledge of diffusion, I need information about how atoms move. Diffusion in thin films is closely related to defects. Point defects such as vacancy are the simple defects, and there are several other types of defects such as dislocations, grain boundaries, and free surfaces. Since the mobility of atoms following these defects is much higher than that of atoms in lattice, these defects serve as high diffusion paths. However, in amorphous with disordered structure, the defect mechanism may not be equally applicable. In addition, the crystal structure also has a great influence during the diffusion process. Near the melting point, the diffusion coefficient (D) of the fcc metal is about 10^{-8} cm^2/s to 10^{-9} cm^2/s. On the other hand, in the case of bcc metal, it is about 10^{-7} cm^2/s to 10^{-8} cm^2/s. That is, the diffusion is relatively slow in the dense fcc structure, while diffusion is relatively fast in the low density bcc structure. In order to explain such various diffusion mechanisms, evaluation of barrier properties is important.

The D can be explained in terms of the atomic diffusion mechanism. The interstitial mechanism involves the diffusion of small atoms such as H, C, N, and O in metals. Interstitial mechanism is a mechanism in which solute atoms considerably smaller than lattice atoms are incorporated into the interstitial site to form an interstitial solid solution. Solute atoms at the interstitial site of the host lattice diffuse as they jump to one of the other adjacent interstitial sites. Interstitial atoms diffuse much faster than substitutional atoms because the small size of the interstitial solute can jump somewhat freely between interstitial atoms. Also, since defects are not required to mediate interstitial jumps, the energy of defect formation does not contribute to the activation energy (E_a) of diffusion. In other words, since interstitial atoms do not need defects in order to jump, the D of atoms moving by the interstitial mechanism is quite high. Since the E_a of interstitial diffusion is much smaller than that of substitutional diffusion, the D of interstitial diffusion is tens of times larger than D of substitutional diffusion.

Solute atoms of similar size to the host atom usually form a substitutional solid solution. Diffusion of substitutional solute atoms requires a different mechanism than interstitial diffusion. Kirkendall observed that the diffusion of Cu and Zn was uneven during the interdiffusion between Brass and Cu [71]. Kirkendall's findings are still accepted today as evidence for the substitutional mechanism of metal and alloy diffusion. In other words, vacancy is a mediator of substitutional diffusion in metals in all cases. Vacancy is the most important form of defect caused by heat, and atoms jump to adjacent vacancy by substitutional diffusion.

The grain-boundary of polycrystalline structure serves as a fast diffusion path with improved atomic mobility. Fisher presented for the first time a mathematical model of grain-boundary diffusion. Grain-boundary is expressed as a high diffusivity slab embedded in a low diffusivity crystal. The grain-boundary is described by two parameters: grain-boundary width, δ and grain-boundary diffusion coefficient, D_{gb}. D_{gb} is generally much greater than the lattice diffusion coefficient, D. The δ is widely recognized as about 0.5 nm. There are A, B, C type diffusions related to grain-boundary diffusion in polycrystalline. Figure 5 shows the Harrisons classification of diffusion [72]. This classification is widely used. Type A diffusion is observed in materials with high temperature, long time annealing, and small grain size. The lattice diffusion length, $\sqrt{Dt}$ needs to be slightly larger than the spacing between grain boundaries, d ($\sqrt{Dt} > d$). The concentration profile measured in type A diffusion follows a Gaussian function or an error function. The effective lattice diffusion coefficient, D_{eff} is determined from the profile. In general, D_{gb} is greater than D_{eff}. This explains why the D of polycrystalline is greater than that of single crystal. Type B diffusion occurs in materials with sufficiently large grain sizes at low temperatures, relatively short time annealing. Under these conditions, the $\sqrt{Dt}$ is smaller than the d and larger than δ ($\delta < \sqrt{Dt} < d$). Type C diffusion is a condition in which lattice diffusion is practically absent. Therefore, diffusion occurs only along the grain boundary without leakage into adjacent grains. This situation occurs at a sufficiently low temperature and annealing for a very short time.

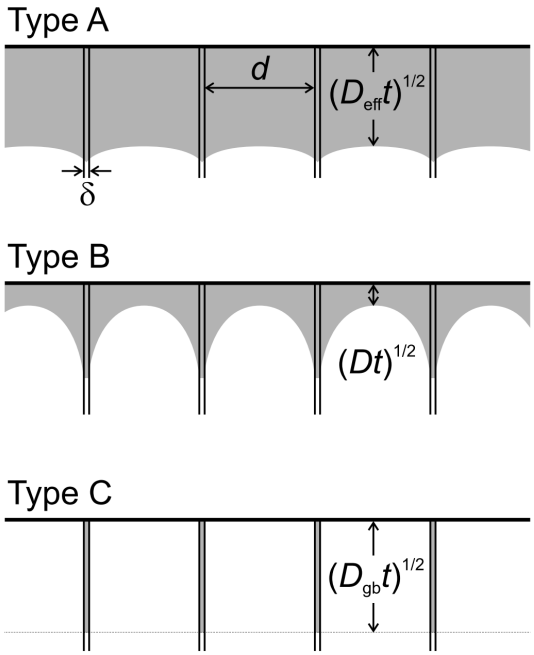

Fig 5. Type A, B, and C diffusion regimes in a polycrystalline according to Harrisons classification [72].

Diffusion in solids is generally quite strongly dependent on temperature. The temperature dependence of the *D* follows the Arrhenius formula:

$$D = D_0 exp\left(-\frac{E_a}{k_B T}\right) \qquad (1.1),$$

where, D_0 is a pre-exponential factor, also called a frequency factor, E_a is the activation energy of diffusion, T is the absolute temperature, and k_B is the Boltzmann constant. Both E_a and D_0 are the activation parameters of diffusion. The D_0 is expressed as follows.

$$D_0 = gfv^0 a^2 exp\left(\frac{\Delta S}{k_B}\right) \qquad (1.2),$$

where, ΔS is the diffusion entropy, g is the geometrical factor, f is the correlation factor, v^0 is the trial frequency, and a is the lattice parameter. D_0 can be interpreted differently depending on the diffusion mechanism, type of diffusion process, and lattice shape. An important thing is that Arrhenius behavior occurs for a various reason, from atomic transport mechanisms to micro-structure features such as impurities, grain boundaries, and dislocation.

1.4 Various evaluation methods of barrier properties for Cu diffusion

In this chapter, I discuss how to evaluate barrier properties. Figure 6 systematically classifies the measurement methods of barrier properties reported so far; (a) qualitative, semi-quantitative, quantitative evaluation and (b) indirect, direct evaluation. The difference between the indirect and direct evaluation methods is whether to measure the diffused Cu directly or to measure some properties changed by the diffused Cu. The most important factor to evaluate barrier properties is the *D*. The unit of *D* is (cm^2/s). It means the distance that an atom has moved during a unit time. Basically, if we can measure the quantity of Cu diffused across the barrier layer, we can get *D*. Obtaining *D* means that the barrier properties can be quantitatively evaluated. However, since there are few methods to accurately measure trace quantify of diffused Cu, it is important to develop a new measurement method.

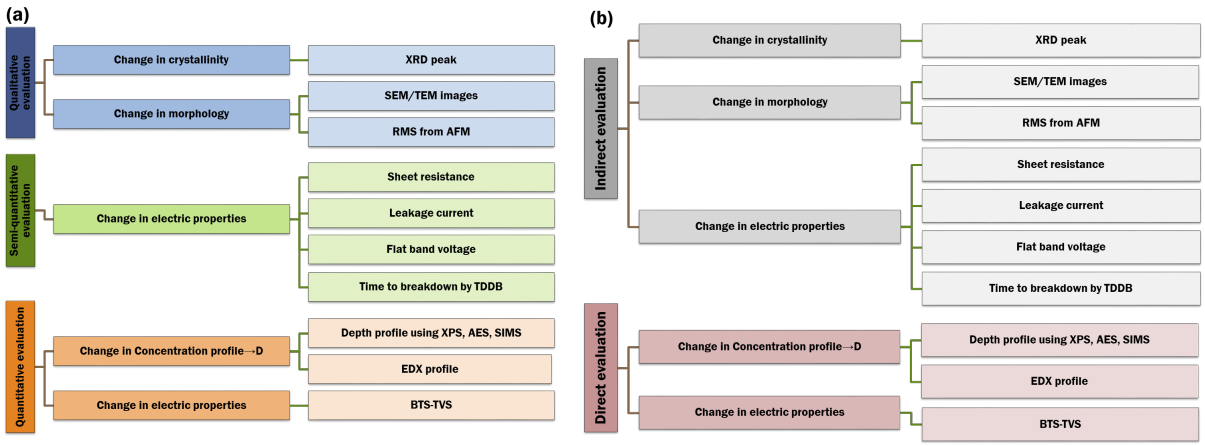

Fig 6. Classification of methods for evaluating barrier properties.

1.4.1 Qualitative evaluation method

The method in which any numerical discussion cannot be made from the measurement results is called a qualitative evaluation method. The qualitative evaluation method only evaluates whether the barrier layer prevents diffusion or whether the barrier layer has lost its barrier properties due to diffusion. The biggest difference from the other two methods is that it is not possible to discuss any numerical results with respect

to the measurement, and the barrier properties are judged by the subjectivity of the researcher. Therefore, while the barrier properties can be easily evaluated immediately after the measurement is completed, subjective interpretation is deeply involved in the measurement results. Qualitative evaluation methods can be classified into two categories; (1) Change in crystallinity and (2) Change in morphology. Many researchers have already reported many results with various measurement techniques using qualitative evaluation method.

X-ray diffraction (XRD) is mainly used to qualitatively evaluate barrier properties by detecting changes in crystallinity. By using XRD, information about the crystal structure inside the material can be obtained. The incident X-ray causes diffraction, and the crystallinity in the material can be determined by using the diffracted X-ray. When the diffraction phenomenon occurs, the following relationship, called the Bragg law, is established between the wavelength of the incident X-ray (λ), the incident angle (θ), and the spacing between the lattice planes (d).

$$n\lambda = 2d \sin\theta \qquad (1.3),$$

That is, when the incident angle θ is determined, the lattice spacing d can be obtained. Several diffraction peaks can be obtained according to the change of the incident angle θ, and a crystal pattern can be obtained from this. In general, when diffusion occurs, the sample material is crystallized or a newly formed compound is crystallized. As explained in Chapter 1.2, the crystallized thin film undergoes rapid diffusion through a high-speed diffusion path such as grain boundaries, which deteriorates the barrier properties.

XRD measurements can also be classified as indirect evaluation methods. When the barrier properties are deteriorated by annealing, the barrier itself is crystallized or Cu diffusion occurs. As a result, the crystalline peak of the newly formed Cu compound and the crystalline peak of the barrier layer are obtained. That is, what we can know by XRD measurement is whether a new Cu compound is formed and whether the barrier layer is crystallized. Since the diffused Cu is not directly measured in this process, it corresponds to the indirect evaluation method.

Min et al. investigated the diffusion barrier properties of Ta for Cu interconnects using XRD [29]. Ta has a relatively high melting point and is thermodynamically stable with respect to Cu, so it has been widely

studied as a diffusion barrier for Cu. [300-nm-thick Cu/50-nm-thick Ta/Si substrate] sample structure is annealed without breaking the vacuum. Figure 7 shows the XRD results of Cu/Ta/Si sample after annealing and the sample structure at that time. It can be seen that Cu_3Si was formed at 600°C and Cu_3Si and $TaSi_2$ were formed at 650°C. From this result, it can be seen that the Ta barrier layer was failed at 600°C. If the size of each peak and the degree of crystallization can be quantitatively compared, semi-quantitative or quantitative evaluation of barrier properties may be possible. However, no information can be obtained beyond this and no numerical discussion can also be made on the barrier properties. The only information we can know from this result is that the new compound was formed due to crystallization of the barrier layer by annealing.

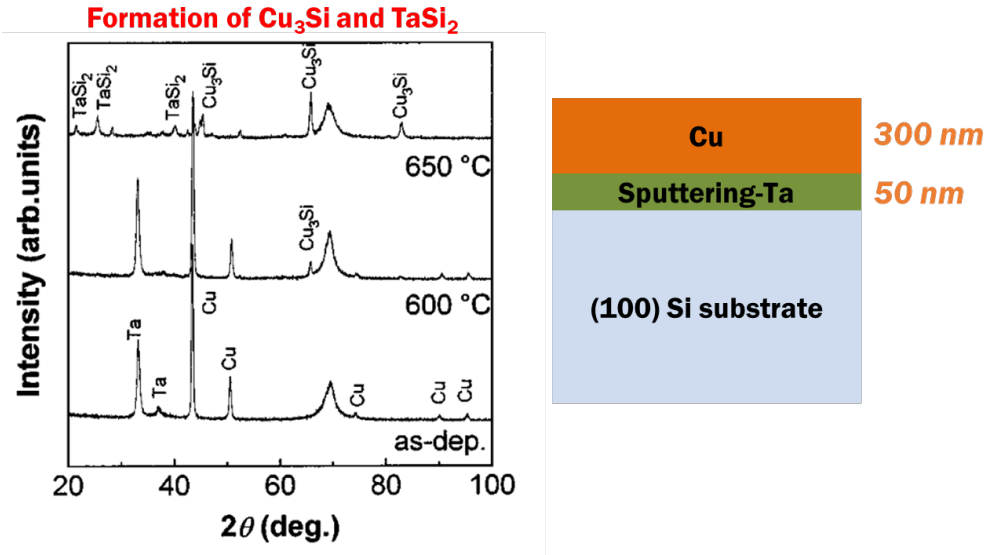

Fig 7. Change of XRD peak for Cu/Ta/Si structure and the schematic diagram of sample [29].

The barrier properties can be qualitatively evaluated by observing the morphology change of the cross-section of the sample by electron microscope such as a transmission electron microscope (TEM) or a scanning electron microscope (SEM). TEM is suitable for obtaining the cross-sectional image. A feature of SEM is that relatively large specimens can be observed three-dimensionally. In general, when diffusion occurs in a thin film, a new compound or crystal structure is changed. As a result, the contrast of the barrier

layer is changed or the sharpness of the interface of the barrier layer is deteriorated. By observing this change using TEM or SEM images, the researcher determines whether the barrier properties are maintained or deteriorated. Therefore, the method using TEM/SEM observation also belongs to the indirect evaluation method.

Kim et al. proposed a [5-nm-thick TiN/2-nm-thick Al/5-nm-thick TiN] structure by sputtering and conducted a study to prevent Cu diffusion. Subsequently, Shin et al. conducted a follow-up study on barrier properties with TiN thin film made by CVD having good step coverage [73]. Since TiN was generally used as a diffusion barrier for Al metallization, extensive studies using TiN thin films have also been conducted in Cu interconnects. In order to evaluate the barrier properties, a 100-nm-thick Cu thin film was deposited on the [25-nm-thick CVD-TiN/CVD-Al/25-nm-thick CVD-TiN/Si substrate] structure by sputtering. After Cu deposition, the samples were annealed for 30 min using rapid thermal annealing (RTA). Figure 8 shows the cross-sectional image of the Cu/TiN/Al/TiN/Si structure using STEM and the composition of the elements using EDX in each point after 600°C annealing. As a result of STEM observation, change in structure due to annealing was not observed. The Cu concentration was about 4-7 at. % in the upper TiN layer and about 2 at. % in the lower TiN layer. It can be seen that the Al layer acts as a barrier to prevent Cu diffusion through the TiN film. In fact, Al reacted with oxygen in the surrounding TiN thin film to produce Al_2O_3. This is because the change in Gibbs free energy of Al_2O_3 is lower than that of TiO_x. From the consistent results of the two measurement methods (STEM and EDX), the reliability of the results of this study was secured.

However, no numerical discussion can be made from the results of these evaluations. If a tighter EDX measurement had been performed, a detailed concentration profile could have been obtained. Then, a quantitative evaluation from the concentration profile would have been possible.

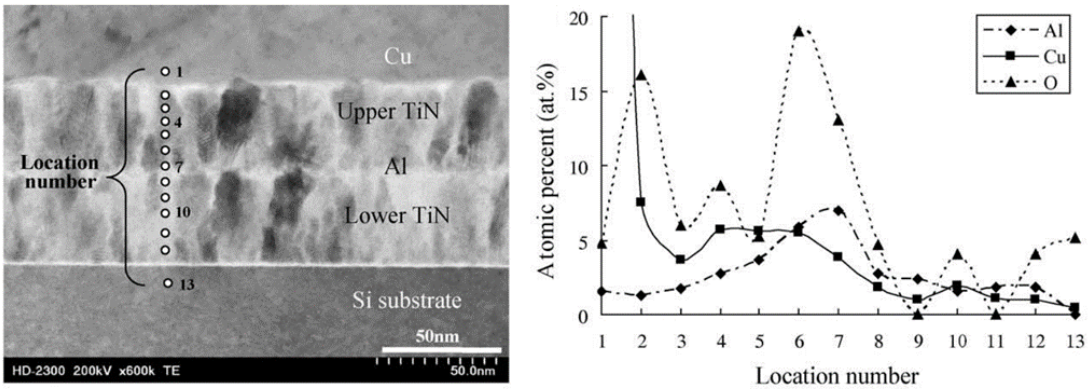

Fig 8. Cross-sectional image of Cu/TiN/Al/TiN/Si structure measured using STEM and composition of elements using EDX in each point [73].

1.4.2 Semi-quantitative evaluation method

Qualitative evaluation method could only evaluate whether or not the barrier properties work. On the other hand, since the semi-quantitative evaluation method can obtain a certain number related to diffusion from the measurement result, it is possible to numerically evaluate the change in barrier properties. However, since the quantity of diffused Cu cannot be known from the numerical value of the measurement result, it cannot be regarded as quantitative evaluation. If it is possible to prove a consistent relationship between the quantity of diffused Cu and the values obtained from the experimental results, a quantitative evaluation will be possible. Since the electric properties are very sensitive, it is possible to know the moment when the barrier properties are deteriorated more quickly than conventional methods. Representatively, methods of measuring change in sheet resistance, leakage current, flat band voltage shift, and breakdown time by time-dependent dielectric breakdown (TDDB) belong to semi-quantitative evaluation using changes in electric properties.

When a new compound is formed or the crystal structure is changed by diffusion, the resistivity of the material changes rapidly. Sheet resistance is generally used as a measure of the resistivity of a material. The unit of sheet resistance is expressed in ohm/sq. Here, Sq means an infinite area. Line resistance is measured with two probes over an arbitrary distance, but in the case of sheet resistance, it is measured with four probes with equal intervals. This method allows you to evaluate barrier properties very simply. In

addition, the evaluation method using the change in sheet resistance can be classified as an indirect evaluation method. When the barrier properties are deteriorated by annealing, interdiffusion between Cu and SiO_2 occurs, and a new Cu compound is generated on the surface. As a result, the sheet resistance increases rapidly, and the corresponding change is measured. Therefore, it is classified as an indirect method.

Lee et al. reported that a TaSiN ternary amorphous thin film shows excellent barrier properties against Cu diffusion[74]. They used sheet resistance to evaluate the barrier properties of the [100-nm-thick Cu/30-nm-thick TaSiN/Si] structure. Figure 9 shows the change in sheet resistance of two barriers ($Ta_{43}Si_{12}N_{45}$, $Ta_{39}Si_9N_{52}$) versus annealing temperature and the sample structure at that time. For both barriers, the sheet resistance remains constant at about 0.2 ohm/sq up to 700°C. At 750°C, the sheet resistance of the $Ta_{43}Si_{12}N_{45}$ barrier rises rapidly. On the other hand, the $Ta_{39}Si_9N_{52}$ barrier still remains constant at about 0.4 ohm/sq even at 750°C, and the sheet resistance rapidly increases from 800°C. This means that Cu passes through the barrier layer (TaSiN) and diffuses to Si, forming copper silicide with high resistivity.

However, the numerical value of the barrier properties cannot be determined with this method. All we know is the annealing temperature at which the resistivity begins to change and the resistivity value at that time. From this result alone, it is not known how many Cu atoms passed through the TaSiN barrier. If a new theory that can link resistivity and the quantity of diffused Cu is proposed, quantitative evaluation could be attempted using it.

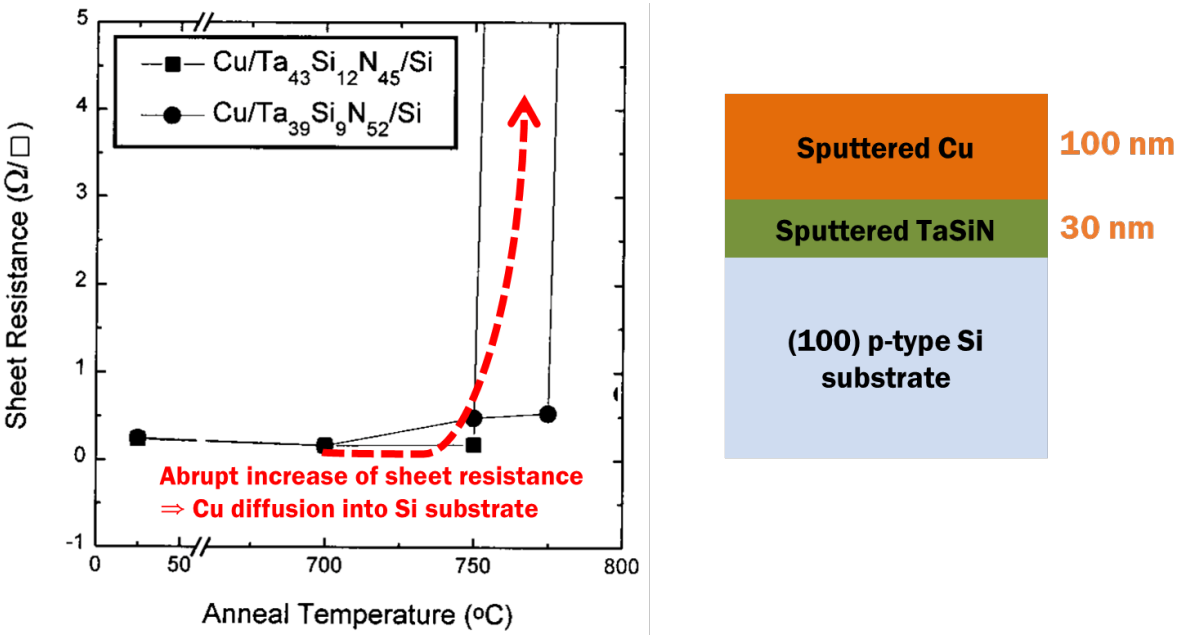

Fig 9. Changes in sheet resistance in Cu/TaSiN/Si structures and the schematic diagram of sample [74].

The barrier properties can be evaluated using the leakage current. In general, no current flows through the barrier layer. However, under the condition of a strong electric field, a minute current can flow through the barrier. This current is called leakage current. In the same electric field, the smaller the leakage current, the better the barrier properties will be. Also, the method using leakage current is classified as an indirect evaluation method. When the barrier properties are deteriorated by annealing and a fast diffusion path such as a grain boundary is created in the barrier, fine Cu diffusion occurs through the path. If a voltage is applied when a Cu path exists in the barrier layer, current flows through the Cu path, and the researcher evaluates the barrier properties by measuring the result. Therefore, the method of measuring leakage current is also an indirect evaluation method.

Perng et al. evaluated a diffusion barrier properties of Ru(P) for direct Cu plating[47]. They chose Ru(P), which allows for low electrical resistance and direct Cu plating, as the diffusion barrier. The preparation of Cu/Ru(P)/p-ULK/Si/Al structure for measuring the leakage currents is as follows. (1) 250-nm-thick SiCOH was deposited on the Si wafer by PECVD. (2) 12-nm-thick Ru(P) film was deposited on the SiCOH by RF sputtering. (3) 190-nm-thick Cu was deposited on Ru(P). (4) Al was deposited on the back

side of the sample to form a metal-insulator-metal (MIM) structure. Figure 10 shows the change in leakage current density as the electric field changes for the as-depo sample and the sample structure at that time. This result shows that the leakage current is dependent on the phosphorus concentration of the Ru film. As the phosphorus concentration increases, the leakage current of the Ru(P) barrier decreases. For example, in the same electric field of 1.0 $(MV/cm)^2$, the current density of Ru is about 4.0 x 10^{-2} A/cm^2, Ru(P) low is about 3.5 x 10^{-3} A/cm^2, and Ru(P) high is 8.5 x 10^{-4} A/cm^2. The lower the leakage current, the smaller the quantity of Cu diffused to Si. That is, this result indicates that Ru(P) has better barrier properties than Ru. This is because the Ru(P) thin film has an amorphous structure thanks to the addition of P. Since the amorphous structure does not form a grain boundary, it is more effective in preventing Cu diffusion.

However, it is not known how good the barrier properties between them. This is because the fact that the leakage current is reduced by half does not mean that the barrier properties are doubled. We do not yet know the numerical relationship between leakage current and barrier properties.

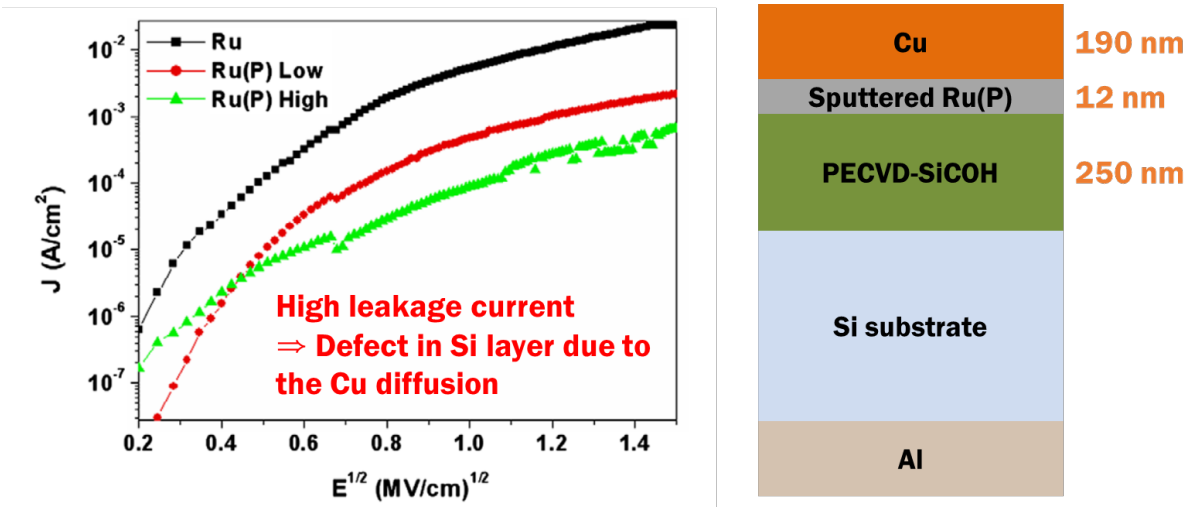

Fig 10. Changes in leakage current in Cu/Ru(P)/p-ULK/Si/Al structures and the schematic diagram of sample [47].

The change in the barrier properties can be evaluated from the shift of the flat band voltage in the capacitance–voltage (C-V) curve for MOS capacitor. In general, MOS capacitor go through an accumulation

region, a depletion region, and an inversion region according to a change in voltage applied. Also, the flat band voltage corresponds to the inflection point of the C-V curve in the depletion region. In the depletion region, in addition to the capacitor by the existing oxide layer, a new capacitor by the depletion layer is created in the doped Si substrate, so the total capacitance is reduced. As a result, a decrease in the C-V curve appears. Therefore, if the flat band voltage is shifted to the left, it means that the capacitor by the depletion layer appears even at a lower applied voltage. In the capacitor by the depletion layer, carriers (electrons or holes) in the doped Si substrate are concentrated toward oxide layer by the applied voltage. Therefore, the shift in the flat band voltage even at a lower applied voltage means that surface Cu is diffused toward the Si substrate. That is, the shift of the flat band voltage indicates that the barrier properties are deteriorated. In addition, since the method of measuring the shift of flat band voltage cannot directly measure the quantity of diffused Cu, it can be classified as an indirect evaluation method.

Kohn et al. evaluated the barrier properties of electroless deposited $Co_{0.9}P_{0.1}$ using high conformality, low deposition temperature, and electroless technology capable of depositing Cu without a seed layer [3]. A schematic image of the MOS structure is shown on the left in Figure 11. The MOS capacitor is prepared by the following process. (1) 100-nm-thick SiO_2 was prepared on p-type Si substrates by thermal oxidation. (2) 4-nm-thick Ti layer was sputtered on SiO_2. (3) 10-nm-thick sputtering Co seed layer was deposited. (4) On the Co seed layer, 30-nm-thick $Co_{0.9}P_{0.1}$ barrier, 150-nm-thick Cu layer, and 30-nm-thick $Co_{0.9}P_{0.1}$ encapsulation layer were electroless deposited in order. (5) 200-nm-thick Al layer was sputtered on the back side. The results of the C–V measurements for the 30-nm-thick $Co_{0.9}P_{0.1}$ barrier using MOS capacitors are shown on the right in Figure 11. The flat band voltage after initial annealing at 300°C for 30 minutes was -0.29±0.05 V. Subsequently, by annealing at 450°C for 4 hours and 12 hours, the flat band voltage shifted in the negative direction. After annealing for 12 hours, the flat band voltage shifted in the negative direction of about 0.15 V. This shift may be due to Cu^+ ions diffused into the SiO_2.

However, the flat band voltage can be shifted not only by diffusion of Cu, but also by formation of compounds by oxygen and moisture in SiO_2. In addition, the method using the C-V curve is an indirect

method in which the quantitative relationship between the shift of flat band voltage and the quantity of diffused Cu cannot be known.

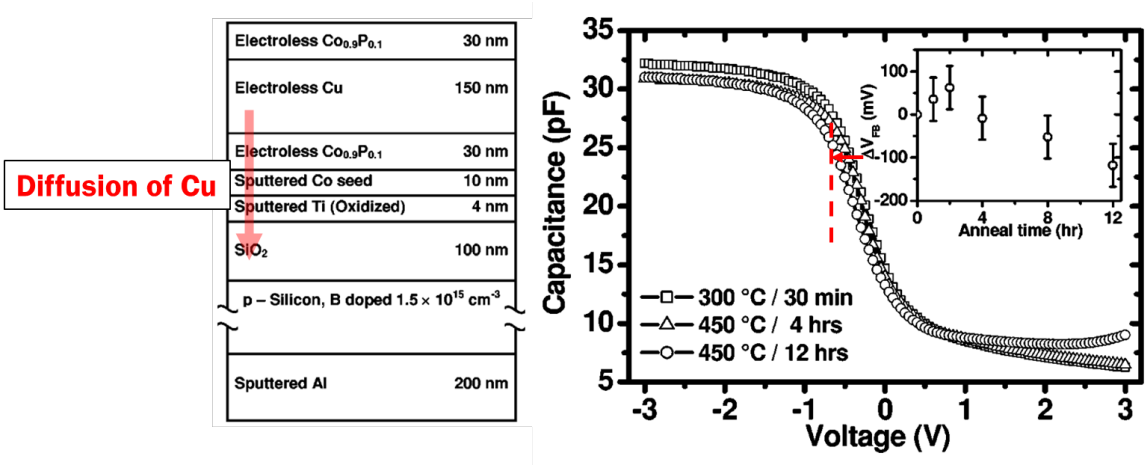

Fig 11. MOS structure and C-V curve at that time [3].

TDDB is a phenomenon that occurs when a relatively low electric field is applied to the device for a long time. Cu diffused into SiO_2 by the electric field creates a conducting path therein, resulting in device breakdown. The time it takes for SiO_2 to fail in this constant electric field is called time-to-breakdown (t_{BD}). Therefore, if the barrier layer prevents Cu diffusion, less Cu will diffuse in SiO_2, resulting in longer t_{BD} of the device. In addition, the method using TDDB belongs to the indirect evaluation method. This method measures the time when a conducting path occurs between Cu and SiO_2 when the barrier layer in the MIS structure is deteriorated, not the quantity of diffused Cu.

Lo et al. proposed 2D layered material as an alternative to diffusion barrier[9]. They fabricated 0.62-nm-thick MOCVD-MoS_2 at 400°C using ($Mo(CO)_6$) and (DES) as precursors on SiO_2. The sample structure for TDDB measurement is shown on the left of Figure 12. For the TDDB measurement, a Cu electrode having a thickness of 30 nm and a diameter of 100 μm was deposited on SiO_2 and MoS_2 with an E-beam evaporator, respectively. Subsequently, an E-beam evaporated Al layer was deposited on the top of the Cu electrode and on the back side of the Si substrate to prevent electrode oxidation and ensure good electric contact. The

change in leakage current in a constant electric field of 5 MV/cm is shown in the left graph of Figure 12. The device with the MoS_2 barrier breakdown later than the device without the barrier. The results of TDDB measurements in various electric fields are shown as a cumulative distribution plot on the right of Figure 12. It can be seen that the use of the MoS_2 barrier increases t_{BD} regardless of the magnitude of the applied electric field. The medium-time-to-failure ($TTF_{50\%}$) was also increased.

If any quantitative relation between t_{BD} and the quantity of diffused Cu is found, quantitative evaluation will be possible. However, the quantity of diffused Cu cannot be known by TDDB measurement.

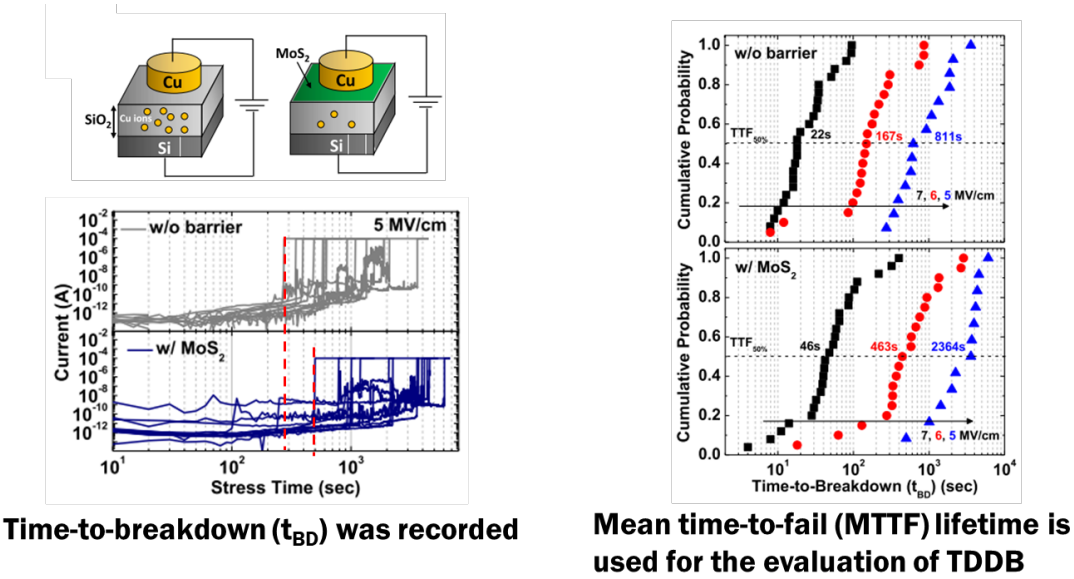

Fig 12. TDDB measurement results for MOS structures [9].

1.4.3 Quantitative evaluation method

For quantitative evaluation to be accepted, the quantity of diffused Cu must be obtained through measurement. In addition, if *D* can be derived using that quantity, we can quantitatively discuss the barrier properties of materials. For example, the barrier properties can be systematically summarized for each material, each composition, and each structure through comparison of the inherent *D* of the material. Among the studies so far, in order to obtain the most reliable *D*, the experimental results should be compared with the diffusion behavior based on Fick's law. Among them, the method using the concentration profile of

diffused Cu is the most accurate. To obtain a concentration profile, the depth profile method of a surface analysis equipment such as X-ray photoelectron spectroscopy (XPS) can be used. The quantity of diffused Cu can also be obtained through electric properties such as bias temperature stress (BTS)-triangular voltage sweep (TVS) method.

D can be calculated by fitting the concentration profile obtained from the depth profile results using XPS to the theoretical concentration profile based on Fick's law. The diffusion mechanism can be predicted by examining the temperature dependence of *D* obtained in this way. The content related to the method using the concentration profile was described in detail in Chapter 2. In addition, the depth profile method is included in the direct evaluation method because it directly measures the quantity of Cu diffused in the barrier layer.

Shimizu et al. evaluated the barrier properties of ALD-Co(W) single layer as an alternative to the PVD-Ta/TaN double layer[52]. ALD-Co(W) single layer was successfully prepared using two oxygen-free precursors [$(C_5H_5)_2Co$, $(C_5H_5)_2WH_2$]. The process of evaluating barrier properties is as follows. (1) On the Cu layer, a 20-nm-thick Co(W) film and a 20-nm-thick Co film were deposited, respectively. (2) Co(W)/Cu and Co/Cu samples were annealed at 400, 500, 600°C. (3) The Cu concentration is measured by depth profile method using XPS. (4) *D* is obtained by fitting the actual concentration profile obtained from XPS with the concentration profile calculated from Fick's law. The Cu concentration profile in the Co(W) film is shown on the left side of Figure 13. Even after annealing, the concentration profile of Co(W) changed only slightly. The center of Figure 13 shows the Arrhenius plot of *D* of the ALD-Co(W), ALD-Co, and PVD-TaN. Low *D* means that the thin film has excellent barrier properties against Cu diffusion. The Arrhenius plot also shows the results of the PVD-TaN reported by Oku et al[21]. The improved barrier properties for Cu diffusion that they observed are due to the addition of W. The E_a for Cu diffusion can also be obtained from the slope of the Arrhenius plot. As a result, it can be seen that ALD-Co(W) has a high E_a of 2.0 ± 0.2 eV. Since there is no diffusion through the grain boundary at this level of E_a, it is expected to have a grain boundary stuffing structure. The barrier properties using *D* can be quantitatively evaluated.

The only limitation is that a barrier layer of some thickness is required to obtain a concentration

profile. They used 20-nm-thick ALD-Co(W).

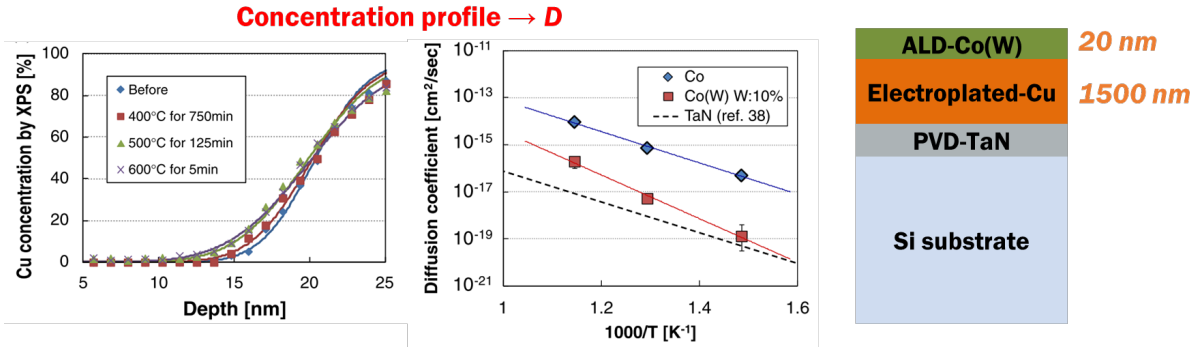

Fig 13. Concentration profile of Cu diffused in Co(W) and the Arrhenius plot using *D* and the schematic diagram of sample [52].

The BTS-TVS method is a voltage-current measurement method that detects the quantity of ions diffused by an applied voltage. The current density of the diffused ions is measured from the peak of the diffused ions in TVS plot, and the diffused ions is quantified therefrom. During the BTS, an elevated temperature and an electric field cause Cu ion drift towards the dielectric. Immediately after BTS, Cu ions were detected and quantified from TVS plot using an analog voltage ramp. In addition, since the number of diffused Cu ions can be obtained from the area of the TVS plot, the BTS-TVS method can be classified as a direct evaluation method.

H. Wojcik et al. reported the results of the barrier properties of PVD Ru-Mn measured using BTS-TVS [66),75)]. The preparation of the sample is as follows. First, a 15-nm-thick Ru-Mn (1-5 at. %) barrier and 500-nm-thick Cu were deposited by sputtering on p-Si wafers having a 100 nm thermal SiO_2 on top. Then, test dots were made through the wet etch process of Cu and the reactive-ion etching (RIE) process of Ru–Mn. A 40-nm-thick TaSiN passivation layer was deposited over the dots to prevent Cu oxidation during BTS. The left side of Figure 14 shows a cross-sectional view of the test structure. The change in leakage current during BTS for metal-insulator-semiconductor (MIS) structures of three different barrier films is shown in the center of Figure 14. The MIS structure without barrier began to fail immediately after the BTS was applied.

In the MIS structure including the Ru barrier film, the leakage current rapidly increased after a short relaxation. In contrast, no increase in leakage current was observed in the MIS structure including the Ru-Mn or TaN barrier. The TVS plot corresponding to after the BTS is shown on the right in Figure 14. Large Cu peaks can be seen in the Cu and Ru/Cu samples. However, it remained flat in the Ru-Mn or TaN samples. The Cu peak represents the ionic current due to the diffusion of Cu ions. The integration of this peak indicates the quantity of Cu ions inside SiO_2. Therefore, using the Cu peak shown here, the number of diffused Cu ions can be quantitatively evaluated. Originally, this method was used to measure sodium and potassium impurities, but this method is applied to Cu ions that are detected at higher voltages.

However, since this method requires a unique structure such as test dots different from the general MOS structure, sample preparation is cumbersome. In addition, for a material having excellent barrier properties, it is difficult to measure because a peak due to diffusion of Cu ions hardly appears.

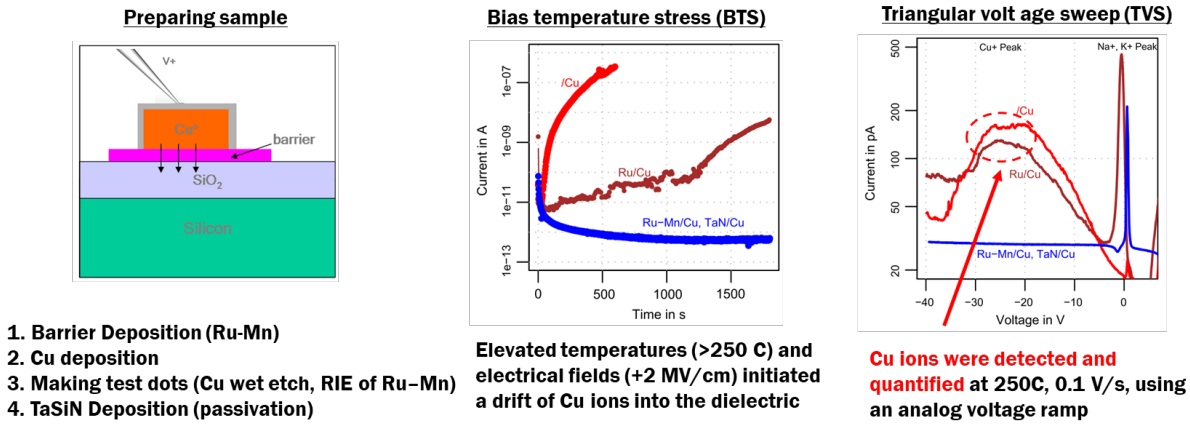

Fig 14. Preparation process and results of BTS-TVS measurement for MOS structure [66),75)].

1.5 Purpose and Overview of the Dissertation

This dissertation focused on the development of a new method for the quantitative evaluation of barrier properties in preparation for continued miniaturization of ULSI devices. As described in chapter 1.4, except for Shimizu et al. most of the evaluation methods for barrier properties have rarely been studied from the temperature dependence for diffusion to the obtaining E_a. Therefore, the evaluation method that I want to develop is not only the quantitative evaluation of the barrier properties using D, but also a quantitative evaluation method that enables discussion on the diffusion mechanism from the temperature dependence for diffusion. For this, a modified time-lag method is proposed as a new quantitative evaluation method. This method has been used so far for the diffusion of hydrogen gas to rubber membranes. I first applied it to the Cu interconnects of ULSI devices. This dissertation is organized into five chapters.

Chapter 1 introduces the problems caused by the miniaturization of Cu interconnects, and explains the requirements for solving them from a metallurgical, structural, and manufacturing point of view. As a result, PVD-Co(W) single layer was selected as the barrier layer. Next, in order to develop a new barrier property evaluation method, various barrier property evaluation methods studied so far were classified. In addition, examples of each evaluation method were given and their principles were explained.

Chapter 2 covers the principles and experimental methods to evaluate the barrier properties, crystallinity, and resistivity of a 20-nm-thick PVD-Co(W) single layer. Subsequently, the results of the experiment are discussed. To quantitatively evaluate the barrier properties of a 20-nm-thick PVD-Co(W) single layer, depth profile method using XPS was used. After discussing the barrier properties, crystallinity, and resistivity results, the optimal composition of Co and W was estimated. The significance of this chapter is that it is a starting point for quantitative evaluation of the barrier properties of PVD-Co(W) single layer. If quantitative evaluation is successfully introduced, it will be possible to predict what will happen in the initial stage of thin film growth.

Chapter 3 deals with the process of establishing a quantitative evaluation method for barrier properties below 10 nm. In Chapter 2, a quantitative evaluation of the barrier properties of PVD-Co(W) using

the depth profile method has already been completed. However, the depth profile method is difficult to apply to ultra-thin films such as 1 or 2 nm, because it does not obtain concentration profiles for such a thin film. Therefore, it is essential to develop a method capable of quantitative evaluation of ultra-thin films. First, quantitative evaluation using atomic probe tomography (APT) was attempted. Then, considering the reason why the APT measurement failed, I introduced the results of the modified time-lag method using wavelength dispersive X-ray fluorescence (WDXRF) and inductively coupled plasma-optical emission spectrometer (ICP-OES). The barrier properties of PVD-Co(W) were quantitatively evaluated using the modified time-lag method, and the reliability of the results was also secured.

In Chapter 4, the thickness dependence of the barrier properties of thinned PVD-Co(W) was discussed using the modified time-lag method. The thickness dependence of barrier properties is important because the starting point for miniaturization of Cu interconnects depends on the thickness of the barrier layer. For this, I derive E_a and D_0 to estimate the nanostructure of PVD-Co(W). As a result, it was confirmed that the thinned PVD-Co(W) also had excellent barrier properties. In addition to the barrier properties of thinned PVD-Co(W) thin films, I further discussed crystallinity and adhesion.

In Chapter 5, I organized the contents of achievements through my research. Based on the research results, several proposals were made for the diffusion field of Cu interconnects. Finally, the remaining tasks were arranged.

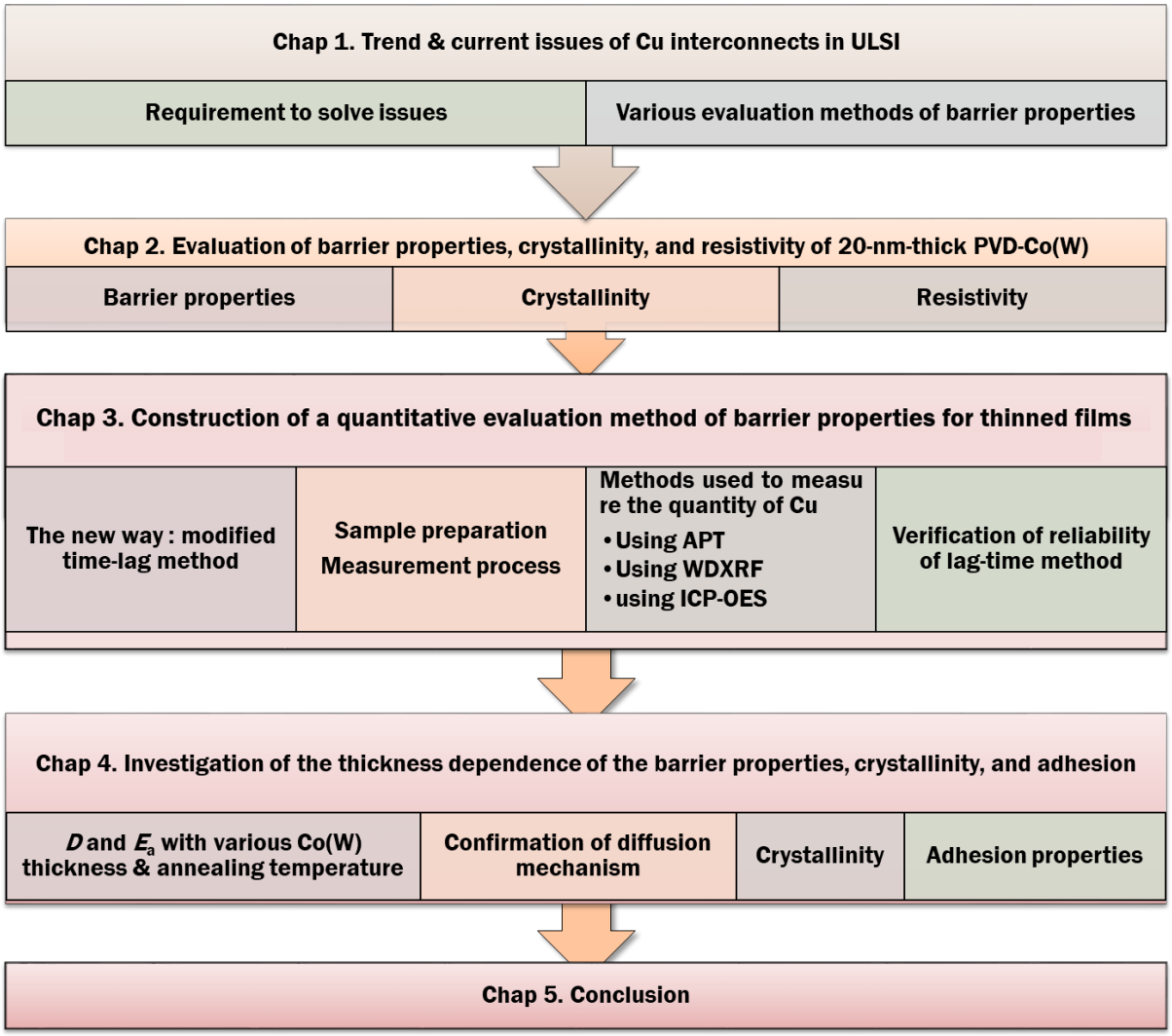

Fig 15. The overall structure of the dissertation.

Reference

1) IRDS™ 2020: Executive Summary - IEEE International Roadmap for Devices and Systems™, https://irds.ieee.org/editions/2020/executive-summary, (accessed 31 July 2020).

2) A. E. Kaloyeros and E. Eisenbraun, Annu. Rev. Mater. Sci **30**, 363 (2000).

3) A. Kohn, M. Eizenberg and Y. Shacham-Diamand, J. Appl. Phys. **94** [5], 3015 (2003).

4) B. Li, T. D. Sullivan, T. C. Lee and D. Badami, Microelectron. Reliab. **44** [3], 365 (2004).

5) D. Edelstein, J. Heidenreich, R. Goldblatt, W. Cote, C. Uzoh, N. Lustig, P. Roper, T. McDevitt, W. Motsiff, A. Simon, J. Dukovic, R. Wachnik, H. Rathore, R. Schulz, L. Su, S. Luce and J. Slattery, Int. Electron Devices Meet. IEDM Tech. Dig. **4**, 773 (1997).

6) W. Holt, Jefferies 2013 TMT Conference Presentations, https://www.jefferies.com/OurFirm/Conferences/551, (accessed 22 November 2021).

7) J. W. Pyun, W. C. Baek, J. Im, P. S. Ho, L. Smith, K. Neuman and K. Pfeifer, J. Appl. Phys. **100** [2], 023532 (2006).

8) M. T. Bohr, Proc. Int. Electron Devices Meet. 241 (1995).

9) C. L. Lo, K. Zhang, R. Scott Smith, K. Shah, J. A. Robinson and Z. Chen, IEEE Electron Device Lett. **39** [6], 873 (2018).

10) R. Brain, Tech. Dig. - Int. Electron Devices Meet. IEDM 9.3.1 (2017).

11) Y. Shacham-Diamand, J. Electron. Mater. **30** [4], 336 (2001).

12) M.-A.NICOLET, Thin Solid Films **52**, 415 (1978).

13) S. P. Murarka and S. W. Hymes, Crit. Rev. Solid State Mater. Sci. **20** [2], 87 (1995).

14) H. Ono, T. Nakano and T. Ohta, Appl. Phys. Lett. **64** [12], 1511 (1994).

15) S. Tsukimoto, T. Morita, M. Moriyama, K. Ito and M. Murakami, in *Journal of Electronic Materials* (Minerals, Metals and Materials Society, 2005) Vol. 34 pp. 592.

16) K. Holloway, P. M. Fryer, C. Cabral, J. M. E. Harper, P. J. Bailey and K. H. Kelleher, J. Appl. Phys. **71** [11], 5433 (1992).

17) M. Uekubo, T. Oku, K. Nii, M. Murakami, K. Takahiro, S. Yamaguchi, T. Nakano and T. Ohta, Thin Solid Films **286** [1–2], 170 (1996).

18) G. P. Tiwari, R. S. Mehrotra and Y. Iijima, in *Diffusion Processes in Advanced Technological Materials* (Springer Berlin Heidelberg, 2005) pp. 69.

19) C. Lee and Y.-L. Kuo, *The Evolution of Diffusion Barriers in Copper Metallization* (2007).

20) J. Uhm and H. Jeon, Jpn. J. Appl. Phys. **40**, 4657 (2001).

21) T. Oku, E. Kawakami, M. Uekubo, K. Takahiro, S. Yamaguchi and M. Murakami, Appl. Surf. Sci. **99** [4], 265 (1996).

22) Y. Wang and R. Y. Lin, Mater. Sci. Eng. B **112** [1], 42 (2004).

23) P. Alén, M. Ritala, K. Arstila, J. Keinonen and M. Leskelä, J. Electrochem. Soc. **152** [5], G361 (2005).

24) J. S. Becker and R. G. Gordon, Appl. Phys. Lett. **82** [14], 2239 (2003).

25) J. S. Becker, S. Suh, S. Wang and R. G. Gordon, Chem. Mater. **15** [15], 2969 (2003).

26) Z. Li, R. G. Gordon, D. B. Farmer, Y. Lin and J. Vlassak, Electrochem. Solid-State Lett. **8** [7], G182 (2005).

27) D. Edelstein, C. Uzoh, C. J. Cabral, P. DeHaven, P. Buchwalter, A. Simon, E. Cooney, S. Malhotra, D. Klaus, H. Rathore, B. Aganvala and D. Nguyen, Interconnect Technol. Conf. 2001. Proc. IEEE 2001 Int. 9 (2001).

28) G. S. Chen, P. Y. Lee and S. T. Chen, Thin Solid Films **353** [1], 264 (1999).

29) K.-H. Min, J. Vac. Sci. Technol. B Microelectron. Nanom. Struct. **14** [5], 3263 (1996).

30) W. Luh, W. Wu, D. Liu and C. Wu, Solid. State. Electron. **45**, 149 (2001).

31) H. Wang, A. Tiwari, X. Zhang, A. Kvit and J. Narayan, Appl. Phys. Lett. **81** [8], 1453 (2002).

32) H. C. Chung and C. P. Liu, Surf. Coatings Technol. **200** [10 SPEC. ISS.], 3122 (2006).

33) J. P. Gambino, Proc. Int. Symp. Phys. Fail. Anal. Integr. Circuits, IPFA [DOI:10.1109/IPFA.2010.5532242].

34) A. Isobayashi, Y. Enomoto, H. Yamada, S. Takahashi and S. Kadomura, IEEE Electron Devices Meet. 2

(2004).

35) B. Zhao, H. Kim and Y. Shimogaki, Japanese J. Appl. Physics, Part 2 Lett. [DOI:10.1143/JJAP.44.L1278].

36) B. Zhao, T. Momose and Y. Shimogaki, Japanese J. Appl. Physics, Part 2 Lett. [DOI:10.1143/JJAP.45.L1296].

37) S. Yokogawa and H. Tsuchiya, J. Appl. Phys. **101** [1], 013513 (2007).

38) K. Maekawa, K. Mori, N. Suzumura, K. Honda, Y. Hirose, K. Asai, A. Uedono and M. Kojima, Microelectron. Eng. **85** [10], 2137 (2008).

39) K. Shima, Y. Tu, H. Takamizawa, H. Shimizu, Y. Shimizu, T. Momose, K. Inoue, Y. Nagai and Y. Shimogaki, Appl. Phys. Lett. **105** [13], 133512 (2014).

40) J. Koike and M. Wada, Appl. Phys. Lett. **87** [4], 85 (2005).

41) R. K. Singh Raman, P. Chakraborty Banerjee, D. E. Lobo, H. Gullapalli, M. Sumandasa, A. Kumar, L. Choudhary, R. Tkacz, P. M. Ajayan and M. Majumder, Carbon N. Y. **50** [11], 4040 (2012).

42) H. C. Lee, M. Jo, H. Lim, M. S. Yoo, E. Lee, N. N. Nguyen, S. Y. Han and K. Cho, Carbon N. Y. **149**, 656 (2019).

43) H. Shimizu, K. Shima, Y. Suzuki, T. Momose and Y. Shimogaki, J. Mater. Chem. C **3**, 2500 (2015).

44) A. Datta, K. T. Nam, S.-H. Kim and K.-B. Kim, J. Appl. Phys. **92** [2], 1099 (2002).

45) S.-H. Kim, K. T. Nam, A. Datta, H.-M. Kim, K.-B. Kim and D.-H. Kang, J. Vac. Sci. Technol. B Microelectron. Nanom. Struct. **21** [2], 804 (2003).

46) J. S. Reid, E. Kolawa, R. P. Ruiz and M. A. Nicolet, Thin Solid Films **236** [1–2], 319 (1993).

47) D. C. Perng, K. C. Hsu, S. W. Tsai and J. Bin Yeh, Microelectron. Eng. **87** [3], 365 (2010).

48) L. B. Henderson and J. G. Ekerdt, Thin Solid Films **517** [5], 1645 (2009).

49) R. Li, M. Li, C. Jiang, B. Qiao, W. Zhang and J. Xu, J. Alloys Compd. **773**, 482 (2019).

50) J. W. Yeh, JOM **65** [12], 1759 (2013).

51) J. Koike and M. Wada, Appl. Phys. Lett. **87** [4], 11 (2005).

52) H. Shimizu, K. Sakoda, T. Momose and Y. Shimogaki, Jpn. J. Appl. Phys. **51** [5 PART 2], 1 (2012).

53) K. Shima, H. Shimizu, T. Momose and Y. Shimogaki, ECS J. Solid State Sci. Technol. **4** [2], P20 (2014).

54) P. Moon, V. Dubin, S. Johnston, J. Leu, K. Raol and C. Wu, IEEE Int. Electron Devices Meet. 2003 [C], 35.1.1 (2003).

55) A. KINBARA, J. Vac. Soc. Jpn. **53** [9], 539 (2010).

56) H. Kim, T. Koseki, T. Ohba, T. Ohta, Y. Kojima, H. Sato and Y. Shimogaki, J. Electrochem. Soc. **152** [8], G594 (2005).

57) H. Kim, T. Koseki, T. Ohba, T. Ohta, Y. Kojima, H. Sato and Y. Shimogaki, J. Electrochem. Soc. **152** [8], G594 (2005).

58) H. Kim, Y. Kojima, H. Sato, N. Yoshii, S. Hosaka and Y. Shimogaki, Jpn. J. Appl. Phys. **45** [No. 8], L233 (2006).

59) H. Kim, Y. Naito, T. Koseki, T. Ohba, T. Ohta, Y. Kojima, H. Sato and Y. Shimogaki, Japanese J. Appl. Physics, Part 1 Regul. Pap. Short Notes Rev. Pap. **45** [4 A], 2497 (2006).

60) K. T. Jang, S. Y. Lee, S. K. Na, S. K. Lee, J. M. Baek, W. K. You, O. H. Park, R. H. Kim, H. S. Oh and Y. C. Joo, IEEE Electron Device Lett. **39** [7], 1050 (2018).

61) C. C. Yang, S. Cohen, T. Shaw, P. C. Wang, T. Nogami and D. Edelstein, IEEE Electron Device Lett. **31** [7], 722 (2010).

62) T. Nogami, J. Maniscalco, A. Madan, P. Flaitz, P. DeHaven, C. Parks, L. Tai, B. St Lawrence, R. Davis, R. Murphy, T. Shaw, S. Cohen, C. K. Hu, C. Cabral, S. Chiang, J. Kelly, M. Zaitz, J. Schmatz, S. Choi, K. Tsumura, C. Penny, H. C. Chen, D. Canaperi, T. Vo, F. Ito, O. Straten, A. Simon, S. H. Rhee, B. Y. Kim, T. Bolom, V. Ryan, P. Ma, J. Ren, J. Aubuchon, J. Fine, P. Kozlowski, T. Spooner and D. Edelstein, 2010 IEEE Int. Interconnect Technol. Conf. IITC 2010 [111], 10 (2010).

63) C. C. Yang, T. Spooner, S. Ponoth, K. Chanda, A. Simon, C. Lavoie, M. Lane, C. K. Hu, E. Liniger, L. Gignac, T. Shaw, S. Cohen, F. McFeely and D. Edelstein, in *2006 International Interconnect*

Technology Conference, IITC (2006).

64) H. K. Jung, H. B. Lee, M. Tsukasa, E. Jung, J. H. Yun, J. M. Lee, G. H. Choi, S. Choi and C. Chung, IEEE Int. Reliab. Phys. Symp. Proc. 307 (2011).

65) J.-B. Yeh, D.-C. Perng and K.-C. Hsu, J. Electrochem. Soc. **157** [8], H810 (2010).

66) H. Wojcik, C. Krien, U. Merkel, J. W. Bartha, M. Knaut, M. Geidel, B. Adolphi, V. Neumann, C. Wenzel, M. Bendlin, K. Richter and D. Makarov, Microelectron. Eng. **112**, 103 (2013).

67) S. Kondati Natarajan, C. L. Nies and M. Nolan, J. Mater. Chem. C **7** [26], 7959 (2019).

68) Y. Shacham-Diamand and S. Lopatin, Electrochim. Acta **44**, 3639 (1999).

69) H. Shimizu, K. Sakoda and Y. Shimogaki, Microelectron. Eng. **106**, 91 (2013).

70) H. Shimizu, A. Kumamoto, K. Shima, Y. Kobayashi, T. Momose, T. Nogami and Y. Shimogaki, ECS J. Solid State Sci. Technol. **2** [11], P471 (2013).

71) A. Paul, T. Laurila, V. Vuorinen and S. V. Divinski, *Thermodynamics, diffusion and the kirkendall effect in solids* (Springer International Publishing, 2014) Vol. 9783319074.

72) L. G. Harrison, Trans. Faraday Soc. **57** [0], 1191 (1961).

73) Y. H. Shin and Y. Shimogaki, Sci. Technol. Adv. Mater. **5** [4], 399 (2004).

74) Y.-J. Lee, B.-S. Suh, M. S. Kwon and C.-O. Park, J. Appl. Phys. **85** [3], 1927 (1999).

75) H. Wojcik, R. Kaltofen, U. Merkel, C. Krien, S. Strehle, J. Gluch, M. Knaut, C. Wenzel, A. Preusse, J. W. Bartha, M. Geidel, B. Adolphi, V. Neumann, R. Liske and F. Munnik, Microelectron. Eng. **92**, 71 (2012).

Chapter 2

Evaluation of barrier properties, crystallinity, and resistivity of 20-nm-thick PVD-Co(W) single layer for ULSI-Cu interconnects

The importance of this chapter is that it is the starting point for the quantitative evaluation of the barrier properties of PVD-Co(W). As mentioned in Chapter 1, most barrier properties up to now have relied on qualitative evaluation methods. However, information that can be obtained from the results of qualitative evaluation of barrier properties in miniaturized Cu interconnects is limited. Inherent information on the material of barrier layer that can be evaluated numerically is required. If quantitative evaluation was successfully introduced, it would be possible to predict what would happen in the initial stage of thin film growth. And from the results, it will be possible to discuss the origin of the barrier properties of the thin film.

This chapter firstly deals with the principles and experimental methods of evaluating the barrier properties, crystallinity, and resistivity of 20-nm-thick PVD-Co(W) single layer. Next, I discuss the results of each experiment. For the barrier properties, it is necessary to find out how to quantitatively evaluate the barrier properties of 20-nm-thick PVD-Co(W) single layer. At this time, I used a depth profile method for 20-nm-thick PVD-Co(W) single layer. Subsequently, after discussing the results of barrier properties, crystallinity, and resistivity, the optimal composition was estimated by investigating how the composition of Co and W affects the above three properties.

2.1 Experimental

2.1.1 Sample preparation

The sample preparation and structure of the sample for barrier properties are as follows. The structure of the sample to evaluate barrier properties was Cu/Co(W)/SiO_2/Si as shown on the left of Figure 1. The substrate was a 300 mm diameter silicon wafer with a 100-nm-thick thermal oxide. Prior to the deposition, the sputter chamber was evacuated to 1.3×10^{-6} Pa. The SiO_2/Si substrate was used without any pretreatment. The deposition was performed in a plasma sputter chamber (FC7100; CANON ANELVA) with multiple targets (Cu, Co, and W) under an argon (Ar) atmosphere. The substrate was transferred to the sputter

chamber through the load lock chamber. Then, while the chamber was being purged with Ar, the pressure was set to 3.0×10^{-2} Pa. This pressure was maintained until the sample preparation was completed. 20-nm-thick PVD-Co(W) films with W concentration of 23, 35, 43, 51, 58, and 70 at. % were deposited using dual target plasma sputtering. Note that, as diffusion coefficient (D) of Cu in Co(W) was estimated from Cu concentration profile in Co(W), Co(W) should have enough thickness, though their thickness in Cu interconnects is critically thin of 1-2 nm, and thus it was set to 20 nm in this study. Subsequently, Cu films were deposited in the same chamber. The power applied to each target was controlled to change the composition of the Co(W) thin film. Direct current (DC) plasma was generated for Co(W) and Cu deposition. For the Co(W) deposition, the Co and W concentration were adjusted while the total power was held constant at 500 W for the Co and W targets, but the power ratio was varied. For the Cu deposition, 1 kW of power was applied to the Cu target to deposit Cu at a growth rate of 24 nm/min. The composition of the Co(W) film was confirmed by X-ray photoelectron spectroscope (XPS; 1600C; Ulvac Phi) after removing the surface contaminations by 5-min-long Ar ion etching with acceleration voltage of 2.1 kV and emission current of 25 mA. Note that Cu was not deposited on the samples to evaluate crystallinity and resistivity as shown on the right of Figure 1. Deposition conditions for these samples were the same as that for evaluating barrier properties except for Cu deposition.

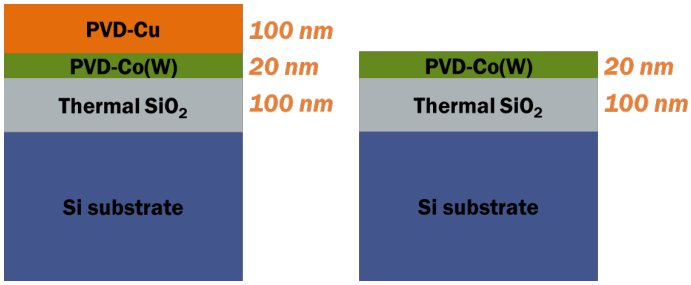

Fig 1. Schematic of a sample for evaluating barrier properties and for evaluating crystallinity and resistivity.

2.1.2 Measurement process

The D of Cu in PVD-Co(W) was estimated by evaluating Cu concentration profile in the Co(W) film after annealing to accelerate the Cu diffusion. In this chapter, method to anneal the sample and method to measure the Cu concentration profile is explained. Samples were annealed to accelerate the Cu diffusion into the Co(W). To ensure the same diffusion length ($\sqrt{Dt}$) of Cu in Co(W), 4-6 nm in this case, annealing temperature and period was determined. Hence, the concentration profile did not vary significantly among samples annealed at any temperature. Resulting annealing conditions were summarized in Table 1.

Table 1. Annealing conditions for evaluation of Cu diffusion barrier properties.

Temp	W 23 at.%	W 35 at.%	W 43 at.%	W 51 at.%	W 58 at.%	W 70 at.%
500°C	750 min	750 min	750 min	750 min	750 min	750 min
550°C	450 min	450 min	450 min			
600°C	150 min	150 min	378 min	150 min	12 min	150 min
650°C		29 min	60 min			
700°C	10 min	2.5 min	5.5 min	25 min	1 min	25 min

The basic procedure for evaluating the Cu diffusion barrier properties was as follows. Samples with stacked structure of 100-nm-thick Cu/20-nm-thick Co(W)/100-nm-thick SiO_2/Si were annealed by rapid thermal anneal (RTA; MILA-3000; ULVAC-RIKO, INC). These were maintained at a constant pressure of 6,666 Pa while supplying 20 sccm of H_2 gas to the RTA furnace. Then, the concentration profile of Cu diffused into Co(W) was measured by XPS. However, when the depth profile of the Cu surface was measured by XPS, a knock-on phenomenon occurred, in which Ar ions pushed Cu inside of Co(W) film. To avoid this phenomenon, depth profiling was conducted from backside of the sample, as shown in Figure 2. For this, following preprocessing was made. First, a 1.5-μm-thick Ti layer was sputtered on top of the structure to stabilize the Cu film, and then another Si substrate was adhered onto the Ti layer using double-sided carbon tape. Thereafter, Si was etched from the backside over a designated area (15 × 8 mm) by deep reactive-ion etching (DRIE; MUC21-ASE Pegasus; SPT) until the backside of Co(W) layer was exposed. Then, the Cu

concentration profile was measured by XPS backside depth profiling.

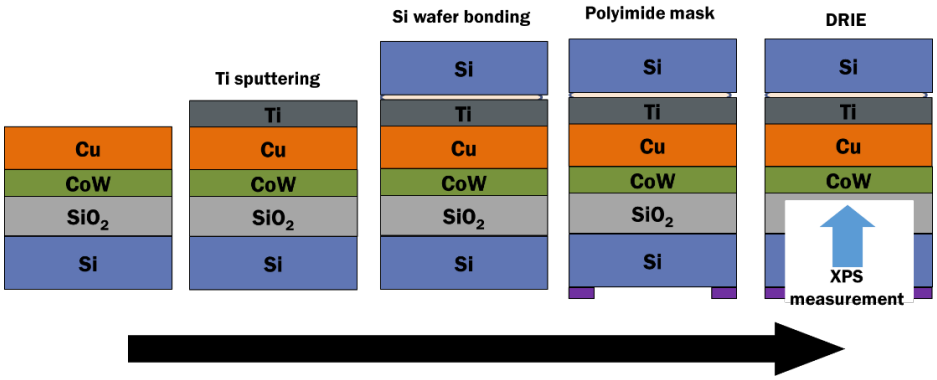

Fig 2. Sample fabrication procedures for diffusivity of Cu within Co(W) films.

For evaluating the crystallinity of Co(W) and Cu, X-ray diffraction (XRD; SmartLab system 9kW; Rigaku) with 2θ-ω mode using Cu Kα X-ray were used. Annealing conditions were the same as those in Table 1 used for barrier properties. At 500°C, all six samples were annealed for 750 min in the same manner. At 700°C, six samples were annealed for 10 min, 2.5 min, 5.5 min, 25 min, 1 min, and 25 min, respectively. Measurement was done from 40° to 50° with an interval of 0.02°. High-resolution transmission electron microscope (HRTEM; JEM-ARM200F; JEOL) were also used for crystallinity evaluation. The pretreatment process of the sample for HRTEM measurement is as follows. The sample was polished from side wall and thinned by ion milling. After that, it was measured by HRTEM with an acceleration voltage of 200 kV and a beam diameter of about 1 nm. This measurement allowed not only TEM cross-sectional images, but also selected area electron diffraction (SAED) patterns. The nanostructure can be predicted from the SAED pattern.

The resistivity of PVD-Co(W) was estimated from sheet resistance and film thickness. Film thickness of Co(W) was measured by field emission scanning electron microscope (FE-SEM; JSM6340F; JEOL). The thickness of all of the Co(W) films was 20 nm. The sheet resistance was obtained by averaging the values measured at 10 different points on the respective sample using a four-point probe (Series 2400

SourceMeter; Keithley). At this time, the relative standard deviation of resistivity of six samples was also obtained (3 % for W 23 at. %, 2 % for W 35 at. %, 2 % for W 43 at. %, 2 % for W 51 at. %, 2 % for W 58 at. %, and 2 % for W 70 at. %). Since the relative standard deviation of six samples is very small as 2%, there is no problem in the accuracy of the resistivity of the sample.

2.1.3 Analysis process

Experimental Cu concentration profiles in Co(W) obtained by XPS were fitted by a theoretical profile based on Fick's second law ($\frac{\partial c}{\partial t} = D\frac{\partial^2 c}{\partial z^2}$), by which *D* was determined. It was first proposed by our group.[1)–4)] Here, the diffusion was treated as semi-infinite diffusion couple. A semi-infinite system refers to a system in which the end of the diffusion couple is not affected by the diffusion of components. The concentration profile can be obtained by applying the appropriate initial and boundary conditions. The actual concentration profile of Cu, *C*(z), is given in the form of an error function; [5)]

$$C(z) = \frac{100}{2\sqrt{\pi}\sqrt{Dt}}\int_0^z exp\left[-\left(\frac{x}{2\sqrt{Dt}}\right)^2\right]dx \quad (2.1),$$

where *x* is distance from the Cu/Co(W) interface, and *t* is annealing period. That is, at *x* = 0 is equivalent to the Cu/Co(W) interface. However, the measured Cu concentration profile by XPS is not exactly the same as the actual Cu concentration, *C*(z), due to large spatial resolution in depth direction, which is typically 2-3 nm. Therefore, the measured Cu concentration showed profile even from the abrupt interface of non-annealed Cu/Co(W), as shown on the right in Figure 3. This is a unique phenomenon that occurs in XPS measurement and cannot be controlled by the user. The relationship between *C*(z) and the apparent concentration profile, *S*(z), can be given by considering the depth resolution of XPS as follows;[6)]

$$S(z) = \int_0^\infty C(z)\cdot exp\left[-\left(\frac{z-s}{2\sigma}\right)^2\right]ds \quad (2.2),$$

where *z* is the depth and *σ* is the XPS depth resolution. This means that *S*(z) is given by the Gaussian convolution of *C*(z). Therefore, I can find *D* using equations 2.1 and 2.2. First, *S*(z) profiles with various Dt values are calculated in advance. Next, the XPS depth profile obtained in the experiment is fitted to the S(z) profile obtained previously. At this time, while changing the *D*t value, I find the result that best fits the profile

obtained in the experiment. Then I can get *D* from the *D*t value of the profile that best fits.

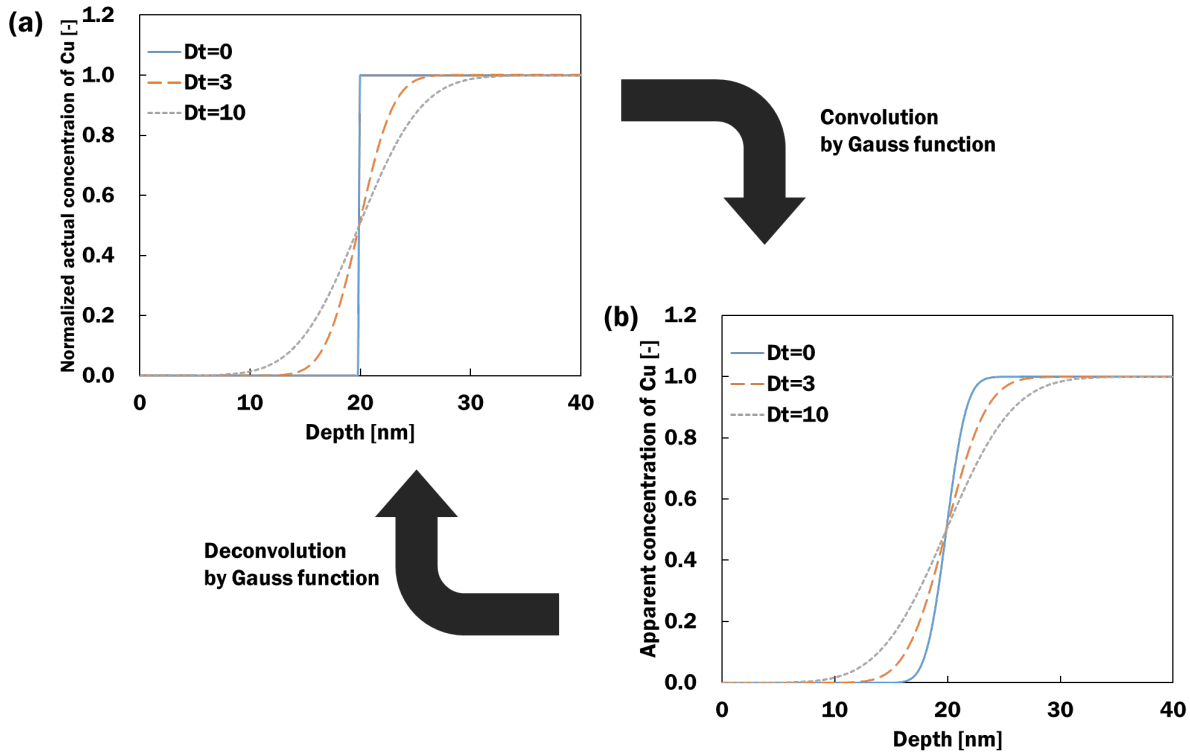

Fig 3. Relationship between (a) actual concentration profile and (b) apparent concentration profile obtained by XPS.

2.2 Barrier properties of 20-nm-thick PVD-Co(W) single layers

2.2.1 Excellent barrier properties of PVD-Co(W)

The *D* of Cu in 20-nm-thick PVD-Co(W) single layers was evaluated by the depth profile method using XPS. This method was first proposed by Shimizu et al.[1)–4)] Since all Cu concentration profiles must be distributed in the Co(W) layer, the thickness of Co(W) was set to 20 nm thicker than the thickness applied to the actual Cu interconnects. The *D* of Cu in 20-nm-thick Co(W) single layers was calculated from Cu concentration profile after annealing for various times (from 1 min to 750 min). The concentration profile of Cu diffused into PVD-Co(W) single layers after annealing at 500°C for 750 min is shown in Figure 4. Fitting to estimate *D* was done for the measured Cu concentration profile below 50 at. %. Good agreement was obtained between the measured profile and *S*(z) when *D* was 2.2×10^{-19} cm^2/s. Same fitting was done for all samples made in this study, and good agreement was obtained, i.e. *D* was successfully estimated in all conditions studied.

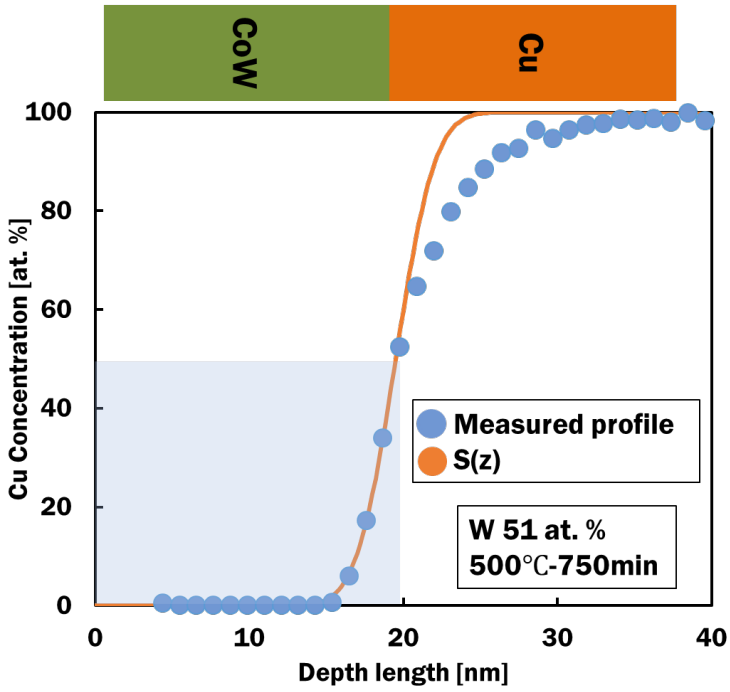

Fig 4. The Cu concentration profile diffused into PVD-Co(W).

Figure 5 shows an Arrhenius plot of D of Cu in PVD-Co(W) single layers with six different W concentrations. The logarithm of D varied linearly against reciprocal of temperature in the range of 500 to 700ºC. This means that the diffusion mechanism (for example, volume diffusion and grain boundary diffusion) of Cu in Co(W) was unchanged in this temperature range, otherwise, high-temperature annealing might allow crystallization of Co(W) to change the diffusion mechanism, thereby the Arrhenius plot being deviated from the linear relation. It will be discussed later in chapter 2.2.3.

The temperature dependence of D is given by;

$$D = D_0 exp\left(-\frac{E_a}{k_B T}\right) \qquad (2.3),$$

where D_0 is a pre-exponential factor, also called a frequency factor, E_a is the activation energy for diffusion, T is the temperature, and k_B is the Boltzmann constant. At temperature T, atoms with average kinetic energy k_BT exist with the Boltzmann distribution. $\exp(-E_a/k_BT)$ represents the ratio of kinetic energy k_BT and E_a at temperature T. That is, as the temperature increases, the proportion of diffusion atoms having a greater kinetic energy than E_a increases. Therefore, as E_a is larger and T is smaller, the probability of diffusion decreases, and finally D becomes smaller. E_a corresponding to the slope in Figure 5 were summarized in Figure 6. The values of E_a were 1.9 eV for W 23 at. %, 1.9 eV for W 35 at. %, 2.2 eV for W 43 at. %, 1.1 eV for W 51 at. %, 2.1 eV for W 58 at. %, and 1.1 eV for W 70 at. %. At low W concentrations (23, 35, 43 at. %), the E_a slightly increased with the W concentration, while E_a fluctuated at higher W concentrations. The accuracy of E_a obtained here is estimated from the relative standard deviation of the D for 6 samples. Since all the relative standard deviations of the six samples are small, around 5%, most of the measurements will be near the Arrhenius line and therefore have sufficient accuracy (6 % for W 23 at. %, 6 % for W 35 at. %, 6 % for W 43 at. %, 4 % for W 51 at. %, 8 % for W 58 at. %, and 4 % for W 70 at. %.). Therefore, the results of W 51 at. % and W 70 at. %, which behave slightly differently, are not due to errors during measurement. However, at W 70 at. %, there is a possibility that crystallization of W starts and grain boundaries are formed, resulting in a decrease in E_a. However, since such crystallization is not seen in W 51 at. %, the cause of the different

behavior is still unknown. D_0 also behaves similarly to E_a. D_0 was 2.0 x10^{-6} - 2.7 x 10^{-7} cm^2/s, nominally around 10^{-6} cm^2/s up to W 43 at. %, while it fluctuated above W 51 at. % similarly with E_a. The scientific meaning of D_0 will be discussed in chapter 2.2.3. Anyhow, since the W 43 at. % had the largest E_a value, it is expected to exhibit the highest barrier property among the six W concentrations. Therefore, PVD-Co(W) thin film with W 43 at. % is considered to be optimal for back end of the line (BEOL) manufacturing processes.

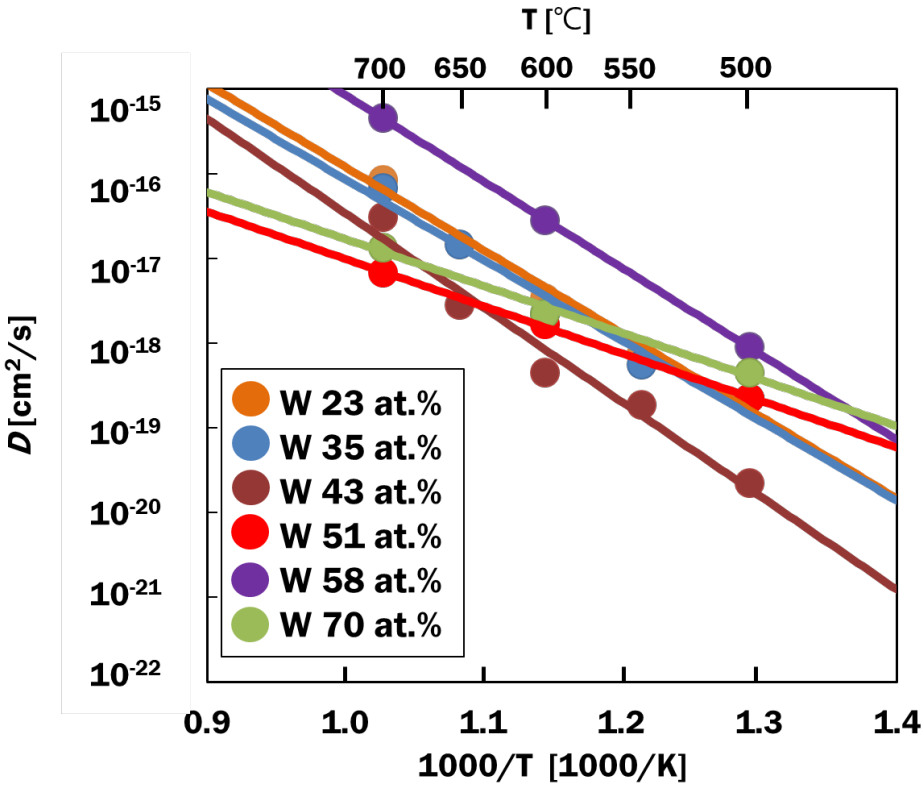

Fig 5. Arrhenius plot with various W concentrations of PVD-Co(W) films.

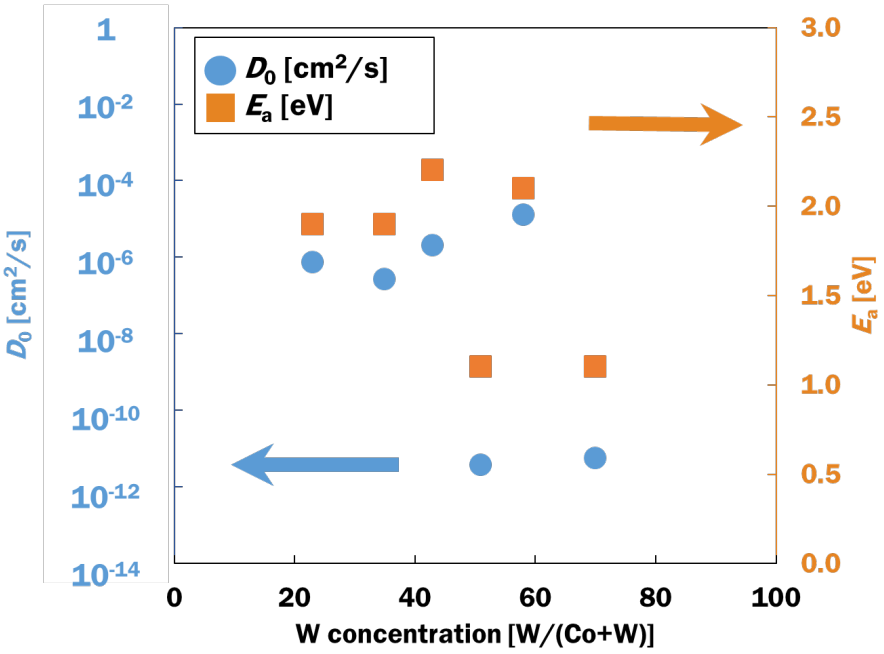

Fig 6. D_0 and E_a obtained from the XPS depth profile method.

PVD-Co(W) with W 43 at. % was then compared with other candidates of the barrier, PVD-TaC[7], CVD-W[8], PVD-TiN[9], and PVD-TaN[10] as shown in Figure 7. ALD-Co(W) with W 20 at. % is also shown, which was the best barrier in the previous study (10-20 at. %)[1]. The D of Cu in PVD-Co(W) was smallest among them in the studied temperature range (500-700ºC). Similar with Figure 6, E_a and D_0 showed the similar tendency, i.e., the higher E_a, the higher D_0. The highest E_a was seen for PVD-Co(W) (2.2 eV), while the others showed 0.76 eV for PVD-TaC[7], 0.46 eV for CVD-W[8], 1.4 eV for PVD-TiN[9], 1.3 eV for PVD-TaN[10], and 1.7 eV for ALD-Co(W)[1]. The value of D_0 was 2.1 x 10^{-11} cm^2/s for PVD-TaC[7], 1.1 x 10^{-13} cm^2/s for CVD-W[8], 1.2 x 10^{-9} cm^2/s for PVD-TiN[9], 2.8 x 10^{-10} cm^2/s for PVD-TaN[10], and 3.9 x 10^{-8} cm^2/s for ALD-Co(W)[1]. From comparison of E_a, PVD-Co(W) showed Cu diffusion barrier properties superior to the other candidates. D_0 exists in a wide range from 10^{-8} to 10^{-13} cm^2/s, which will also be discussed in chapter 2.2.3.

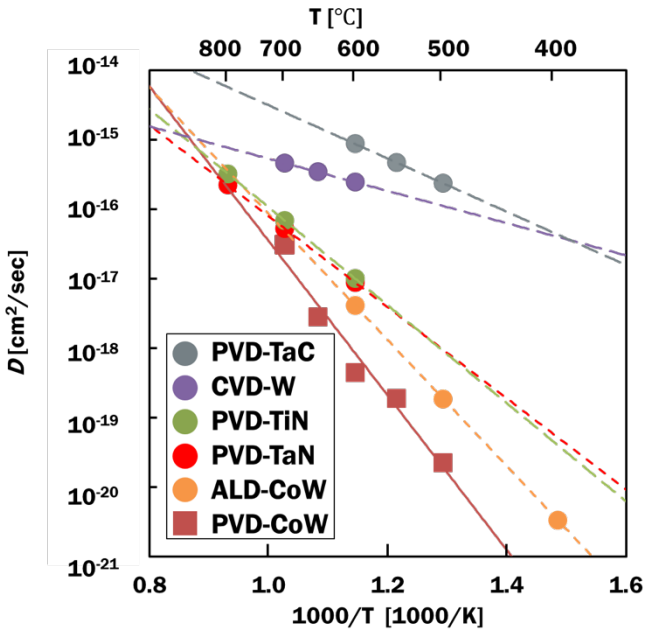

Fig 7. Arrhenius plot of PVD-TaC[7], CVD-W[8], PVD-TiN[9], PVD-TaN[10], ALD-Co(W) (W; 20 at. %)[1], and PVD-Co(W) (W; 43 at. %).

D at 500°C was summarized in Figure 8 because it was the lowest temperature, we studied and closest to the temperature used in the back end of the line (BEOL) manufacturing, thus working as the brief summary of the barrier property. PVD-Co(W) with W 43 at. % was compared with ALD-Co(W) with W 20 at. % and PVD-TaN. *D* of Cu for PVD-TaN was drawn by the horizontal dashed line. Of the W concentrations tested, PVD-Co(W) with W 43 at. % showed the lowest *D*, and thus expecting better Cu diffusion barrier properties than PVD-Ta/TaN and ALD-Co(W), which was consistent with our conclusion based on E_a. Therefore, PVD-Co(W) thin film with W 43 at. % was considered to be optimal for BEOL manufacturing.

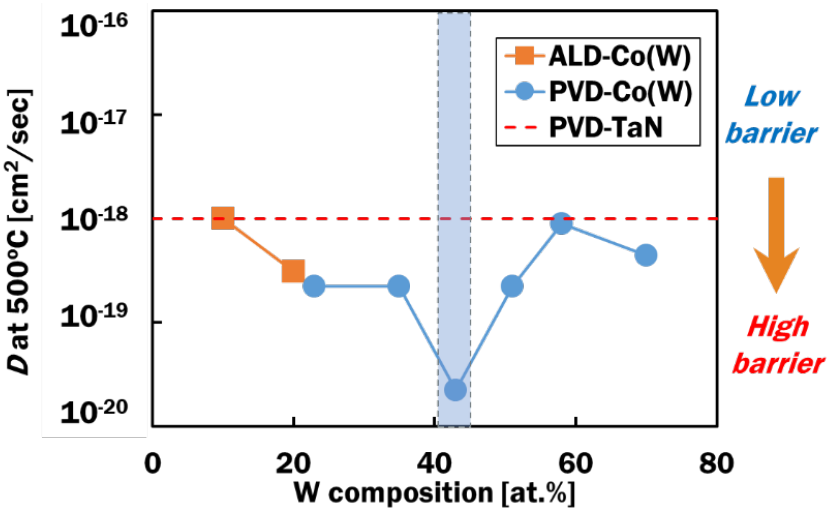

Fig 8. *D* at 500°C with PVD-Co(W), PVD-Ta/TaN, and ALD-Co(W) (W; 20 at. %).

2.2.2 The cause of excellent barrier properties

The maximum E_a of the 20-nm-thick PVD-Co(W) obtained in my research was 2.2 eV. This value is not small compared to other materials. For comparison, E_a for the self-diffusion of various known bulk metals is summarized in Table 2[11]. Note that the state of the material in Table 2 is a bulk metal, not a thin film. Basically, it can be seen that the higher the melting point (M.P.), the higher E_a. In particular, W, a high melting point material, exhibits a fairly high E_a of ~ 5.4 eV. Therefore, the addition of W has a favorable effect on the improvement of the barrier properties. In addition, since the 20-nm-thick PVD-Co(W) exhibits a higher E_a than the self-diffusion of bulk Cu, it can be confirmed that the superior barrier properties of PVD-Co(W).

Table 2. E_a of various bulk metals[11].

	Zn	Mg	Al	Ag	Au	Cu	Mo	Ta	W
Ea (eV)	~ 1.0	~ 1.5	~ 1.3	~ 1.7	~ 1.7	~ 2.0	~ 4.5	~ 4.2	~ 5.4
M.P.(°C)	420	650	660	962	1,064	1,084	2,623	3,017	3,422

Table 3 summarizes the results of the E_a of various materials for Cu diffusion. E_a here is mostly

calculated by simply assuming the thickness of the thin film as $\sqrt{Dt}$. The E_a of the alloy barrier is higher than that of the nitride and carbonized barrier. The reason can be explained as follows. First of all, when it is an alloy barrier, it is easy to have an amorphous structure. In addition, alloys tend to have a higher melting point than pure metals. These properties have the effect of increasing E_a. In addition, when the barrier properties are the same, as an advantage of the alloy barrier, which is superior to the nitride and carbonized barrier in terms of electrical properties. It can be predicted that the alloy barrier is a more advantageous barrier material.

Table 3. E_a of various materials for Cu diffusion.

Group	**Metal**		**Nitride**					**Carbide**	**Alloy**		
	Ta	**W**	**TiN**	**W/WN**	**W_2N**	**Ta/TaN**	**TaN**	**TaC**	**CoP**	**CoW**	**CoWP**
E_a (eV)	2.3	1.2	1.4	1.9	1.0	1.4	1.3	0.9	1.3	2.2	2.4
Ref.	12)	13)	9)	14)	15)16)	17)	10)	7)	18)		19)

The magnitude of E_a in general describes the diffusion mechanism. It is because, the larger E_a, the more difficult for the diffusion of atoms. If the barrier layer is a single crystalline structure or amorphous structure, volume diffusion would occur due to lack of grain boundaries, and thus showing large E_a. Volume diffusion is further classified into substitutional diffusion (vacancy diffusion) and interstitial diffusion. When the size of matrix atom and diffused atom is largely different, interstitial diffusion would occur, otherwise, substitutional diffusion would occur. If the barrier layer is a polycrystalline structure that includes grain boundaries, atoms are diffused along the grain boundaries with much smaller E_a. In short, even for the same material, E_a varies depending on nanostructure, especially presence/absence of grain boundary. Note that to grow single crystalline film, very high temperature typically above 500°C and the substrate coherent with deposits is necessary, but it is hard to be achieved in the BEOL manufacturing, and thus single crystalline film was excluded from the discussion hereafter. As E_a is not theoretically estimated, 13 existing reports on

E_a of Cu in various metals were surveyed. Although there are no reports fairly comparing E_a of Cu in the same metal but different nanostructure, previous reports revealed the range of E_a in the respective nanostructure; 0.2-1.4 eV in polycrystals such as Ta [20)21)], Co [1)], W_2N [16)], TiN [9)], TaN [10)], TaC [15)], and CuSn [22)], while 1.8-2.8 eV in amorphous such as Ru(P) [23)], W/WN [14)], TiB_2 [24)], and W-Si-N [25)]. These suggested that diffusion of Cu in amorphous shows E_a above 1.8 eV, while that in polycrystals shows E_a below 1.4 eV. Furthermore, considering their averaged values were 2.1 and 1.0 eV, respectively, there seemed the empirical relation that E_a of Cu in amorphous metals is approximately twice of that in polycrystalline metals [26)27)28)]. Similar phenomenon may also have occurred in the ALD-Co and ALD-Co with W stuffing, i.e. ALD-Co(W); ALD-Co that includes grain boundary showed E_a as low as 1.0 eV [1)], while ALD-Co(W) shows almost twice E_a of 1.7 eV [1)]. In this study, PVD-Co(W) with W 43 at. % showed the largest E_a of 2.2 eV, which was above the criteria for amorphous (1.8 eV), thus consistent with my reasoning. It is presumable that the PVD-Co(W) with W 43 at. % has an amorphous structure without grain boundary, suggesting that diffusion of Cu in PVD-Co(W) is probably caused by volume diffusion, especially substitutional diffusion (vacancy diffusion) due to similarity of atomic radius; Cu; 1.3 Å, Co; 2.0 Å, and W; 2.1 Å. In the meantime, PVD-Co(W) with W 51 and 70 at. % showing E_a of 1.1 eV seemed polycrystalline. Previously, Studies of metallic compounds containing Co and W have shown that W improves their barrier properties [29)30)31)32)33)34)35)36)37)38)39)18)]. Note that, my further analysis on the nanostructure of Co(W) to be shown in Figure 9 denied it and found these were also amorphous, though the reason was not elucidated so far.

To explain the relationship between E_a and the crystal structure in my experimental results, nanostructure of PVD-Co(W) films was evaluated by XRD and TEM-SAED. The nanostructure affect the barrier properties. Basically, the higher the density of atoms in the unit cell, the better the barrier properties. Therefore, for the same material, the fcc or hcp structure tends to have superior barrier properties rather than the bcc structure. If there are defects such as grain boundaries or dislocations in the material, E_a is greatly reduced. Figure 9(a) shows XRD results of PVD-Cu/PVD-Co(W)/SiO_2 samples with six different W concentrations before annealing. Peak intensity was normalized based on that of Cu (111). PVD-Co(W) with

W 23 at. % had a very little Co (111) peak, but almost negligible. The other samples showed no peaks related to any Co and W, i.e., amorphous as expected. More attention should be paid for unwanted crystallization during annealing. Figures 9(b) show XRD patterns of the annealed samples at 500 and 700°C, respectively. Annealing time was described in Table 1. At 500°C, for the PVD-Co(W) with W 51, 58, and 70 at. %, Co (111) peak (44.1°) and W (110) peak (40.3°) were not found, suggesting that amorphous structure was maintained even after the annealing at 500°C. The samples with W 23, 35, and 43 at. % showed a small Co (111) peak (44.1°), meaning that crystallization occurred in the sample. However, their peak intensities were very small, and thus it was difficult to say that Co(W) was entirely crystallized, rather small portion of the film was crystallized. Other possible peaks such as Co_3W (20-21) at 46.6° and W (111) at 41.4° were not found. At 700°C, any peak was not observed from W 51 and 58 at. %, while small Co (111) peak was observed from W 23, 35, and 43 at. %, while small W (110) peak was observed from W 70 at. %. In short, the sample with W 51 and 58 at. % were not crystallized during the annealing, while the others were crystallized; however, due to smallness of the intensity, very limited region of the film seemed crystallized, which was probably small Co or W grains buried in the amorphous Co(W). Note that Co(W) alloy such as Co_3W was not detected from any samples. This means amorphous structure might be preserved in most regions of the film after annealing, while crystallized in very limited region. Therefore, the diffusion mechanism was not changed from amorphous phase, in other words, obtained *D* could be regarded as *D* of Cu in amorphous PVD-Co(W). It was reasonable from the Arrhenius plot shown in Figure 5, in which all the results could be fitted by the single straight line without exception. Similar results were obtained by TEM-SAED. Figure 9(c) shows the cross-sectional TEM image and SAED pattern of the W 58 and 70 at. % samples after annealing at 650°C - 44 min. Note that this annealing condition was much harsher than those used for the barrier property evaluation, i.e., 600°C - 12 min and 700°C - 1 min. Appropriate annealing time to evaluate *D* at 650°C could be anticipated as only a few minutes, i.e., this sample was annealed 10 times longer than that for the barrier property evaluation. Nevertheless, any periodic pattern corresponding to crystal structure was not observed from the TEM cross-section image; furthermore, one dim circle was observed with faint spots

on the outside from the SAED pattern. Considering that polycrystalline structure gives many concentric circles around the origin in the SAED pattern, while amorphous structure gives halo ring pattern around the central bright spot, my Co(W) film annealed in the significantly harsh condition was slightly crystalized but close to amorphous. Hence, my PVD-Co(W) film after the annealing for the barrier property evaluation would preserve the amorphous structure. According to the XRD and TEM-SAED observations combined with the Arrhenius plot shown in Figure 5, it was certain that Co(W) was amorphous or almost amorphous even after the annealing, and thus obtained *D* could be regarded as *D* of Cu in amorphous PVD-Co(W).

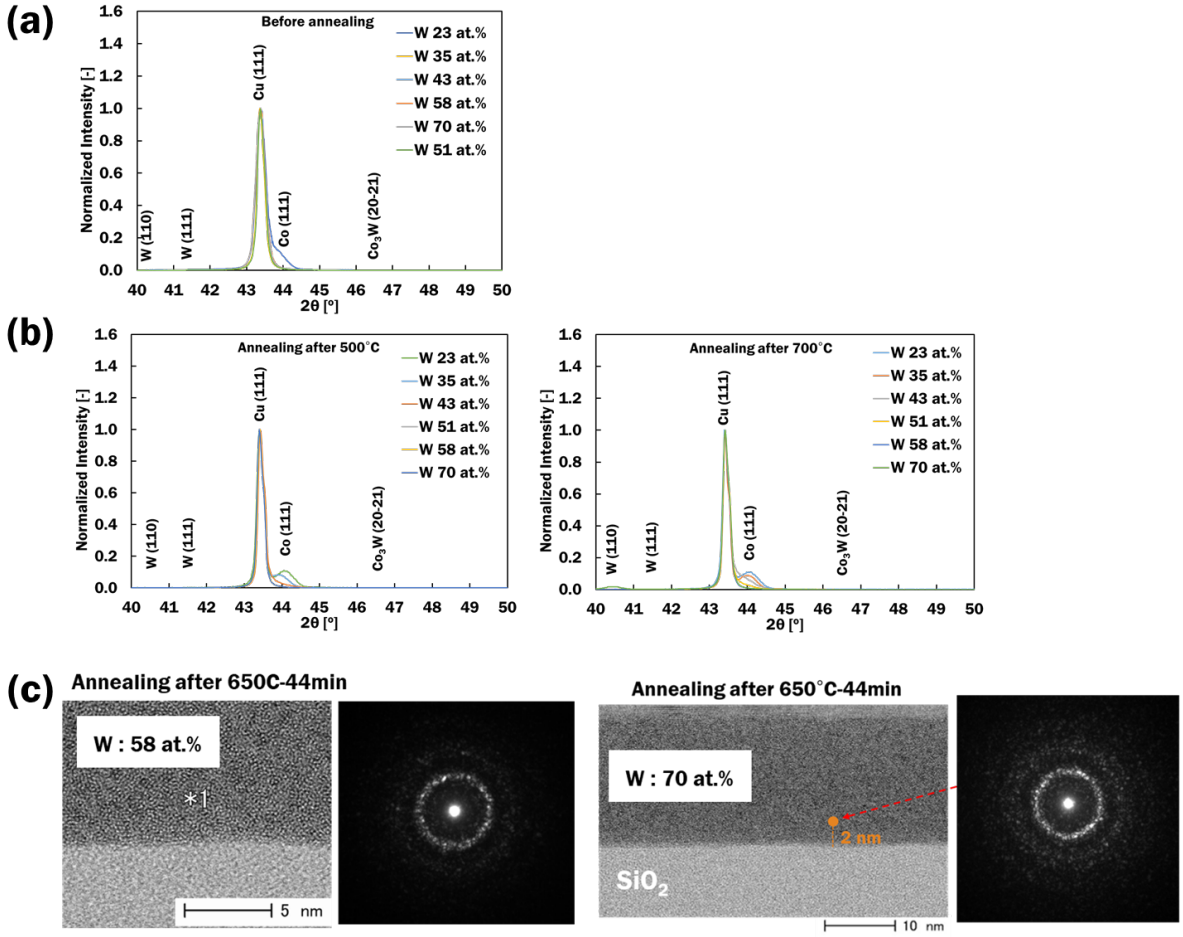

Fig 9. (a) XRD and (b) TEM results of PVD-Co(W) after annealing.

To strengthen my claim that PVD-Co(W) film was almost amorphous after annealing, grain size of Co in PVD-Co(W) with 35 at. % W was calculated from XRD peak obtained using the Scherrer equation.

Peak intensity was normalized based on the peak intensity of Cu (111). Figure 10 shows the normalized XRD results of the W 35 at. % before and after annealing at 700°C - 2.5 min. Before the annealing, no peaks related to Co and W were observed; however, a very small Co (111) peak appeared after the 2.5-minutes annealing. This 2.5 minute was the annealing period used for the barrier properties evaluation, thus same with that in Figure 9(b). Based on this fact, the structure of Co(W) after 2.5 min annealing is estimated as follows. In crystallography, using the Scherrer equation, the grain size can be inferred from the full width at half maximum (FWHM) of the Co (111) peak, which was about 0.51°. The Scherrer equation can be written as,

$$\tau = \frac{K\lambda}{\beta \cos\theta} \qquad (2.4),$$

where τ is average size of grains, K is dimensionless shape factor (typically 0.94), [40] λ is the X-ray wavelength used for XRD measurement (1.5405 nm in this experiment), and β is FWHM (about 0.51 in the case of Co (111)), θ is the Bragg angle of the peak (22.0° in this case). The average grain size of Co was therefore estimated as 3.1 nm. I also considered instrumental broadening by XRD apparatus. For the same XRD apparatus, XRD measurement was performed for Si powder (198-05455; FUJIFILM Wako Pure Chemical Corporation). At this time, the difference in FWHM of Si powder peak was 0.03°. Considering this, it can be seen that the change in grain size due to instrumental broadening is negligible. Grains with 3.1 nm in diameter were small compared with the film thickness of 20 nm, so that it can be recognized that very small Co grains were buried in the amorphous Co(W). It was consistent with my reasoning in the previous chapter. That is, in the current annealing condition for barrier property evaluation (2.5 min), only a part of Co formed crystalline grains with 3.1 nm in diameter, while W was not crystallized, i.e., amorphous like state.

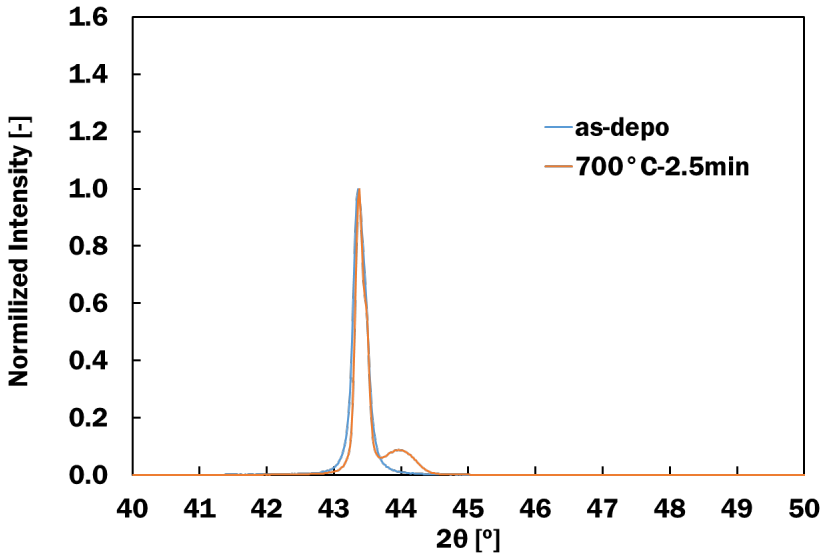

Fig 10. Normalized XRD results of the W 35 at. % sample before annealing & annealed at 700°C - 2.5 min.

2.2.3 Verification of amorphous structure of Co(W) by E_a and D_0

In the preceding chapter, Co(W) was proved to have amorphous structure by XRD and TEM analyses. In this chapter, it was also verified from the relationship between D_0 and E_a. In the Arrhenius formula, D consists of the pre-exponential factor, D_0, and the exponential function, $\exp(-E_a/k_BT)$. At certain temperature, kinetic energy of atoms distributes according to Boltzmann distribution with average of k_BT. Considering that vacancy diffusion of Cu occurred in my Co(W), E_a is the activation energy required for Cu atoms to diffuse in Co(W) barrier via vacancy, in which E_a is equivalent to the formation vacancy inside Co(W) rather than movement of Cu atoms to that vacancy. Anyhow, larger E_a means more energy is required to break the bond of Co(W) barrier, i.e. Cu atoms that can diffuse into Co(W) becomes less.

Like E_a, D_0 is also a parameter affected by the diffusion mechanism. The D_0 is expressed as follows.

$$D_0 = gfv^0a^2exp\left(\frac{\Delta S}{k_B}\right) \qquad (2.5),$$

where, ΔS is the entropy for diffusion, g is the geometrical factor, f is the correlation factor, v^0 is the attempt frequency with the order of the Debye frequency of the lattice, and a is the lattice parameter. Except for ΔS, the change in all other factors is not significant. (g is usually a value between 1/6 and 1, f is usually a value between about 1/3 and 1, v^0 is in the range of 10^{12} to 10^{13} s^{-1}, a is typically several angstroms.) Only ΔS

greatly affects the change in D_0. When equation 2.5 is expressed for ΔS, it is as follows.

$$\Delta S = k_B ln\left(\frac{D_0}{gfv^0a^2}\right) \qquad (2.6),$$

According to statistical mechanics analysis, $\frac{D_0}{gfv^0a^2}$ means the number of cases in which diffusion atoms are distributed. That is, the greater the D_0, the greater the probability that the diffusion atoms will be distributed more disorderly. As a result, the change in the entropy of diffusion, ΔS, becomes large, and diffusion occurs more and more irreversibly. That is, when D_0 is large, diffusion atoms exist in a relatively more disordered state. The order of D_0 reported for amorphous structure shows a very wide change of about $10^{-11} \sim 10^{17}$ cm^2/s [41),42)]. This deviation is much greater than the D_0 reported for crystalline structure (about $10^{-2} \sim 10^6$ cm^2/s).

Although, individual discussion on E_a and D_0 is difficult, past researches on diffusion of various metals in amorphous alloys clarified that there is an empirical relation between D_0 and E_a [43)41)],

$$D_0 = Aexp\left(\frac{E_a}{B}\right) \qquad (2.7),$$

where A and B are fitting parameter. This relationship is valid for amorphous and crystalline alloys. In the case of amorphous alloys, A was reportedly about 10^{-15} to 10^{-16} cm^2/s and B was about 0.055 eV, while, for crystalline metals, A was about 10^{-3} cm^2/s and B was about 0.41 eV [43)41)44)45)]. These suggest that different diffusion mechanisms for amorphous and crystalline alloys result in significantly different values of A and B. Figure 11 shows the relationship between D_0 and E_a in crystalline metals and amorphous alloys shown above, and our PVD-Co(W) shown in Figure 6. The slope of this graph is 1/B, and the y-intercept is ln(A). The result of PVD-Co(W) with six different W concentration exhibited a straight line with A of 2.3×10^{-18} cm^2/s and B of 0.077 eV. It suggests that all of my Co(W) follows the empirical relationship. That is, all six PVD-Co(W) samples have the same nanostructure. Furthermore, as A and B values for my Co(W) were closer to amorphous alloys rather than crystalline alloys, all of my Co(W) can be recognized as amorphous structure. Summarizing, Co(W) was verified as amorphous structure by both of structural analysis by XRD and TEM, and also kinetic analysis using D_0 and E_a.

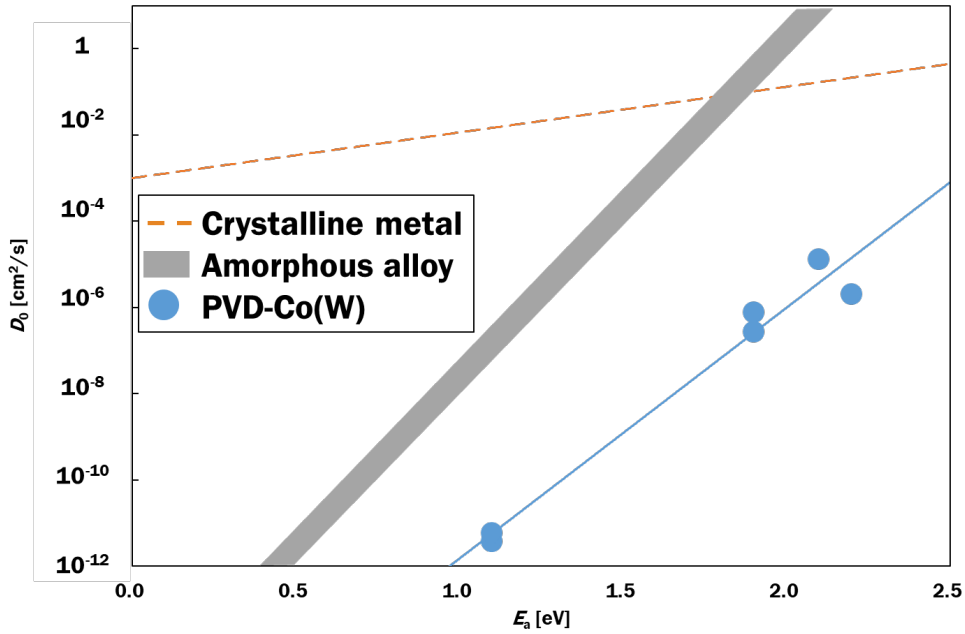

Fig 11. Relationship between D_0 and E_a in crystalline metals and amorphous alloys [43)41)].

2.3 Relationship between the composition of Co(W) and resistivity

Figure 12 shows the resistivity of PVD-Co(W) films with various W compositions. The resistivity increased to W 51 at. %, then decreased again. The relatively high resistivity of PVD-Co(W) compared to PVD-Co is not unusual. In general, alloys are made by introducing another element into pure metal as an impurity. This distorts the crystal structure, which hinders the movement of free electrons, thereby increasing the resistivity. Figure 12 also shows the resistivity of a 20-nm-thick ALD-Co(W) film fabricated from an amidinato precursor and a 25-nm-thick PVD-TaN film[2)46)]. The results showed that PVD-Co(W) and ALD-Co(W) have almost the same resistivity. ALD-Co(W) is a stuffing structure, in which W is segregated at grain boundaries of Co. On the other hand, PVD-Co(W) does not exhibit any grain boundaries when the W concentration is high. In this structure, there is no fast pathway for free electrons, so the resistivity of amorphous alloy without grain boundaries is higher than that of the crystalline metal. In terms of impurity, ALD is still likely to contain trace impurities derived from precursors, while PVD can completely block impurities. In the case of sputtering, the film was formed in a vacuum condition (3.0×10^{-2} Pa in this experiment), and since the purity of the sputtering target (at least 99.999%) is very high, the possibility of mixing of impurities is very low. Therefore, the effect of impurities is negligible. On the other hand, in the case of CVD/ALD, if a precursor containing oxygen is used, oxygen may be included in the thin film. The Co(W) thin film containing oxygen has less segregation of W at the grain boundary, so the stuffing effect is decreased. Moreover, since the resistance also increases by mixing of oxygen, it is disadvantageous as a barrier film. Therefore, an additional operation to remove oxygen impurities by annealing in a reducing atmosphere is required. In addition, it is necessary to use an amidinato precursor that does not contain oxygen from the beginning. In the case of CVD/ALD-Co(W) made using the amidinato precursor, oxygen was suppressed below the lower detection limit of XPS [2)]. That is, PVD is advantageous from the perspective of impurity control, and ALD is advantageous from the perspective of nanostructure. As a result, it is expected that PVD-Co(W) and ALD-Co(W) will have similar levels of resistivity due to these two factors (impurities and nanostructures) cancelling each other out.

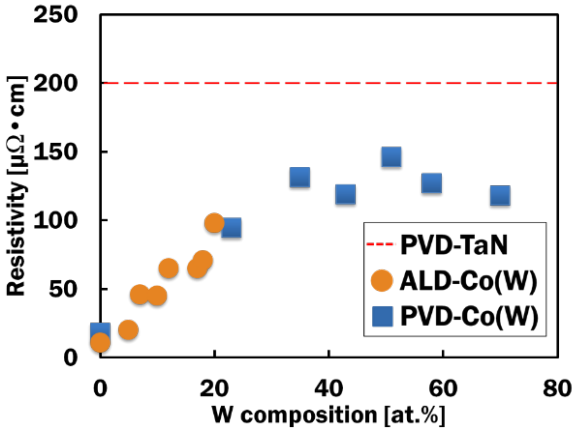

Fig 12. The resistivity of Co(W) films formed by PVD, ALD, and PVD-TaN.

2.4 Adhesion properties of thinned PVD-Co(W) films

2.4.1 Sample preparation and measurement process for adhesion properties

Figure 13 describes the basic principle for measuring adhesion, the contact angle, and the sample structure used at that time. The Young-Dupre equation is used to evaluate adhesion. The surface Cu condensed by annealing forms a contact angle by the influence of the substrate. The smaller the contact angle is, the higher the adhesion. All deposition conditions are the same as those used in chapter 2.1.1. Only the deposition time was adjusted to make the thickness of the Cu film 20 nm and the thickness of the Co(W) film 2 and 3 nm.

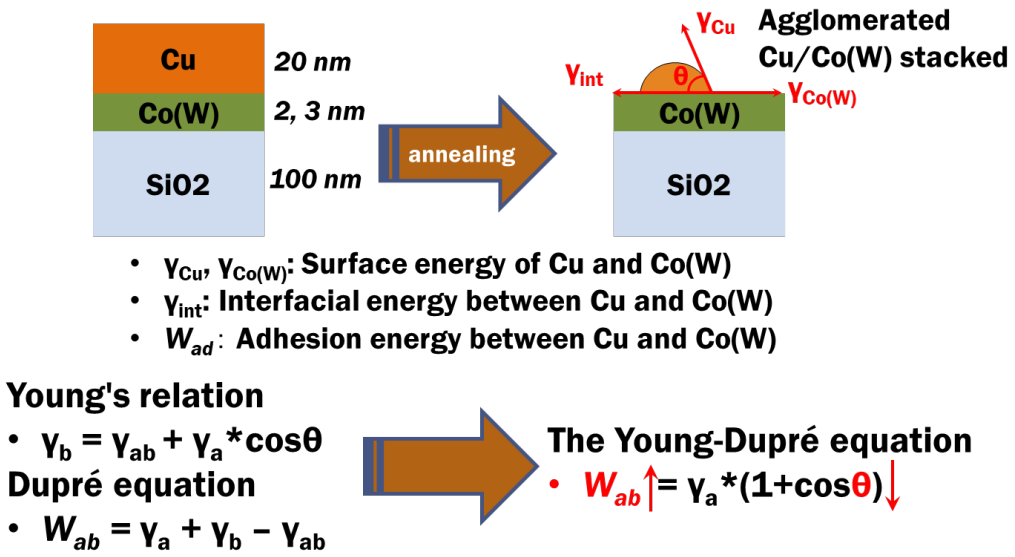

Fig 13. Basic principle and sample structure for measuring adhesion: contact angle.

The measurement process for adhesion evaluation is as follows. First of all, the most important thing is that the PVD-Co(W) layer should not be crystallized by annealing. In order to confirm this, it was checked whether or not it was crystallized using XRD with Cu Kα X-ray. Annealing conditions were the same as in chapter 2.1.2, and annealed for 400, 500, 600, 700°C - 120 min. After annealing, the cross section of the sample was observed with an SEM to find the condensed position as shown in figure 14. The contact angle of the condensed position at 30 locations was measured.

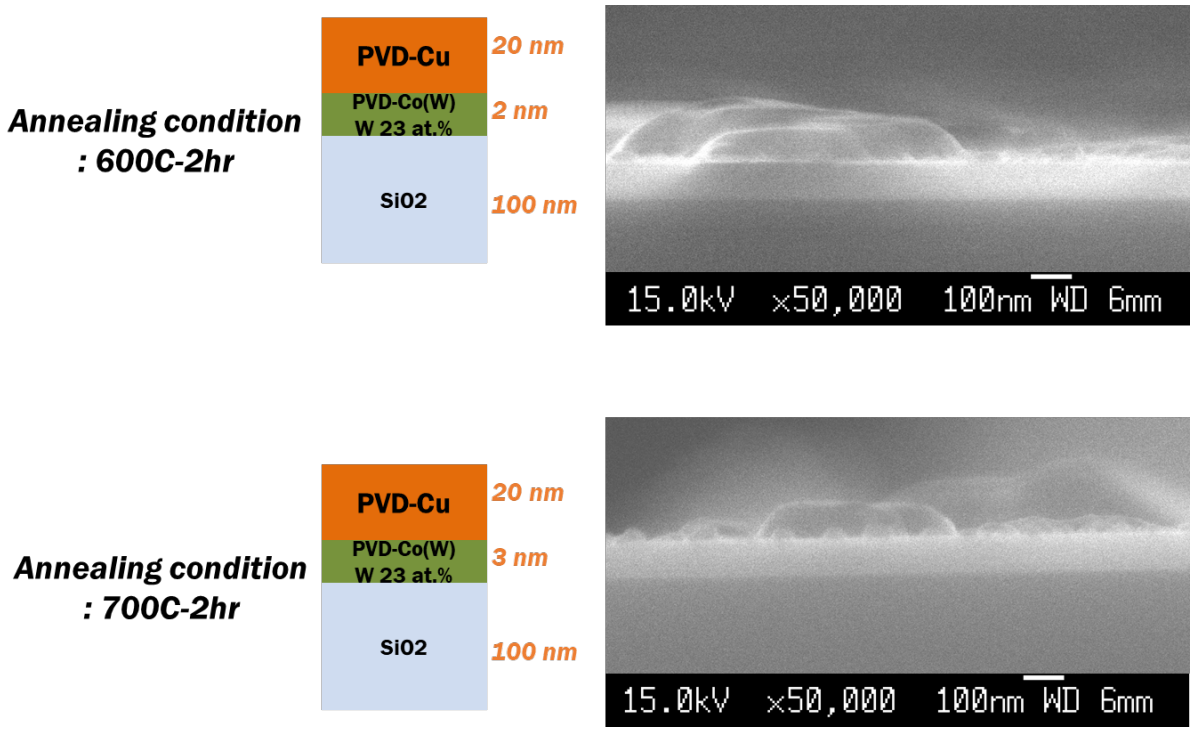

Fig 14. The cross section of the sample with an SEM to find the condensed position.

2.4.2 Evaluation of adhesion properties from the result of contact angle measurement

The contact angle is plotted in the form of a cumulative distribution to investigate the relationship between adhesion and W concentration as shown in figure 15. First, at 400°C and 500°C, condensation of Cu did not occur. In the previous adhesion study using ALD-Co(W), condensation of Cu had already occurred at 400°C [47]. This means that the absolute adhesion of PVD-Co(W) is better than ALD-Co(W). The change in adhesion according to the change in the W concentration is also examined. In 2 and 3-nm-thick PVD-Co(W), the dependence on the W concentration is not large, but it can be seen that the contact angle increases as the W concentration increases. Therefore, as the W concentration increases, the adhesion is expected to decrease. Since W has a bcc crystal structure, it is expected that lattice mismatch with Cu of the fcc crystal structure is large. Because of this difference, the W concentration and adhesion properties tend to be inversely proportional.

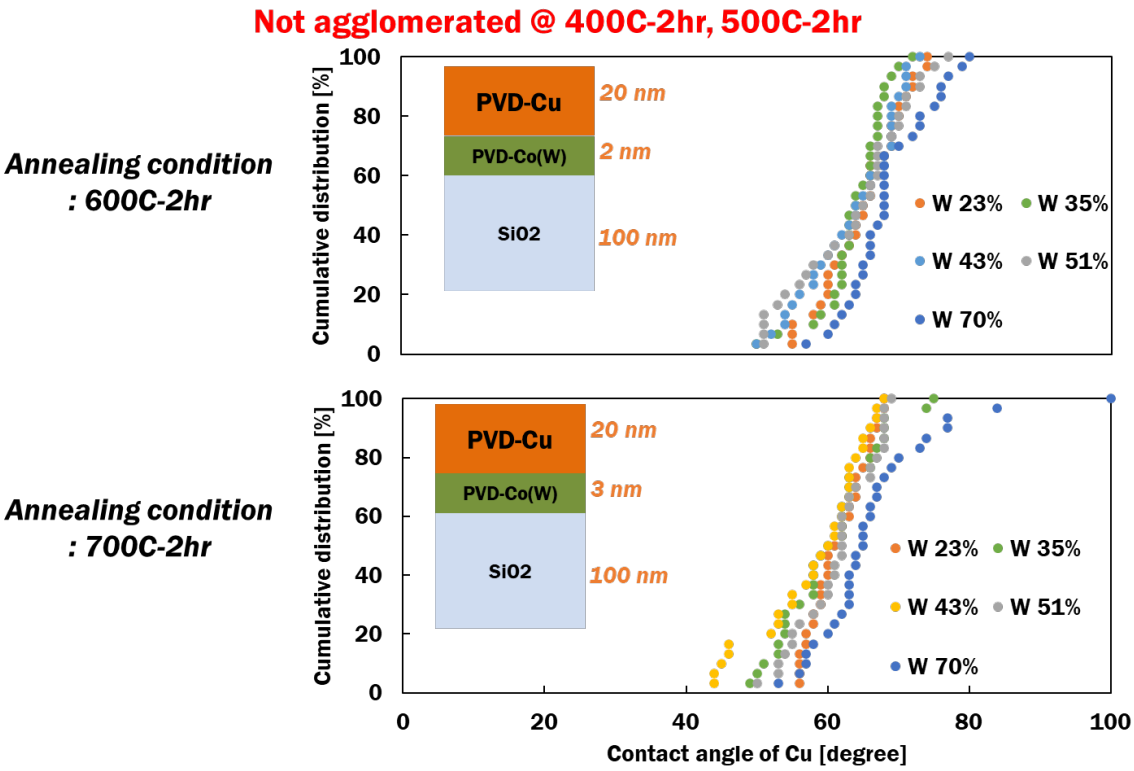

Fig 15. Cumulative distribution of contact angle with PVD-Co(W).

A comparison with the previously studied ALD-Co(W) is also performed. In figure 16, contact angle result of PVD-Co(W) with W 23 at. % is plotted with the contact angle result of ALD-Co(W) [47]. Looking at the results of ALD-Co(W), the contact angle increases as the W concentration increases, indicating a decrease in adhesion properties. Therefore, the W concentration and adhesion of ALD-Co(W) clearly tend to be inversely proportional. Next, for the same W 23 at. %, the average contact angle of ALD-Co (W) is 59°. This is slightly smaller than the average contact angle of PVD-Co(W) of 65°. In other words, if the W concentration is the same, it means that ALD-Co(W) has slightly better adhesion than PVD-Co(W). This is because the surface energy of 10-nm-thick ALD-Co(W) is larger than that of 2-nm-thick PVD-Co(W). As the surface energy of Co(W) increases, the adhesion increase. In general, there may be a trace quantity of impurities or defects present at the interface as a cause of the increase in surface energy.

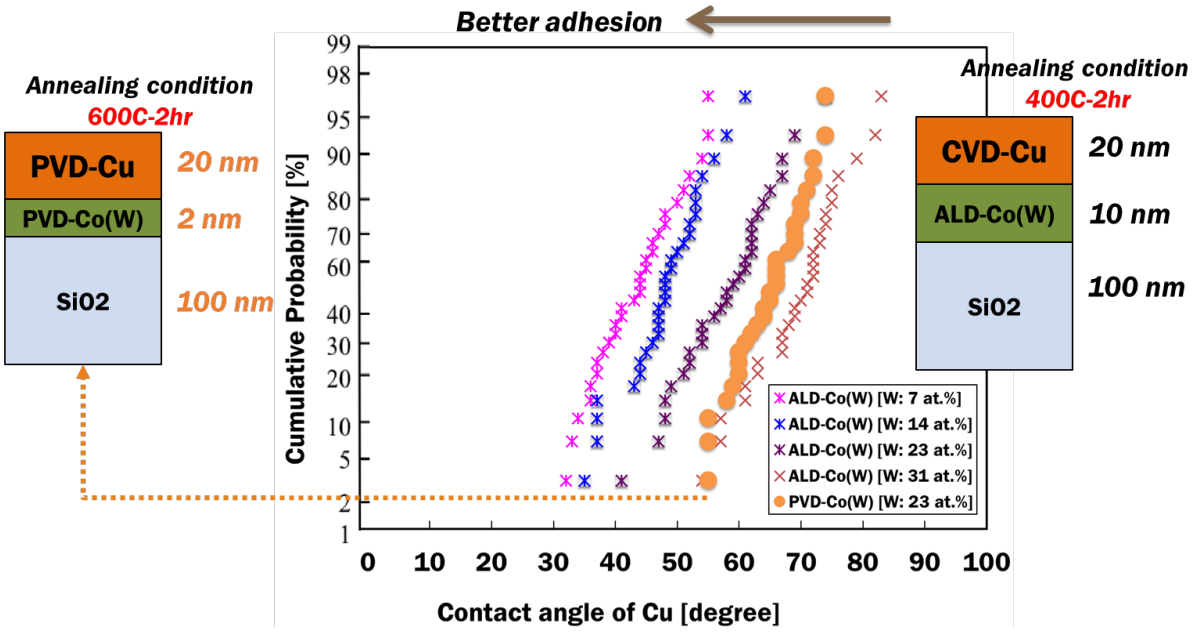

Fig 16. A comparison with the previously studied ALD-Co(W) [47].

2.5 Summary of the three properties

Figure 17 summarizes the above results in one graph, and through this, the optimum W concentration of the PVD-Co(W) single layer can be obtained (W 43 at. %). Figure 17(a) shows the adhesion of Cu according to the W concentration when 2-nm-thick PVD-Co(W) was annealed at 600°C. Above W 43 at. %, the average contact angle tends to slightly increase, but the change is not large, so it is considered that the adhesion is not significantly affected by the W concentration. Figure 17(b) shows the change in resistivity according to the change in W composition. As the W concentration increased, the resistivity increased slightly overall, but the increase rate was not so large. In particular, in the case of W 35 at. % or more, the increase in resistivity is small despite the increase in W concentration. Figure 17(c) shows the change in barrier properties according to the change in W composition. The result of W 43 at. % has the smallest D at 500°C and the E_a is the largest. From the viewpoint of crystallinity, the crystal structure changes from the partially crystallized structure to the amorphous-like structure starting at W 43 at. %. Summarizing the above results, it can be concluded that the optimum W concentration is 43 at. %.

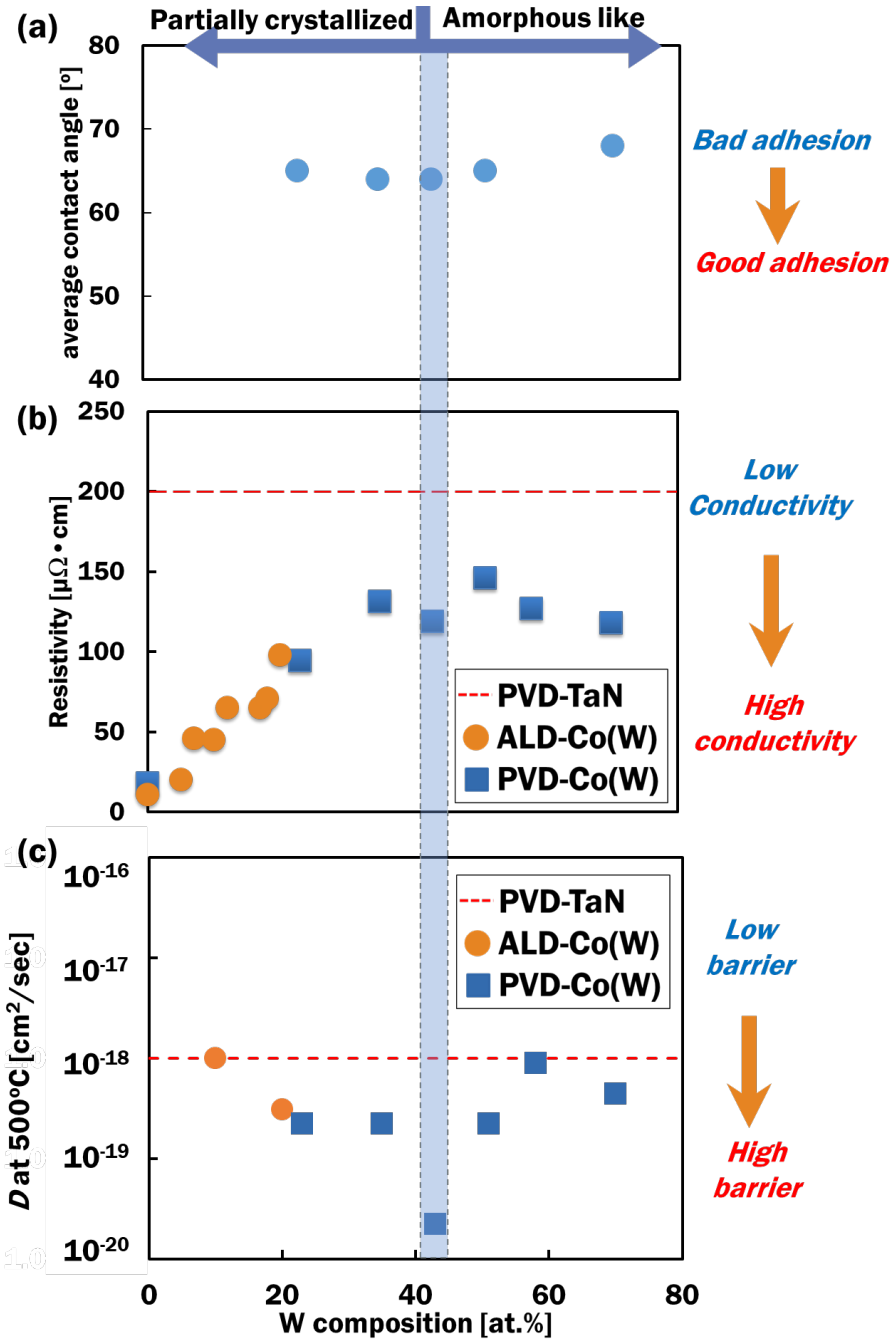

Fig 17. Summary of the three properties.

2.6 Conclusion

The significance of this chapter is the possibility of quantitative evaluation of barrier properties. As explained in Chapter 1, most of the barrier properties in the field of Cu interconnects are qualitative evaluations. In this chapter, using the depth profile method first proposed by Shimizu et al., D of Cu in 20-nm-thick PVD-Co(W) is obtained from the concentration profile and even quantitative evaluation is also completed. At this time, in order to avoid the knock-on effect during XPS analysis, the back-side XPS depth profile method was applied for the first time to obtain the correct D. For 20-nm-thick PVD-Co(W) having six different W concentration, the barrier properties, crystallinity, and electrical properties were investigated. The adhesion was additionally discussed. To evaluate adhesion, the contact angle of the cross-sectional image of SEM was used. The contact angle measured for the evaluation of adhesion was summarized in the form of cumulative distribution. From the result, the dependence of the adhesion on the change of the W concentration was investigated. The excellent adhesion of PVD-Co(W) was confirmed through comparison with the results of ALD-Co(W). Summarizing the above results, the optimal composition of the barrier layer was investigated. The diffusion mechanism was predicted from the magnitude of E_a, which is substitutional diffusion (vacancy diffusion). It is reasonable because all of my Co(W) films have amorphous-like structure as confirmed using structural analysis by XRD and TEM, and kinetic analysis using D_0 and E_a. In addition, use of PVD-Co(W) single liner/barrier layer ensures more cross-sectional area for Cu in the interconnect architecture rather than use of the conventional double layered structure. Thus, PVD-Co(W) single liner/barrier layers are promising alternatives to traditional PVD-Ta/TaN as liner/barriers, and are competitive with ALD-Co(W).

Quantitative evaluations will be very useful for further evaluation of Cu diffusion barrier properties. In the future, 20-nm-thick PVD-Co(W) will be made thinner, to 1 nm, which will be suitable for actual Cu interconnects. This underlines the importance of evaluating Cu diffusion barrier properties based on D. The next task is to develop a new evaluation method that can quantitatively evaluate the thinned barrier layer, which is the limit of the depth profile method.

Reference

1) H. Shimizu, A. Kumamoto, K. Shima, Y. Kobayashi, T. Momose, T. Nogami and Y. Shimogaki, ECS J. Solid State Sci. Technol. **2** [11], P471 (2013).

2) H. Shimizu, K. Shima, Y. Suzuki, T. Momose and Y. Shimogaki, J. Mater. Chem. C **3**, 2500 (2015).

3) H. Shimizu, K. Sakoda, T. Momose and Y. Shimogaki, Jpn. J. Appl. Phys. **51** [5 PART 2], 1 (2012).

4) H. Shimizu, K. Sakoda and Y. Shimogaki, Microelectron. Eng. **106**, 91 (2013).

5) K. A. Jackson, *Kinetic Processes: Crystal Growth, Diffusion, and Phase Transitions in Materials, 2nd Edition | Wiley* (2010).

6) A. Taylor, J. Chem. Technol. Biotechnol. **53** [2], 215 (2007).

7) J. Imahori, T. Oku and M. Murakami, Thin Solid Films **301** [1–2], 142 (1997).

8) k. vieregge and d, gupta, in a, crowson and e.s. chen (eds.), Miner. Met. Mater. Soc. 231 (1991).

9) M. Moriyama, T. Kawazoe, M. Tanaka and M. Murakami, Thin Solid Films **416** [1–2], 136 (2002).

10) T. Oku, E. Kawakami, M. Uekubo, K. Takahiro, S. Yamaguchi and M. Murakami, Appl. Surf. Sci. **99** [4], 265 (1996).

11) G. P. Tiwari, R. S. Mehrotra and Y. Iijima, in *Diffusion Processes in Advanced Technological Materials* (Springer Berlin Heidelberg, 2005) pp. 69.

12) K. Holloway, P. M. Fryer, C. Cabral, J. M. E. Harper, P. J. Bailey and K. H. Kelleher, J. Appl. Phys. **71** [11], 5433 (1992).

13) M. Mercier, S. Weber, A. Jacques, H. Hirabayashi, H. Ohkawa and M. Kinoshita, Defect Diffus. Forum **143**–**147**, 1285 (1997).

14) S. Asgary, M. R. Hantehzadeh, M. Ghoranneviss and A. Boochani, Appl. Phys. A Mater. Sci. Process. **122** [5], 1 (2016).

15) H. Mori, J. Imahori, T. Oku and M. Murakami, in *Fourth international workshop on stress induced phenomena in metallization* (AIP Publishing, 2009) Vol. 418 pp. 475.

16) M. Uekubo, T. Oku, K. Nii, M. Murakami, K. Takahiro, S. Yamaguchi, T. Nakano and T. Ohta, Thin

Solid Films **286** [1–2], 170 (1996).

17) C. K. Hu, L. Gignac, E. Liniger, B. Herbst, D. L. Rath, S. T. Chen, S. Kaldor, A. Simon and W. T. Tseng, Appl. Phys. Lett. **83** [5], 869 (2003).

18) A. Kohn, M. Eizenberg and Y. Shacham-Diamand, J. Appl. Phys. **94** [5], 3015 (2003).

19) J. R. Lloyd, M. W. Lane and E. G. Liniger, IEEE Int. Integr. Reliab. Work. Final Rep. **2002-Janua** [3], 32 (2002).

20) C. K. Hu, R. Rosenberg and K. Y. Lee, Appl. Phys. Lett. **74** [20], 2945 (1999).

21) G. Erdélyi, G. Langer, J. Nyéki, L. Kövér, C. Tomastik, W. S. M. Werner, A. Csik, H. Stoeri and D. L. Beke, in *Thin Solid Films* (Elsevier, 2004) Vol. 459 pp. 303.

22) J. P. Gambino, Proc. Int. Symp. Phys. Fail. Anal. Integr. Circuits, IPFA [DOI:10.1109/IPFA.2010.5532242].

23) L. B. Henderson and J. G. Ekerdt, Thin Solid Films **517** [5], 1645 (2009).

24) J. Pelleg and G. Sade, J. Appl. Phys. **91** [9], 6099 (2002).

25) Y. Shimooka, T. Iijima, S. Nakamura and K. Suguro, Japanese J. Appl. Physics, Part 1 Regul. Pap. Short Notes Rev. Pap. **36** [3 SUPPL. B], 1589 (1997).

26) C. M. Tan and A. Roy, *Mater. Sci. Eng. R Reports*, 2007, 58, 1–75.

27) J. Nabayan and J. Washburn, Philos. Mag. **26** [5], 1179 (1972).

28) S. P. Murarka and S. W. Hymes, Crit. Rev. Solid State Mater. Sci. **20** [2], 87 (1995).

29) T. K. Tsai, S. S. Wu, C. S. Hsu and J. S. Fang, Thin Solid Films **519** [15], 4958 (2011).

30) A. Kohn, M. Eizenberg, Y. Shacham-Diamand and Y. Sverdlov, *Mater. Sci. Eng. A*, 2001, 302, 18–25.

31) J. Gambino, J. Wynne, J. Gill, S. Mongeon, D. Meatyard, B. Lee, H. Bamnolker, L. Hall, N. Li, M. Hernandez, P. Little, M. Hamed, I. Ivanov and C. L. Gan, Microelectron. Eng. **83** [11–12], 2059 (2006).

32) S. M. S. I. Dulal, H. J. Yun, C. B. Shin and C. K. Kim, Appl. Surf. Sci. **255**, 5795 (2009).

33) T. Itabashi, H. Nakano and H. Akahoshi, Proc. IEEE 2002 Int. Interconnect Technol. Conf. IITC 2002 285 (2002).

34) A. Kohn, M. Eizenberg, Y. Shacham-Diamand, B. Israel and Y. Sverdlov, Microelectron. Eng. **55** [1–4], 297 (2001).

35) H. Nakano, T. Itabashi and H. Akahoshi, J. Electrochem. Soc. **152** [3], C163 (2005).

36) S. M. S. I. Dulal, T. H. Kim, H. Rhee, J. Y. Sung and C. K. Kim, J. Alloys Compd. **467** [1–2], 370 (2009).

37) Y. M. Namkoung, H. M. Lee, Y. S. Son, K. Lee and C. K. Kim, Korean J. Chem. Eng. **27** [5], 1596 (2010).

38) A. Kohn, M. Eizenberg and Y. Shacham-Diamand, J. Appl. Phys. **92** [9], 5508 (2002).

39) H. Einati, V. Bogush, Y. Sverdlov, Y. Rosenberg and Y. Shacham-Diamand, Microelectron. Eng. **82** [3-4 SPEC. ISS.], 623 (2005).

40) E. Olson, *PARTICLE SHAPE FACTORS AND THEIR USE IN IMAGE ANALYSIS-PART 1: THEORY*.

41) F. Faupel, W. Frank, M. P. Macht, H. Mehrer, V. Naundorf, K. Rätzke, H. R. Schober, S. K. Sharma and H. Teichler, *Rev. Mod. Phys.*, 2003, 75, 237–280.

42) V. Naundorf, M. P. Macht, A. S. Bakai and N. Lazarev, J. Non. Cryst. Solids **224** [2], 122 (1998).

43) V. Naundorf, M.-P. Macht, A. S. Bakai and N. Lazarev, *The pre-factor D0 of the diusion coefficient in amorphous alloys and grain boundaries*.

44) S. K. Sharma, M. P. MacHt and V. Naundorf, Phys. Rev. B **49** [10], 6655 (1994).

45) S. K. Sharma, M. P. Macht and V. Naundorf, Defect Diffus. Forum **95**–**98**, 1145 (1993).

46) X. Sun, E. Kolawa, J. S. Chen, J. S. Reid and M. A. Nicolet, Thin Solid Films **236** [1–2], 347 (1993).

47) K. Shima, H. Shimizu, T. Momose and Y. Shimogaki, ECS J. Solid State Sci. Technol. **4** [2], P20 (2014).

Chapter 3

Construction of a quantitative evaluation method of barrier properties for thinned films

In the previous chapter, the quantitative evaluation of the barrier properties of Co(W) using the depth profile method has been completed. However, depth profile method is difficult to apply to ultra-thin films such as 1 or 2 nm. This is because 1 or 2 nm are too thin to obtain a concentration profile. Therefore, it is essential to develop a method capable of quantitative evaluation for ultra-thin films. This chapter deals with the process of establishing a quantitative evaluation method for such a thin film. First of all, the contents of the attempted quantitative evaluation using atom probe tomography (APT) are dealt with. Then, the reason why the APT measurement failed at that time is considered, and then the results of the modified time-lag method using wavelength dispersive X-ray fluorescence (WDXRF) and inductively coupled plasma-optical emission spectrometry (ICP-OES) are introduced. In this chapter, the barrier properties of PVD-Co(W) were quantitatively evaluated using the modified time-lag method.

A 20-nm-thick barrier layer and a 1-nm-thick barrier layer are different. Although only the growth rate of thin film deposition is different, the state of the 1-nm-thick barrier layer and the state of the 20-nm-thick barrier layer will have other properties besides the thickness. In particular, since the initial stage of thin film growth is greatly influenced by the substrate, the crystal structure, the number of defects, and the type of defects of the 1-nm-thick barrier layer will be different from those of the 20-nm-thick barrier layer. Therefore, it is meaningful to compare the barrier properties of the 1-nm-thick barrier layer obtained using the method established in this chapter with the barrier properties of the 20-nm-thick barrier layer. Through that comparison, first of all, it will be possible to know whether the barrier properties have changed. In addition, it is possible to discuss the cause of the barrier properties when the barrier layer becomes thinner. Therefore, establishing a quantitative evaluation method for thinned barrier layer is important in itself, but it is also of great help in studying the change in barrier properties according to the growth of the thin film.

3.1 Challenges for the quantitative evaluation of ultra-thin Co(W) barrier for Cu diffusion

For the thinned barrier layer, quantitative evaluation using the concentration profile in the barrier layer is no longer possible. So I used a method to measure the number of trace Cu atoms diffused across the barrier layer to the opposite side. Through this method, a quantitative evaluation of the barrier properties of the thinned barrier layer was performed. In order to accurately measure the number of Cu atoms diffused through the barrier layer, it was first decided to use atom probe tomography (APT; LEAP4000X HR; CAMECA). In general, transmission electron microscopy (TEM) analysis is widely used to visualize the cause of phenomena occurring inside a thin film such as a grain boundary. However, since there is a limit to the minimum size of the electron-beam to be measured, it is difficult to accurately analyze the composition of the atoms diffused in the thin film. APT is very good in terms of this spatial resolution. In the APT measurement, an electric field is applied to a probe-type sample to remove ionized atoms one by one, and quantitative analysis is performed at ppm level based on the mass of the atom. In addition, the position of the atom can be reproduced as a three-dimensional image. Since the APT analysis method can be analyzed at the atomic level, it is a very useful method for studying the distribution of diffused trace atoms.

APT measurements have the following advantages. (1) three-dimensional analysis is possible. APT measurements allow direct observation of three-dimensional images of trace Cu atoms at the atomic level. Through this, the three-dimensional structure and spatial distribution of diffused Cu atoms at a level that has not been seen until now can be identified. In addition, the size and distribution of defects such as grain boundaries formed in the thin film can be confirmed with a three-dimensional image. Integrating these three-dimensional images with the results of the diffusion coefficient will allow for a more in-depth discussion on the diffusion mechanism. (2) Quantitative analysis at ppm level is possible with sub-nm level spatial resolution. In terms of spatial resolution, APT measurements can distinguish atoms at the sub-nm level and has a detection limit at the ppm level, so it is very excellent for trace analysis. (3) All atoms including hydrogen (H_2) and helium (He) can be distinguished.

On the other hand, the limitations of APT measurements are as follows. (1) Measurement and evaluation are possible only for very localized areas. For this reason, it is not clear whether the measurement result represents the characteristics of the entire thin film. Therefore, it is necessary to increase the precision through several measurements. (2) Because control of field evaporation is very difficult, distortion may occur between the actual sample and the three-dimensional image reconstructed by the computer. (3) Preliminary preparation for measurement is very difficult. For APT measurements, a flat sample should be made into a needle shape with a diameter of several tens of nanometer using a focused ion beam (FIB).

Several studies using APT measurements have been reported [1)–7)]. Among them, Shima et al. developed an excellent Cu diffusion barrier system with a combination of a Cu(Mn) seed layer and a Co(W) single layer [1)]. At this time, APT measurements were used to prove the superiority of barrier properties. They succeeded in visualizing the distribution of W and Mn with sub-nm resolution using APT measurements. Figure 1 shows their measurement results using APT. It can be seen that W is segregated to the grain boundary of Co, preventing diffusion of Cu through the grain boundary. It has been found that Mn diffuses from the Cu(Mn) layer to the Co(W) layer and is selectively segregated with W at the Co(W) grain boundary to enhance the barrier properties of the Co(W) layer.

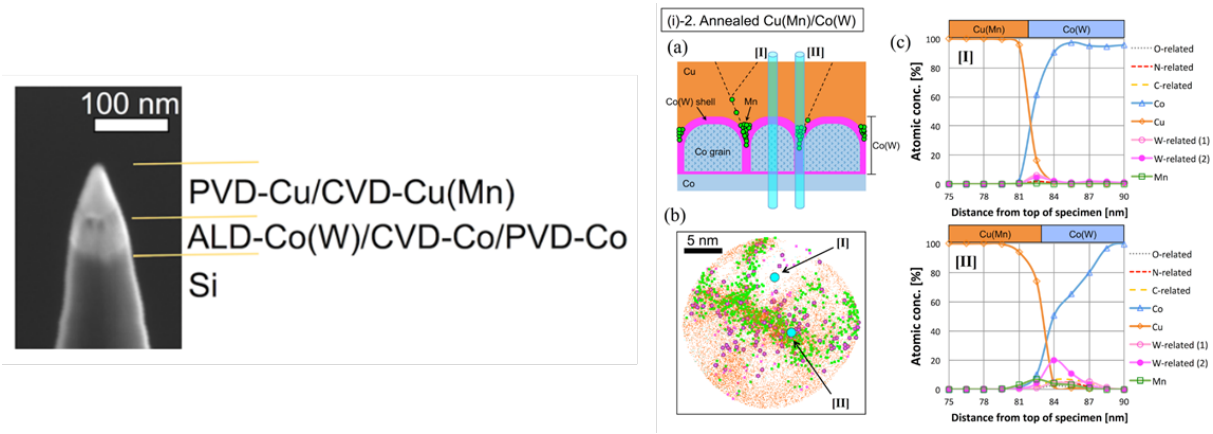

Fig 1. Visualizing the distribution of W and Mn with sub-nm resolution using APT [1)].

Now, I will explain the results I have obtained using APT. I first measured the 20-nm-thick PVD-

Co(W) using APT. The sample used here is the same as the sample used in Chapter 2. The biggest difference from the studies of Shima et al. is that in my study there is a SiO_2 layer between the Co(W) layer and Si wafer. The reason for experimenting with this structure is that low-k materials such as SiO_2 are required in actual Cu interconnects. Figure 2 shows the sample structure and APT results at that time. During the APT measurement, fracture occurred in the SiO_2 region and the measurement failed in the middle. The main cause of the fracture is the pulsed electric field applied during APT measurement. A magnetic field is created by the pulsed electric field, which stresses the sample, resulting in fracture. It is assumed that this is because the field evaporation efficiency in each element is different. In order to prevent fractures during the measurement, it is necessary to reduce the SiO_2 region that is highly stressed by the electric field.

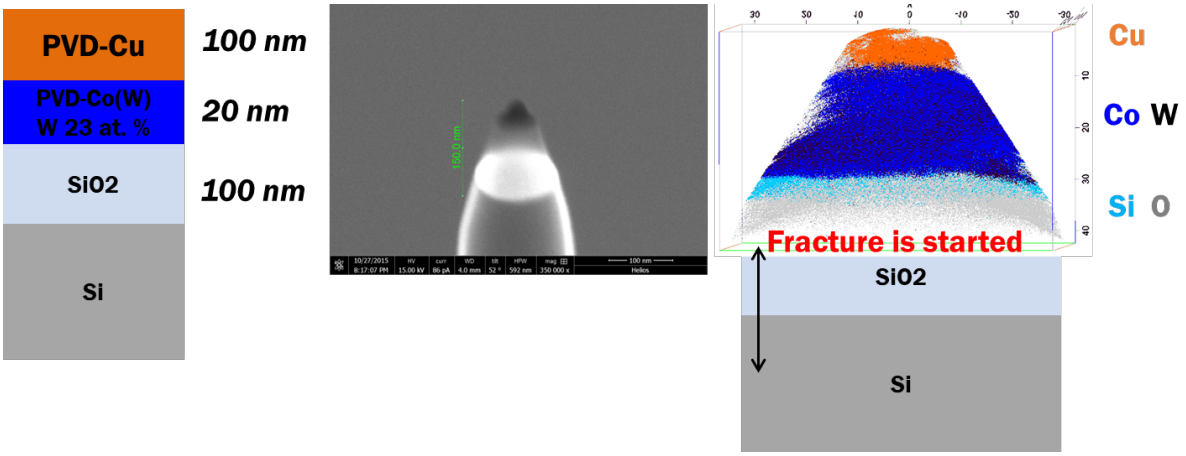

Fig 2. Sample structure and APT results.

There are several factors that influence the APT measurement. Among them, the diameter of the sample, the measurement temperature, laser power, laser pulse frequency, and the wavelength of the laser can be considered as major factors. Table 1 summarizes the changes in various measurement conditions. Among the above-mentioned factors, it was confirmed that the fracture decreased when the laser power was increased, and the laser pulse frequency was decreased. Under the conditions of Table 1, when the laser power was 250 pJ and the laser pulse frequency was 100 kHz, the only APT measurement was possible to Si without fracture. However, at this time, almost no Co(W) and SiO_2 regions were detected. In particular, W and O

were not detected at all. This means that the area has micro-fractured. Still, there were many difficulties in optimizing the measurement conditions.

Table 1. The changes in various measurement conditions.

Sample	Annealing condition	Temp. [K]	Laser Power [pJ]	Laser pulse frequency [kHz]
W:23at.%	As-depo	50	70	160
	700C-25min	50	70	160
	As-depo	35	150	100
	As-depo	50	160	100
W:58at.%	As-depo	50	100	160
	700C-25min	50	100	160
	As-depo	50	250	100

Specimen size : 50–100 nm, Laser wavelength : 355 nm

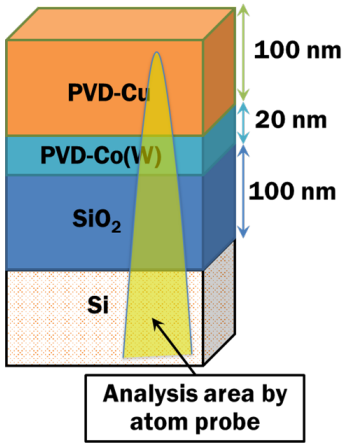

Figure 3 shows the structure and APT measurements result of [200-nm-thick Cu/1-nm-thick Co(W), W 70 at. %/1-nm-thick SiO_2/Si substrate]. As mentioned earlier, the SiO_2 layer was reduced to 1 nm to prevent the fracture caused by the electric field. As a result, APT measurement was successfully performed without fracture to the Si substrate. From this result, it can be seen that the thickness of SiO_2 has the greatest correlation with the occurrence of fracture. However, even before annealing, there was a phenomenon in which Co and W appeared to diffuse into the Si substrate. As a few possible reasons for this, it is thought that Co and W did diffuse through the side created while processing the sample into a needle shape by FIB process. As another reason, among the results of previous basic research, the barrier properties of the structure in which PVD-Co(W) is deposited on PVD-Cu have been evaluated. At that time, it was discovered that PVD-Cu penetrated PVD-Co(W) and spewed out to the surface during annealing. This means that PVD-Co(W) is severely affected by the substrate. Therefore, 100-nm-thick SiO_2 and 1-nm-thick SiO_2 have different surface

properties, as a result, the barrier properties did not appear at all in the PVD-Co(W) deposited thereon. So, diffusion may have occurred even before annealing, as shown in Figure 3. However, the above discussions are only speculation. From the results of the time-lag method to be described later, further discussion will be required.

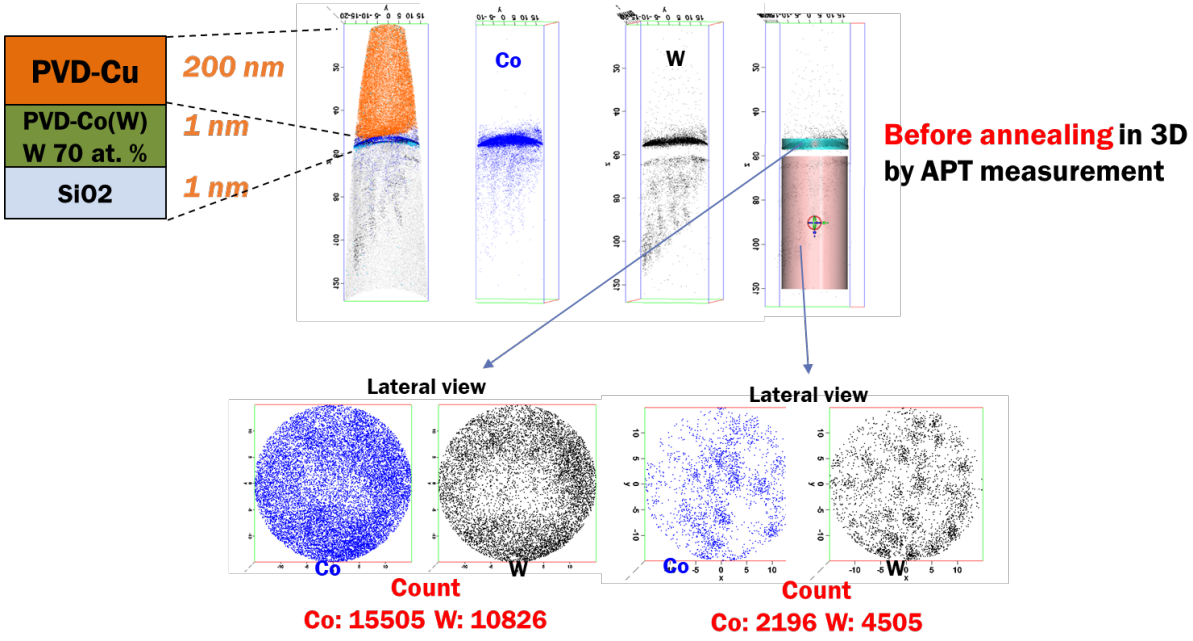

Fig 3. APT measurement result of [200nm Cu/1 nm Co(W), W 70 at. %/1nm SiO2/Si substrate].

3.2 The new way of quantitative evaluation for thinned films: modified time-lag method

In the chapter 3.1, quantitative evaluation using APT was challenged, but satisfactory results were not obtained. Here, the time-lag method used in the gas barrier field is applied to the Cu interconnects field to quantitatively evaluate the barrier properties of PVD-Co(W). Figure 4 shows the characteristics of the two evaluation methods (depth profile method vs. modified time-lag method). The depth profile method covered in Chapter 2 evaluated the barrier properties quantitatively by using the concentration profile of Cu diffused in the Co(W) barrier layer. However, since it is difficult to apply to an extremely thin barrier layer, a new modified time-lag method was used. Since the time-lag method measures the trace element reached the opposite side by passing through the barrier layer, theoretically, no matter how thin the barrier layer is, there is a no problem with the measurement. Thanks to its simplicity, the time-lag method can obtain *D* directly from experimental results. However, this time-lag method has not yet been applied to the Cu interconnects field. Therefore, if this method is successfully introduced into Cu interconnects field, the *D* of Cu in ultra-thin barrier layer such as 1 or 2 nm can be obtained. Therefore, this method is used for the first time for quantitative evaluation of barrier properties in the barrier layer of Cu interconnects.

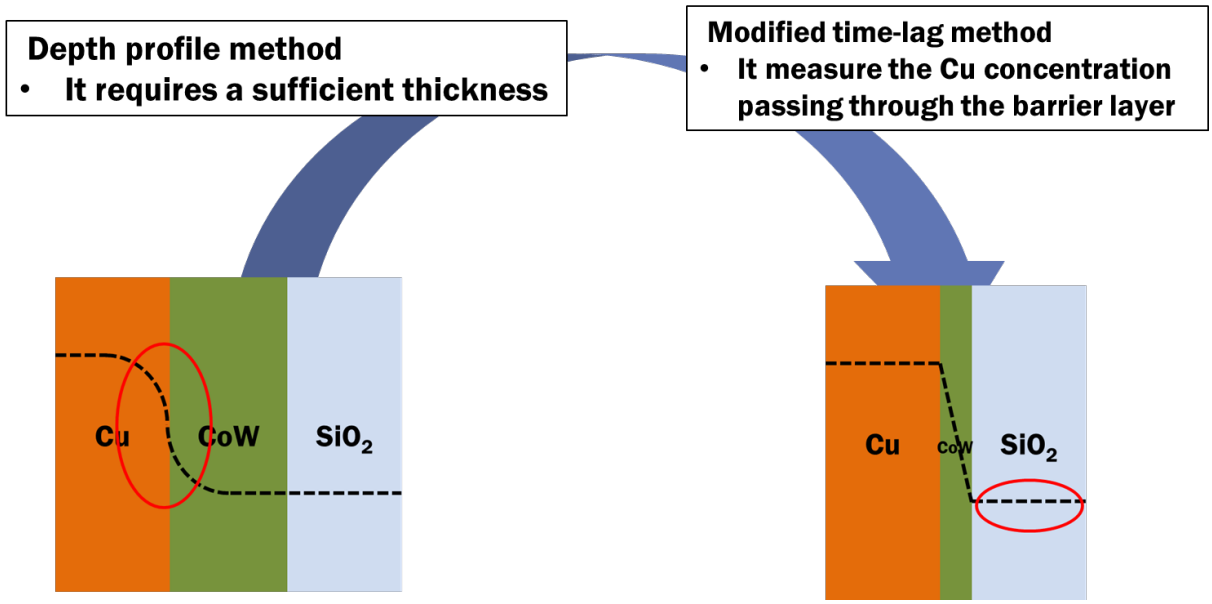

Fig 4. Two evaluation method (depth profile method and modified time-lag method).

3.2.1 Principle of time-lag method

The time-lag method was first designed by H. A. DAYNES et al. in 1920 to evaluate the diffusivity of gaseous H_2 in rubber membrane (i.e., barrier), and measured the time-evolution of H_2 concentration across the membrane [8]. Figure 5 shows the experimental equipment they used in the study and the measurement results at that time. The detailed configuration of the experimental equipment is as follows. (1) A hydrogen chamber that receives H_2 from the outside, (2) a rubber membrane that divides the H_2 chamber and the air chamber, (3) an air chamber that stores diffused H_2, and (4) a katharometer that measures the concentration of H_2. When the experiment begins, H_2 is introduced into the hydrogen chamber. Then, a trace quantity of H_2 diffuses into the air chamber through the rubber membrane. When H_2 enters the katharometer connected to the air chamber, it changes the temperature inside the katharometer. The concentration of diffused H_2 can be obtained from the change of resistance according to the temperature change of the katharometer. With the H_2 concentration measured in the air chamber as the y-axis and the measurement time (time starting when H_2 enters the hydrogen chamber) as the x-axis, a curve in the shape of the right side of Figure 5 can be obtained.

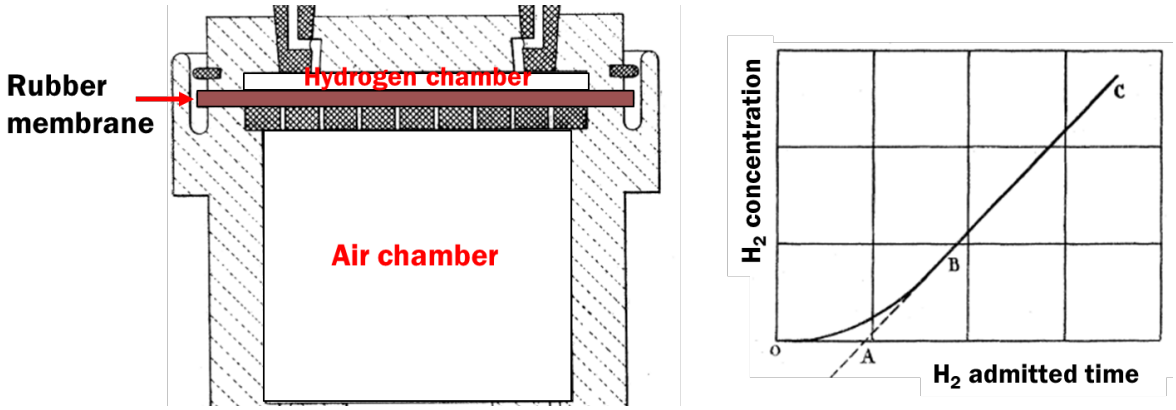

Fig 5. Experimental equipment of time-lag method for H_2 gas and its results [8].

Following the measurement, D is derived from the H_2 flux using Fick's second law, which was detailed elsewhere [8)9)10]. Note that derivation of D is possible without involving any complex procedures like fitting thanks to a simplicity of the time-lag method. Figure 6 shows a schematic relation between a total

quantity of the substance passing through the barrier per unit area (Q) and a measurement time (t) used in the time-lag method, which is in called the Q-t plot. After the measurement begins, Q keeps zero for a while, which is the time necessary for the substance to pass through the barrier. Then, Q starts to increase gradually due to passage of the substance, up to which it is in transient state. Afterwards, Q proportionally increases with time, at which it is in steady state. Thus, the slope denotes a flux of diffused substance passing through the barrier. The delay time to reach the steady state is called "time-lag". Note that, the time-lag is practically estimated by extrapolating the Q-t plot obtained experimentally in steady state, i.e., equivalent to the x-intercept. According to the analytical solution of the diffusion equation, relations between D and x-intercept or slope are given as, [10)]

$$(\text{x intercept, i.e. time-lag}) = \frac{L^2}{6D} \qquad (1),$$

$$(\text{slope, i.e. flux}) = \frac{DC_0}{L} \qquad (2),$$

where C_0 is the concentration of diffused substance at the upstream interface of the barrier, and L is a thickness of the barrier. D is, therefore, obtained by the time-lag and equation (1), since L is known in general prior to the measurement. Besides, D is also obtained by the slope and equation (2), since C_0 is the experimental condition. Therefore, D is obtained by both of the slope (flux) and the x-intercept (time-lag). In the conventional time-lag method, D of water vapor in polymer membrane, for example, was practically obtained only by equation (1), not by equation (2); however, D by reported x-intercept and D calculated by us from the reported slope were almost identical with an error of 5%, suggesting both are feasible [10)].

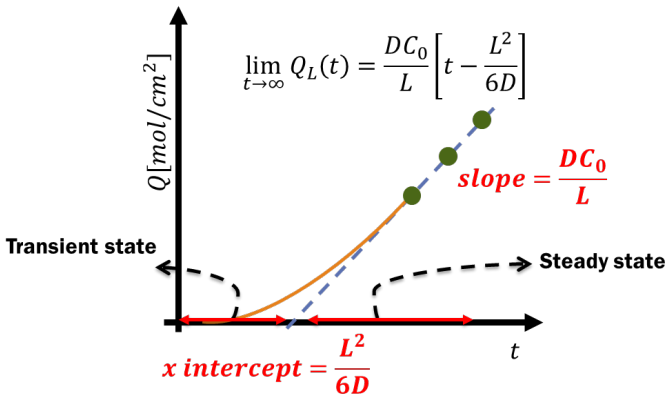

Figure 6. Schematic relation between a total quantity of the substance passing through the barrier per unit area (Q) and an annealing time (t) used in the time-lag method (Q-t plot).

3.2.2 Guideline to modify the time-lag method for Cu Interconnects

Starting with H. A. DAYNES et al., further studies related to the time-lag method were conducted by many researchers. A number of studies have been conducted to determine the permeability and diffusivity of a barrier using the time-lag method [8)–15)]. The conventional time-lag method has been successfully demonstrated for various barrier materials and diffused substances. However, to apply the time-lag method to measure *D* of Cu in the nanometer-thick leak-tight barrier, many modifications are necessary due to differences in sample structures, dimensions, and materials. Roughly speaking, the conventional method was applied to measure *D* of gas in millimeter-thick relatively leaky polymer/rubber membrane (sometimes covered with an inorganic film to enhance barrier property). For example, a polyethylene terephthalate (PET) membrane covered by a silicon nitride (SiN_x) film or an acrylate-polymer/AlO_x film or an organic/inorganic multilayer (i.e. 7-octenyl trichlorosilane/TiO_2) against water vapor diffusion[10)13)16)]. Resulting *D* thereof was typically in the order of 10^{-5}-10^{-13} cm^2/s at room temperature. In the meantime, we want to measure *D* of Cu atoms in the several-nanometer-thick leak-tight barrier formed on the SiO_2/Si substrate, whose *D* is expected to be in the order of 10^{-16}-10^{-19} cm^2/s at 500-700 °C. Cross-sectional schematic of the sample structures measured by the conventional and our methods are sketched in Figure 7. Their differences were summarized in Table 2, and the modification guidelines were explained in the following. Note that the practical solution on the basis of these modification guidelines will be explained in chapter 3.2.3.

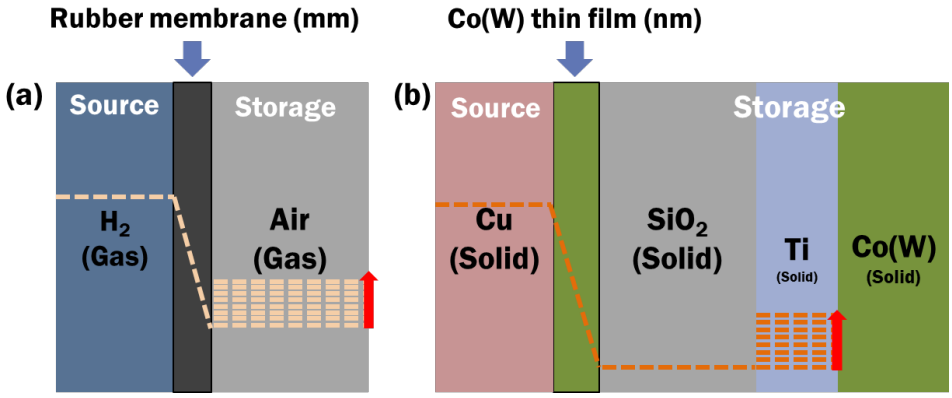

Figure 7. Schematic sample structures measured by (a) the conventional method for gas diffusion and (b) the modified method for solid diffusion.

Table 2. Differences of the conventional and modified time-lag method.

No.	Items	Conventional	Modified
(1)	**Acceleration testing by annealing**	Not required (at room temperature)	Required
(2)	**Sample structure**		
	Source of diffused substance	Gas (flowing gas)	Solid (metal film on the barrier)
	Storage	Gas (chamber filled with air 101325 Pa)	Solid (film under the barrier)
(3)	**Measurement**		
	Timing of measurement	in situ	ex situ (after the annealing)
	Detection method	Thermal conductivity method (abundance of diffused substances)	Trace analytical method
	Removal of source before detection	Not required	Required (difficulty in selective detection of substances in storage)

(1) Acceleration testing by annealing

To discuss the need for annealing, typical flux of the substance in the conventional method was calculated and was compared with that expected in the modified method. For both, reported D, C_0, and L was substituted into Eq. 2, in which D of Cu in the ultra-thin barrier has not been evaluated yet, and thus that in 20-nm-thick Co(W) film was used alternatively. All calculations were conducted at room temperature. For

the conventional method, D was typically 10^{-5}-10^{-8} cm^2/s, C_0 was 10^{-4}-10^{-8} mol/cm^3, and L was 10^{-1}-10^{-3} cm. The resulting flux showed relatively large values ranging 10^{-9}-10^{-12} $mol/cm^2/s$ [8)15)], suggesting ease to obtain sufficient Q. Therefore, the conventional time-lag method was conducted at room temperature. On the other hand, almost no flux and resulting Q at room temperature is expected for the ultra-thin barrier targeted herein. It is because D to be measured by the modified method was predicted to be extremely small as 10^{-31}-10^{-44} cm^2/s at room temperature based on D of Cu in the 20-nm-thick Co(W) films. In addition, C_0 of Cu in Co(W) is nearly zero according to the phase diagram [17)]. Therefore, the modified method requires acceleration testing by annealing to obtain sufficient Q.

(2) Sample structure

In the conventional method, source of the diffused substance is gas, which is spatially uniform and unchanged with time in the upstream of the barrier. On the other hand, in the modified method, source is a Cu film formed on the barrier, in which continuous supply with time can be secured as far as the continuous film morphology remains during the annealing. However, a metal thin film formed on the heterogeneous underlayer is likely to agglomerate, turning into a discontinuous film and further into isolated grains, in which a source is not uniform on the entire barrier [18)]. Therefore, in order to apply the time-lag method to the solid-state diffusion, agglomeration of the source must be prevented, which is enabled by thick-enough film [18)19)].

Storage of the diffused substance also differed. In the conventional method, gaseous substances passing through the barrier is stored in a chamber equipped at a downstream interface of the barrier, which is filled with air. On the other hand, in the modified method, a solid thin film placed below the barrier works as the storage. In addition, since the barrier property is in general largely influenced by the nature of underlayer, it is important to employ the underlayer same with that of Cu interconnects for the modified method [20)–22)23)]. Hence, the sample should be a stacked structure composed of a source film, a barrier film, an underlayer film, and a storage film as sketched in figure 7(b). Attention should also be paid to capacity of the diffused substance in the storage film, which should be large enough compared with the total quantity of the diffused substance; otherwise, the storage is filled with the diffused substance soon after the start of

measurement, thereby reaching the equilibrium. Hence, material and thickness of the storage should be carefully determined based on the solubility of the diffused substance.

(3) Measurement

The timing of measurements is different for the conventional and modified methods. In the conventional method, a relatively large quantity of diffused substance in the gaseous state is rapidly diffused into the storage, so that a relatively high concentration of diffused substance is uniformly distributed in the storage. In particular, a high concentration of diffused substances is preferable for in situ measurement because they can be detected easily. The uniform distribution of diffused substance is also preferable for in situ measurement. As a result, in situ measurement became possible. On the other hand, since the modified method deals with diffusion in the solid state, the concentration of the diffused substance is much lower than that of the diffused substance in the conventional method. Also, since the storage is also in a solid state, the diffused substance is not uniformly distributed in the storage. Therefore, in situ measurement is difficult in the modified method. In general, in situ measurement of diffusion in the solid state is performed only in very special cases. For example, there are some special equipment that can make measurements during annealing (in situ study by TEM[24),25)] and XRD[26)]). However, there are few instruments that can determine the concentration by in situ measurement for diffusion in the solid state. Very rarely, there is a method to measure the concentration of diffused substance in situ from the sample surface using in situ XPS [25)]. However, in my sample structure, since the source of the diffused substance is at the most surface, it is impossible to measure the concentration of diffused substance through in situ measurement from the surface. If there is a measuring instrument that can measure the concentration of a sample in situ in a cross section with high spatial resolution, it may be possible to measure in situ. However, in reality, such measuring instrument does not currently exist. Therefore, ex situ measurement is inevitably necessary.

In the conventional method, since it is a gaseous diffusion, a uniform distribution of the diffused substance is expected in the storage. As a result, a thermal conductivity detector (TCD) was mainly used to detect the quantity of gaseous diffused substances [8)]. Note that the diffused gas is immediately mixed with

the air in the storage and thus averaged. The TCD is connected to the air chamber, and the inside of the TCD is composed of filaments. Before the diffusion experiment, the TCD is adjusted so that no current flows. When the gaseous diffused substance diffuses into the air chamber and diffuses to the TCD, the temperature inside the TCD decreases and the thermal conductivity of the TCD decreases. To compensate for this, a current will flow through the filament, raising the temperature inside the TCD. As a result, an increase in electrical resistance by the heated filament appears as an electrical signal through the TCD. The Q of diffused gas can be obtained from the area of this signal over time. As the lower detection limit of Q of the conventional method is about 10^{-7} mol/cm^2, which is suitable for allowing a relatively large quantity of diffusion [8]. On the other hand, in the modified method, a smaller Q of ppb level diffusion occurs than in the conventional method, so a measurement method with a lower detection limit is required. The modified method also needs to measure the Q of diffused substance in the solid state, but it is almost impossible to analyze the trace quantity at the ppb level in the solid state. Therefore, I measure the quantity of the diffused substance by dissolving the solid-state storage containing the diffused substance.

I tried to use a method to measure the quantity of a diffused substance from a surface. In this case, the source of the surface may interfere with the measurement of the quantity of the diffused substance. Therefore, removal of the source and barrier is necessary after annealing and before measurement, while the underlayer and storage that contain the diffused substance have to be remained. In the case of the conventional method, since the gaseous diffused substance is measured in situ, there is no need to remove the source. On the other hand, in the modified method, since the source is in a solid state, and the source and the storage in which the diffused substance is diffused are only a few nanometers apart, the source of the surface must first be removed for measurement. Accordingly, an etchant selectively removing the source and barrier is required. In addition, there is no direct way to measure the trace quantity of Q in the storage; therefore, the underlayer and storage that contain the Cu should be dissolved into some solution, and then Q in the solution should be measured by some trace analytical method. For this purpose, an etchant capable of selectively removing only the surface source is required.

3.2.3 Modified time-lag method for Cu interconnects

Based on the guidelines proposed in chapter 3.2.2, the time-lag method was modified as follows.

(1) Acceleration testing by annealing

In the modified method, annealing is mandatory and its condition should carefully be designed including temperature, time, and ambient gas, to ensure the sufficient Q. In particular, higher temperature and longer annealing time are required to obtain Q larger than the lower detection limit of trace analytical method to be used. In the meantime, crystal structure and crystallinity of the barrier should be maintained before/after annealing to appropriately measure *D* in the film, and thus annealing condition should not be harsh. It can be evaluated by X-ray diffraction (XRD) for relatively thicker film, while evaluation by transmission electron microscope (TEM) is mandatory for ultra-thin film. In summary, prior to the measurement, an optimal annealing condition range must be found considering such competing factors.

(2) Sample structure

The Cu film must maintain the continuous film morphology even after annealing. Although film thickness of the topmost Cu (source) should be determined by anticipating quantity of the Cu diffusion, it is typically extremely small, which is equivalent to a film with less than several nanometers in thickness (for example 0.27 nm in my case). As the Cu film is easily agglomerated by annealing, the film thickness must be determined to prevent agglomeration rather than the diffusion quantity. Agglomeration strongly depends on its film thickness; for example, a 5-nm-thick Cu film formed on a 100-nm-thick thermal SiO_2 turned into Cu islands in 15 min at 300°C, while a 50-nm-thick Cu film on the same underlayer preserved the film morphology even after 120-min annealing at 300°C [18]. Although it is also influenced by the lattice mismatch of the film and underlayer, generally speaking, thickness of the source Cu film greater than 100 nm can prevent the agglomeration. Therefore, in the modified time-lag method, the thickness of Cu layer was determined in 100 nm.

The modified time-lag method was applied only to the region with a steady state. For this, a sample

structure including the solid storage was designed as shown in figure 8. To avoid reaching equilibrium after steady state, 1000-nm-thick SiO_2/100-nm-thick Ti/150-nm-thick Co(W) structure provides sufficient capacity to dissolve all the trace quantity of Cu that have passed through the barrier layer so that the steady state can be maintained for a long time. 1000-nm-thick SiO_2 was used as the underlayer of Co(W). This SiO_2 is necessary to maintain the barrier properties of Co(W). Since Cu is rarely soluble in SiO_2, it cannot serve as Cu storage. In addition, since D of Cu in SiO_2 (9.3×10^{-12} cm^2/s at 700°C) is about 10^5 times larger than that in Co(W) (8.3×10^{-17} cm^2/s at 700°C), Cu passing through Co(W) will diffuse downwards rapidly in SiO_2[27]. Therefore, 100-nm-thick Ti was inserted underneath it to act as a Cu storage. According to the Cu-Ti phase diagram, Cu and Ti have eutectic systems. When a trace quantity of Cu is dissolved in pure Ti, they form a solid solution of $CuTi_2$ up to 0.33 Cu/(Cu+Ti) [28]. In addition, they also form as a solid solution of Cu_4Ti_3, Cu_3Ti_2, and Cu_4Ti [28]. Anyhow, Cu forms a compound with Ti, suggesting that Cu can be stored in Ti. Another 150-nm-thick Co(W) is placed beneath the storage, which is a preliminary barrier to prevent diffusion of Cu into the Si substrate even if Cu passes through Ti.

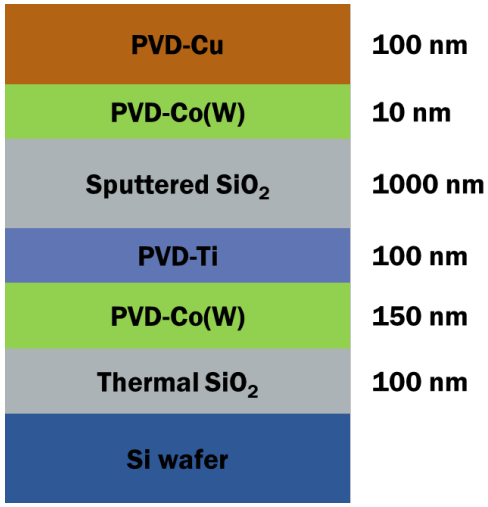

Fig 8. Sample structure for time-lag method.

(3) Measurement

In order to measure the Cu concentration in the 1000-nm-thick SiO_2/100-nm-thick Ti/150-nm-thick

Co(W) structure, it is necessary to etch the topmost 100-nm-thick Cu/9-nm-thick Co(W) structure. For this, $FeCl_3$ solution that dissolves both Cu and Co(W) was used [29]. Since this solution does not dissolve SiO_2, the etching stops on the SiO_2 film [29]. Following this etching, the 1000-nm-thick SiO_2/100-nm-thick Ti/150-nm-thick Co(W) structure was dissolved into [1HF(5%) + 1HNO_3(5%)] mixed solution [29]. For the successful measurement of Cu concentration in the mixed solution without being influenced by the noises, higher Cu concentration is preferred; however, since my Co(W) has the excellent barrier property, it is not realistic. Our preliminary experiments confirmed that Q was in the order of ppb under my typical annealing condition. Therefore, inductively coupled plasma-optical emission spectrometry (ICP-OES; 5100; Agilent Technologies) was used, whose lower detection limit is typically in the ppb range [30)–32)].

3.2.4 General-purpose procedure of the modified time-lag method

The general-purpose procedure of the modified time-lag method for evaluating the Cu diffusion barrier properties is as follows.

(1) A sufficiently thick Cu film and a stacked structure of sufficient thickness are required.

Since the Cu film on the surface is agglomerated by annealing, a Cu film thick enough to maintain the continuous film shape even after annealing is required. In addition, the modified time-lag method uses only a region in a steady state. Therefore, in order to prevent reaching the equilibrium after the steady state, sufficient capacity is required to store the trace quantity of Cu that has passed through the barrier layer.

(2) Appropriate annealing conditions are required.

In the modified time-lag method, annealing is essential. Higher temperature and longer annealing time are required to obtain sufficient Q, whereas short annealing at low temperature is required to maintain the crystallinity of the barrier after annealing. It is necessary to find the optimal range of annealing conditions that can achieve both of these objectives.

(3) Removal of Cu and barrier on the surface by etching solution.

Selective etching is performed by selecting an appropriate etchant capable of etching only the

surface Cu layer and the barrier layer. After etching, clean the sample thoroughly. Then, it is checked whether Cu and the barrier layer are completely removed using a surface analysis equipment such as XPS.

(4) Dissolving trace quantity of Cu in the region where Cu is stored.

It is necessary to dissolve only the region in which the diffused Cu is stored with an appropriate etchant. In order to know the Cu concentration, it is necessary to accurately know the weight of the etchant in which Cu is dissolved and the weight of the sample. Use an analytical sclae to accurately weigh the sample and etchant.

(5) Measuring the Cu peaks using ICP-OES.

The Cu concentration (ppb) in the appropriate etchant is measured using ICP-OES. Among the wavelengths emitted from ionized Cu, the wavelength with the best sensitivity to Cu is selected. The measurement result is converted into Cu concentration (ppb) using a Cu standard solution.

(6) Calculating the trace quantity of Cu (mol/cm^2).

To apply the measurement results to the Q-t plot, the Cu concentration (ppb) must be converted to the number of Cu moles per unit area (mol/cm^2). First, the weight of Cu (g) can be obtained by multiplying the Cu concentration (ppb) by the weight of the etchant (g). Next, it is converted into Cu moles (mol) using the molar mass of Cu. Next, the number of Cu moles per unit area (mol/cm^2) is obtained by dividing the sample area. The above process is repeated to obtain a Q-t plot.

(7) Finding the x-intercept and slope from the Q-t plot.

The obtained data of Q-t plot is divided into two regions; a linear region obtained above the detection limit and a non-linear region below the detection limit. Linear approximation is performed only for the region beyond detection limit. The x-intercept and slope at this time are obtained from the result of the measured data using the method of least squares.

(8) Estimate D in a reliable way.

Equation (1) can be used to estimate D from the x-intercept, and equation (2) can be used to estimate D from the slope. However, in order to use equation (2), C_0 must first be determined. If the annealing

temperature and the type of barrier are known, C_0 can be obtained from the phase diagram.

3.3 Experimental

3.3.1 Sample preparation for barrier properties

The structure for the modified time-lag method was 100-nm-thick Cu/9-nm-thick Co(W)/1000-nm-thick sputtered SiO_2/100-nm-thick Ti/150-nm-thick Co(W)/100-nm-thick thermal SiO_2/Si substrate as shown in figure 8. All thin films were deposited by multi-target direct current (DC) plasma sputtering system (FC7100; CANON ANELVA). Prior to the deposition, the sputter chamber was evacuated to 1.3×10^{-6} Pa. A Si substrate with a thermal SiO_2 film was used without any pretreatment. After loading the substrate through the load lock chamber, the chamber pressure was controlled at 3.0×10^{-2} Pa under an Ar atmosphere. This pressure was maintained until the sample preparation was completed. 150-nm-thick Co(W) films with W concentration of 51 at. % were deposited. Subsequently, Ti and SiO_2 films were deposited. The other Co(W) film with 9-nm in thickness and W composition of 14 at. % was deposited. Finally, 100-nm-thick Cu films were deposited. For the Co(W) deposition, the total power was set to 500W for the Co and W targets, and the W composition was adjusted to be 0.14 W/(Co+W). For the Cu deposition, 1 kW of power was applied to the Cu target to deposit Cu at a growth rate of 24 nm/min. The composition of Co and W of the PVD-Co(W) film was confirmed using ICP-OES. These deposition conditions of Cu and Co(W) are the same as those of the previous 20 nm study.

The sample were annealed in the rapid thermal anneal (RTA) instrument to allow Cu diffusion at a pressure of 6,666 Pa while supplying 20 sccm of H_2 gas (> 99.99999 vol. %). This annealing condition was also same as in the previous 20 nm study. The annealing temperature was 780°C, and the annealing time varied from 50 to 1200 minutes. It took 1 minute to elevate from 25 to 780°C, while took 5 minutes to cool down from 780 to 25°C. In order to confirm that our sample was not crystallized by annealing, the sample before/after the annealing was characterized by 2θ-ω scan XRD with Cu Kα X-ray (SmartLab System 9kW; Rigaku Corporation).

3.3.2 Detail procedure of the modified time-lag method

The whole procedure of the modified time-lag method for evaluating the Cu diffusion barrier properties is as follows.

(1) Removal of Cu and Co(W) on the surface by etching solution.

The 100-nm-thick Cu and 10-nm-thick Co(W) were etched by $FeCl_3$ solution (095-02695; FUJIFILM Wako Pure Chemical Corporation). After etching the sample by 4 % $FeCl_3$ solution for 5 minutes, it was washed with clean water. Complete removal of Cu and Co(W) was confirmed by XPS analysis.

(2) Dissolving trace quantity of Cu exist in [SiO_2/Ti/Co(W)] region with etching solution.

The diffused Cu in the [1000-nm-thick SiO_2/100-nm-thick Ti/150-nm-thick Co(W)] structure was dissolved with [1HF(5%) + 1HNO_3(5%)] mixed solution. In order to know the Cu concentration, it is necessary to accurately know the weight of the etchant in which Cu is dissolved and the weight of the sample. First, I measured the exact weight of sample in the conical tube with 5 significant Figures using an analytical scale (ASP-214; AS ONE CORPORATION). The standard error ($\pm 1.4\times10^{-7}$) was also calculated from the specifications of the scale used to measure the weight of the sample. Next, the mixed solution was added to completely submerge the sample. Next, the total weight after injection of the mixed solution was measured. Next, the weight of the mixed solution and the sample was calculated, respectively. The entire sample was immersed in the mixed solution for about 24 hours to be etched.

(3) Measuring the Cu peaks using ICP-OES.

The Cu concentration (ppb) in the mixed solution was measured using ICP-OES. In order to reduce the error due to impurities during the ICP-OES measurement, the mixed solution after etching in the conical tube was measured without taking out the sample. Among the wavelengths emitted by ionized Cu, we used a wavelength of 213.598 nm. This wavelength has the best sensitivity for Cu during the ICP-OES measurement. The measured date (cps) of Cu peak can be converted to the Cu concentration (ppb) in the mixed solution using the calibration curve of the high-purity Cu standard solution (41621-100ML; SIGMA-ALDRICH).

(4) Calculating the trace quantity of Cu (mol/cm^2).

I need to convert Cu concentration (ppb) into the number of Cu moles per unit area passing through the barrier layer (mol/cm^2). First, the weight of Cu (g) can be obtained by multiplying the Cu concentration (ppb) by the weight of the etchant (g). Next, it was converted into the Cu moles (mol) using the molar mass of Cu. Next, the quantity of Cu atoms per unit area (mol/cm^2) was obtained by dividing the normalized sample area. The normalized sample area is determined based on a standard sample (2cm×2cm, 0.7456 g). For example, if the weight of the measured sample is 0.6964 g, the normalized sample area at this time is 3.7 cm^2. By repeating the above procedure, Q-t plot was obtained. In addition, by repeating these procedures at various annealing temperatures, temperature dependence of *D* was obtained.

Since the quantity of Cu passing through Co(W) is very small, it is necessary to determine the detection limit of modified time-lag method. Therefore, a trace quantity of Cu was measured using ICP-OES. To prepare ICP-OES measurement, I diluted Cu standard solution to make 4 solutions (1000 ppb, 100 ppb, 10 ppb, and 1 ppb). As a diluted solution, [1HF(5%) + 1HNO_3(5%)] mixed solution was used same as the etchant for [1000-nm-thick SiO_2/100-nm-thick Ti/150-nm-thick Co(W)] structure. The precision of quantification is also important. Therefore, the exact weight (5 significant figures) of the solution was measured using an analytical scale. Figure 9 shows the calibration curve using these four solutions. The y-axis is the intensity data obtained from ICP-OES, and the x-axis is the Cu concentration calculated from the Cu standard solution. It can be seen that a straight line is represented only from 1000 ppb to 10 ppb. Thus, the detection limit of ICP-OES in this study was determined to be 10 ppb. By plotting three points, I obtained the equation y = 4.7756x. For reference, under the current experimental conditions, Cu 10 ppb is 3.9×10^{-10} mol/cm^2, and this value corresponds to Cu 0.027 nm.

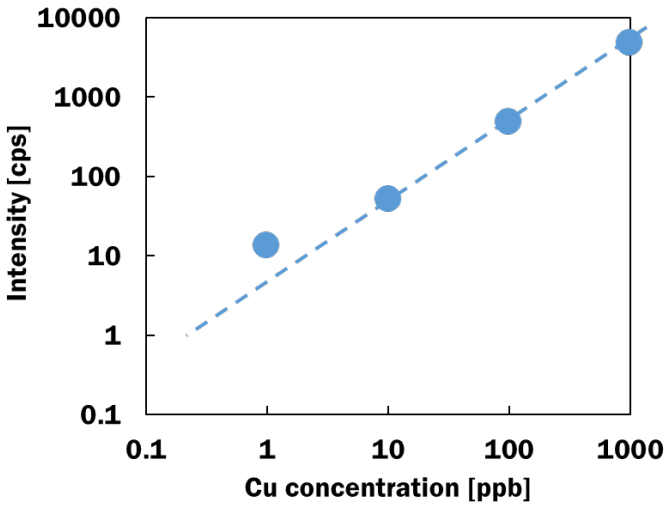

Fig 9. Calibration curve using four solutions (plotted for 3 points).

3.4 Trial and error of modified time-lag method using WDXRF

Before explaining the experimental results of modified time-lag method using ICP-OES, it was attempted to measure the quantity of diffused Cu using WDXRF, which had failed. In this chapter, the experimental conditions and measurement results of modified time-lag method using WDXRF are briefly explained, and the reasons for the failure of the measurement are summarized.

I try to measure the diffused trace quantity of Cu using WDXRF (ZSX Primus II; Rigaku) Spectroscopy. XRF spectroscopy is a non-destructive analytical technique used to identify the types of elements in a material and quantify their composition. The basic measurement principle is as follows. (1) When the sample is irradiated with X-rays with constant energy, the electrons in the electron shell leave their original positions and the positions become holes. (2) Another electron in the outer shell fills the hole. (3) At this time, as electrons in the outer shell transition to hole, energy is emitted in the form of characteristic X-rays. (4) The magnitude of this energy is as much as the difference between the energy level of the outer shell and the energy level of the inner shell. (5) Since all atoms have different energy levels, the type of atom can be determined by measuring the magnitude of this energy (Qualitative analysis). (6) Measuring the number of these energy reveals how many atoms exist (Quantitative analysis).

In particular, WDXRF spectroscopy identifies elements based on the wavelength of characteristic X-rays emitted from a sample. Characteristic X-ray is detected by wavelength based on Bragg's law in the analytical crystal. The measurement result of WDXRF depends on the thickness, type of sample, and the type of incoming X-ray. Basically, the higher the energy of the X-ray, the deeper it reaches the sample. As a result, it is possible to obtain information about the deep inside of the sample. The incoming X-ray used in this experiment is Cu kα and has an energy of about 8.05 eV. Incoming X-ray with this energy reach about 100 μm for SiO_2. Therefore, it is sufficient for use in this experiment. In addition, although there are slight differences depending on the equipment, it is possible to measure a large area enough to measure the area of a circle approximately 40 mm in diameter at once. The detection limit of WDXRF also needs to be noted in order to improve the reliability of measurement results. The commonly known definition of detection limit

is "when the net intensity of the detection peak is more than three times the standard deviation of background noise". The detection limit depends on the element to be measured and the type of matrix element, but heavier elements generally have lower detection limit.

The advantages of WDXRF spectroscopy are as follows. (1) Elements can be detected at concentrations ranging from ppm to 100%. (2) Depending on the material, depths from several nanometers to several millimeters can be analyzed. (3) From the entire wafer to small samples can be analyzed. On the other hand, the disadvantages are as follows. (1) Because WDXRF uses high-energy X-rays, a lot of heat is generated. An external chiller must be used to cool it down. (2) Since the measurement result of WDXRF is sensitive to heat, a constant temperature must be maintained. (3) Light elements such as H, He, Li, and Be cannot be detected.

3.4.1 Measurement process of barrier properties using WDXRF

The sample prepared in Chapter 3.3 was still used in the modified time-lag method using WDXRF. Figure 10 shows the sample structure for WDXRF measurement and the result of the calibration curve of the Cu standard sample for quantitative evaluation. The measurement process using WDXRF is as follows. In order to accurately measure the quantity of Cu, two conditions must be preceded. (1) After annealing, Cu/Co(W) layer should be etched. The etchant and etching method are the same as when using ICP-OES. (2) After Cu/Co(W) etching, WDXRF is used to accurately measure the quantity of Cu diffused in SiO_2/Ti/Co(W).

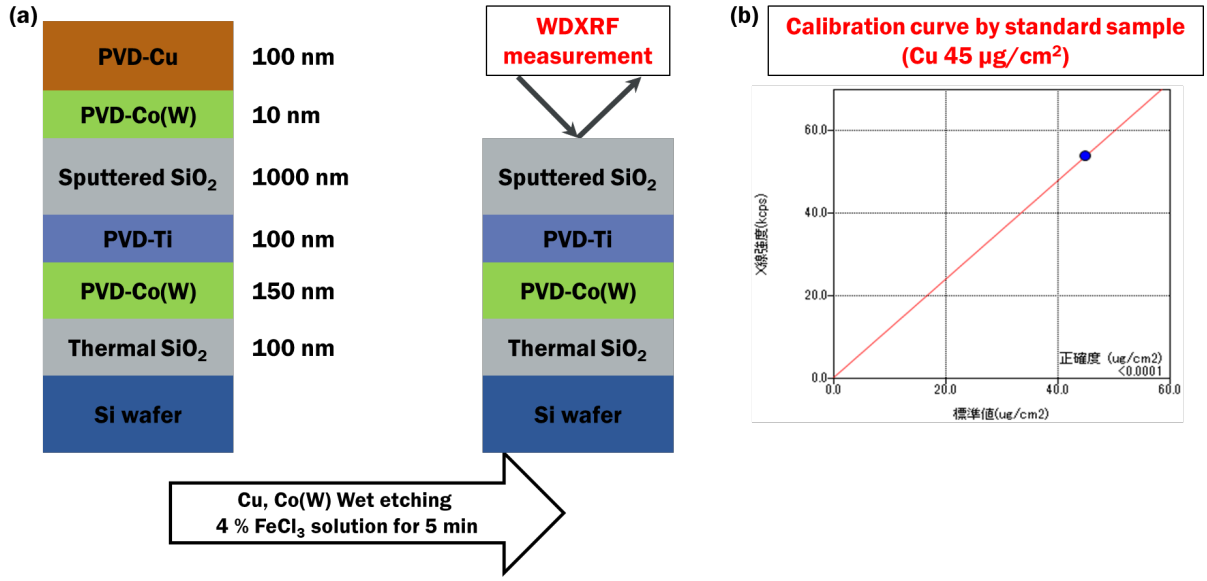

Fig 10. (a) Sample structure for WDXRF measurement and (b) calibration curve of the Cu standard sample.

3.4.2 Obtaining the *D* from the time-lag using WDXRF and its limitation

Figure 11 shows the results of applying a 10-nm-thick PVD-Co(W) sample to the modified time-lag method. The three straight lines in figure 11(a) are the results of annealing at 780, 830, and 855°C. The y-axis represents the number of moles per unit area (Q; mol/cm^2), and the x-axis represents annealing time (t; s). The quantity of diffused Cu increases linearly with the annealing time. This indicates that my assumptions about the modified time-lag method are valid. However, I could not get the x-intercept (i.e., time-lag) that I should know. This is when the detection limit of WDXRF is too high to accurately measure a trace quantity of Cu under the current experimental conditions. Therefore, it is necessary to find a new measurement equipment that can further lower the detection limit. However, since information of the slope can be obtained, it may be possible to predict *D* using the slope, thickness of PVD-Co(W), and C_0 (2.9×10^{-3} mol/cm^3 at 780°C, 3.8×10^{-3} mol/cm^3 at 830°C, and 4.3×10^{-3} mol/cm^3 at 855°C) obtained from the Co-Cu phase diagram into Equation (2).

Figure 11(b) is an Arrhenius plot of *D* obtained from the slope. First of all, the three points of each temperature are connected in a straight line. This indicates that diffusion is taking place by the same diffusion mechanism in the temperature range (780 ~ 855°C). E_a and D_0 of PVD-Co(W) also calculated from the

Arrhenius plot in figure 11(b). For 10-nm-thick PVD-Co(W), E_a is 3.0 eV, and D_0 is 4.2×10^{-4} cm^2/s. Compared with the results obtained using ICP-OES in Chapter 4, E_a obtained from WDXRF was about 0.9 eV smaller than E_a obtained from ICP-OES. In the case of D_0, D_0 obtained from WDXRF was about 10^5 times smaller than D_0 obtained from ICP-OES. Further discussion is needed on this difference.

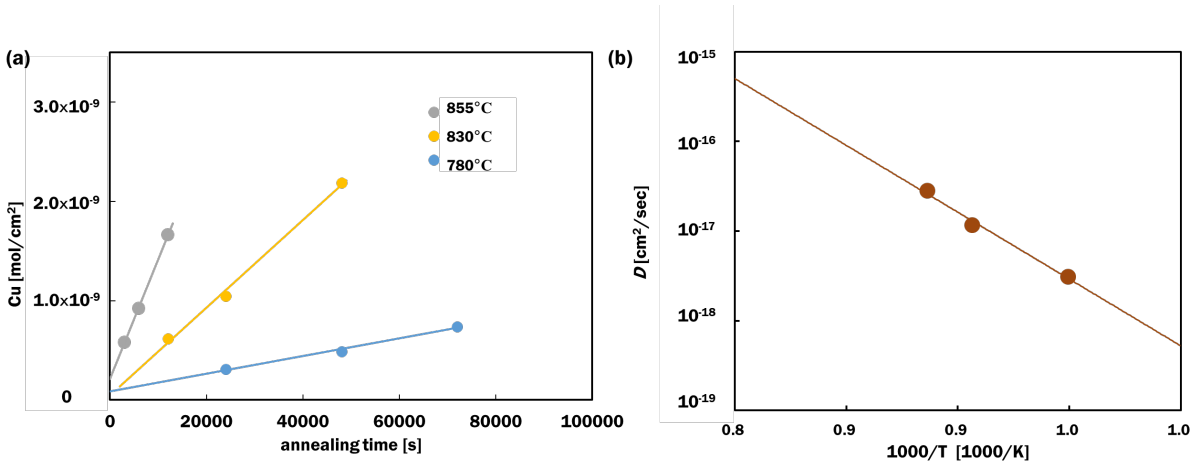

Fig 11. (a) Q-t plot and (b) Arrhenius plot of 10-nm-thick PVD-Co(W) from the slope.

3.5 Results & discussion

3.5.1 Determination of appropriate annealing condition

The crystal structure has a great influence on the barrier properties. Amorphous structures have good barrier properties in general,[33)34)35)] while metal crystallization weakens the barrier properties because it creates grain boundaries allowing fast diffusion of Cu. Therefore, it is necessary to determine the annealing time and temperature in a range where the Co(W) barrier layer will not crystallize while obtaining sufficient Q. From the results of my preliminary experiments, the change in Q of diffused Cu according to the annealing time appeared conspicuously from 780°C and above. Therefore, an annealing temperature of 780°C was determined. In addition, samples with various annealing times are required to diffuse Cu with different concentrations beyond the detection limit. In my experiment, it was set to 50 - 1200 minutes. Figure 12 shows the XRD pattern before and after 780°C-500minutes annealing. According to this result, TiO_2 is crystallized by taking the oxygen of SiO_2 thereon by annealing. However, crystallization of Co and W, which I was concerned about, did not occur.

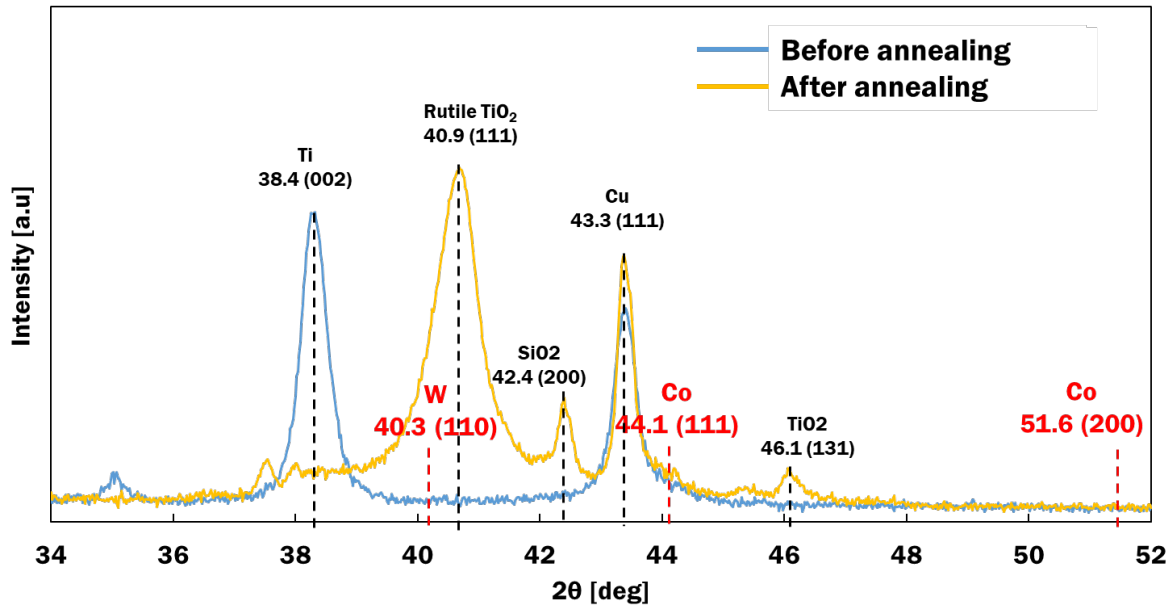

Fig 12. XRD pattern before and after annealing.

3.5.2 *D* estimated by the modified time-lag method using ICP-OES

The key to the modified time-lag method is "how accurately measure the trace quantity of Cu diffused through the barrier layer". The previous chapter dealt with trial and error in applying the modified time-lag method. With the help of the results obtained there, successful measurements using ICP-OES were made possible. The technique of ICP-OES is mainly used for quantitative analysis of metal elements, and the basic measurement process is as follows. (1) Argon gas is converted into plasma at high temperature using an induced magnetic field. (2) A liquid sample is sprayed with aerosol and injected into the plasma. (3) Metals dissolved in the liquid sample are ionized in high temperature plasma. (4) The electron state of the ionized metal atom changes from the ground state to the excite state, and when the electron returns to the ground state, each element emits light of a specific wavelength. (5) Using a spectroscopic device, the emitted light is dispersed for each wavelength. (6) By measuring the intensity of light for each wavelength in the detector, the type and quantity of the contained elements can be known.

The advantages of ICP-OES can be summarized as follows. First, since the efficiency of high-temperature plasma and sample introduction is good, it is possible to qualitatively and quantitatively evaluate very small quantity of elements from ppm to ppb level for most elements. In addition, elements in the sample can be simultaneously detected using high-temperature plasma. On the other hand, the biggest drawback is the matrix effect. The matrix effect occurs for two main reasons. First, in the ICP-OES analysis, the spray efficiency of the solution changes due to the difference in physical properties of the sample solution, which affects the measurement result. Therefore, when preparing the standard solution and the sample solution, the same solvent of the same concentration must be used. Another cause is the problem of overlapping emission spectra. The wavelength of another element overlaps the position of the wavelength of the element to be measured, causing an error in the analysis of the element to be measured. Therefore, it is inevitable to use the second wavelength, avoiding overlapping elements by referring to the data sheet of the wavelength information.

Figure 13 shows a Q-t plot obtained after the annealing ranging from 300 to 72000 s at 780 ℃. The resulting x-intercept and slope of the fitting line were 7778 s and 4.5×10^{-14} mol/cm^2/s, respectively. There are two options to estimate D in the modified time-lag method; from x-intercept using Equation (1) and from slope using Equation (2), for which C_0 has to be determined prior to the analysis.

The way to determine C_0 from the phase diagram was described herein. Since Cu does not dissolve in W, Co-Cu binary phase diagram was considered [17], in which solubility of Cu in Co is 2.2 at. % at 780°C. Note that the Cu solubility is exceedingly small, the volume expansion of Co(W) by Cu dissolution could be neglected. Also, as the solubility of Cu in Co is small, molar density of Cu-Co mixture was approximated to be that of Co. Molar density of Co was calculated as 1.5×10^{-1} mol/cm^3 using the weight density (9.0 g/cm^3) and molar mass (58.9 g/mol) of Co. Then, by multiplying these two values, solubility of Cu in Co was calculated as 3.4×10^{-3} mol/cm^3. Finally, solubility of Cu in Co(W) i.e. C_0 was obtained as 2.9×10^{-3} mol/cm^3. For this calculation, volumetric ratio of Co in Co(W) should be used but unknown, and thus molar ratio of Co in Co(W) [0.86 Co/(Co+W)] was used instead.

D was estimated accordingly. First, D was estimated from the x-intercept using Equation (1). Using L of 10 nm and the time-lag of 7778 s, D was calculated as 2.1×10^{-17} cm^2/s. Subsequently, D was estimated from the slope using Equation (2). Using the slope of 4.5×10^{-14} mol/cm^2/s, C_0 of 2.9×10^{-3} mol/cm^3, and L of 10 nm, D was estimated as 1.6×10^{-17} cm^2/s. These two D values obtained were consistent with 24% deviation, which was as expected in Section 3.2.1. This proves that my modified time-lag method is a reliable method as each D obtained from the x-intercept and slope is almost identical.

Comparison of the two D values obtained from 10-nm-thick Co(W) by the modified time-lag method and that from 20-nm-tchick Co(W) by XPS depth-profiling were examined. Film compositions were same at 0.14 W/(Co+W). D obtained by XPS depth-profiling was 2.5×10^{-16} cm^2/s at 780°C, while D obtained by the modified time-lag method was 2.1×10^{-17} cm^2/s at 780°C. The two D values obtained differently were in the one order. It is indicating as the thickness of the barrier layer decreases, a decrease in D appears.

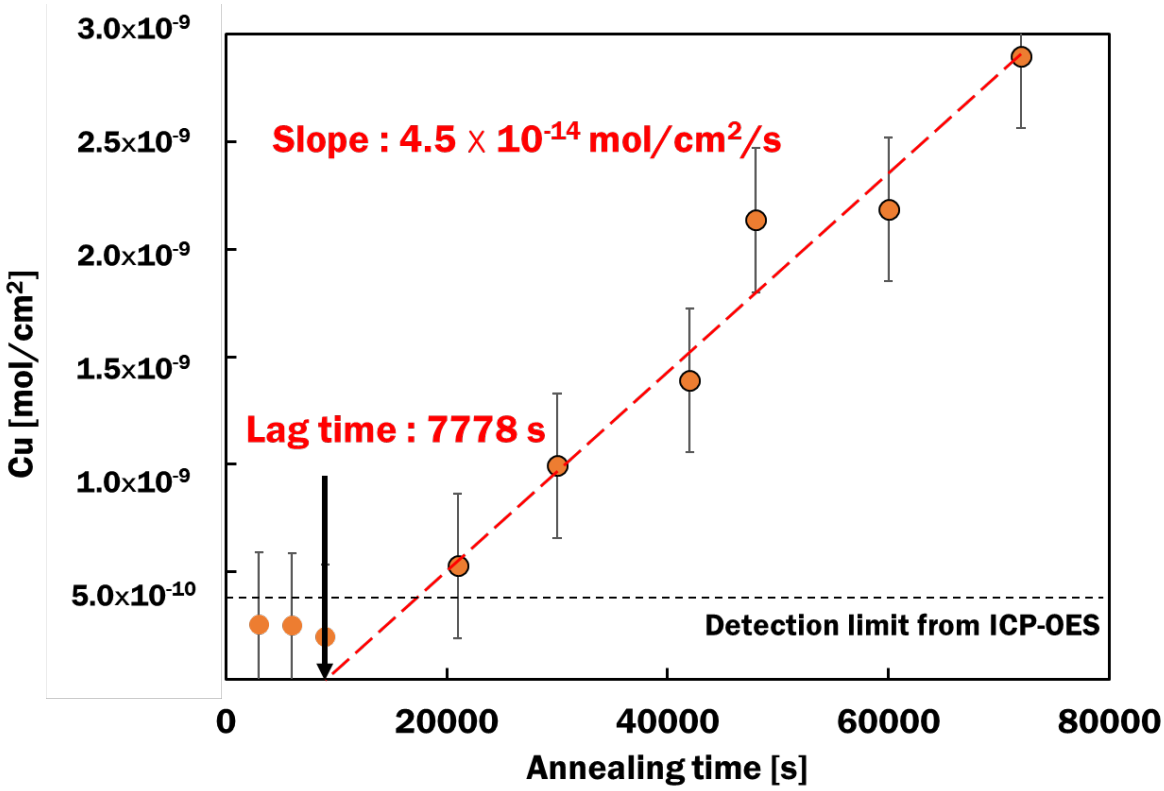

Fig 13. Q-t plot at 780°C using ICP-OES.

3.5.3 Minimization of experimental errors

When the barrier layer becomes extremely thin, the x-intercept will be remarkably close to the origin, and the time-lag will be a few seconds. Then, the deviation of the data of the Q-t plot increases. In Figure 13, the standard error for six samples above the detection limit was $\pm 3.7\times10^{-10}$ cm^2/s, and the average accuracy was 70 %. By the definition, Standard error is the standard deviation for six samples divided by the square root of the number of samples. Average accuracy is the average of [(sample value - standard deviation)/sample value]. Therefore, it is necessary to identify the cause of the experimental error and find a way to reduce it. For the 780°C-10nm sample, two replicates were performed to confirm the reproducibility with an annealing time of 30,000 s. As a result, Cu permeation results of 9.9×10^{-10} and 7.6×10^{-10} (mol/cm^2) were obtained. The difference between the two results is 2.3×10^{-10} (mol/cm^2), which is smaller than the standard error of this measurement ($\pm 3.7\times10^{-10}$ cm^2/s), so it is considered to be reproducible. However, even if it is small, it is not good that the measured value and the standard error of the measured value are in the same order. It is necessary to reduce the standard error by repeating the experiment.

Depending on where the error occurred in the experiment, the solution will be different. (1) If the error occurred during the annealing process, the cause may be defects inside the sample. It is necessary to make a sample in consideration of the possibility that defects may be generated during the sample production process. (2) If the error occurred during the etching process, the cause that can be expected is a trace quantity of impurities generated in the etching process. Of course, I have kept the impurities as low as possible. However, an unavoidable error may have occurred because the concentration handled in my experiment is very small. (3) Finally, if the error occurred in the measurement process of ICP-OES, the cause may be the detection limit of ICP-OES itself. In order to reduce the error in the measurement process, it is worthwhile to use inductively coupled plasma mass spectrometry (ICP-MS), which is a higher precision measuring instrument. In ICP-MS, even trace concentrations can be measured than in ICP-OES. Typical ICP-MS can measure up to ppt (parts per trillion) level, and brand new ICP-MS can measure up to ppq (parts per quadrillion) level. Therefore, if it is possible to measure the detection limit down to 10 ppb or less using ICP-

MS, it may be possible to reduce the error by ICP-MS. Considering the above, more reliable results could be obtained even for the thinner 1nm barrier layer.

3.6 Conclusion

I developed the modified time-lag method to quantitatively evaluate the barrier properties against Cu diffusion in ULSI interconnects. By measuring a trace quantity of Cu passing through the Co(W) barrier layer, D of Cu was obtained. Through comparison with the conventional time-lag method, the items to be modified to change to the modified time-lag method are summarized. As the first challenge of quantitative evaluation, an experiment using APT was conducted. However, it failed due to the influence of the sample structure. Then, a modified time-lag method was performed using WDXRF. However, the time-lag could not be obtained due to the limitation of the precision of the equipment. By overcoming the limitations of WDXRF using ICP-OES, I succeeded in obtaining time-lag. To prove the validity of the modified time-lag method, two D values obtained using the x-intercept and slope from the Q-t plot were compared. It was confirmed that the results obtained from the modified time-lag method are valid. Through comparison with the result of 20-nm-thick PVD-Co(W), it was possible to predict the change in barrier properties according to the change in the thickness of the thin film.

The future work is to validate whether the modified time-lag method is applicable to 1-nm-thick films. When the barrier layer becomes extremely thin, the x-intercept will be very close to the origin, and the time-lag will be a few seconds. Then, the deviation of the time-lag increases. Therefore, it is necessary to use equipment with higher precision to reduce data deviation. Then, reliable results can be obtained even for the thinner 1nm barrier layer. Equipment capable of measuring finer quantities than ICP-OES such as ICP-MS will be needed. By investigating the temperature dependence, the activation energy (E_a) and pre-exponential factor (D_0) for the diffusion of the barrier layer will also be obtained. Through these results, a more in-depth discussion about the barrier properties of the barrier layer will be possible. Also, I will investigate how the obtained D, D_0, and E_a vary according to the change in the thickness of the barrier layer.

Reference

1) K. Shima, Y. Tu, H. Takamizawa, H. Shimizu, Y. Shimizu, T. Momose, K. Inoue, Y. Nagai and Y. Shimogaki, Appl. Phys. Lett. **105** [13], 133512 (2014).

2) K. Stiller, L. Viskari, G. Sundell, F. Liu, M. Thuvander, H.-O. Andrén, D. J. Larson, T. Prosa and D. Reinhard, Oxid. Met. **79** [3–4], 227 (2012).

3) B. Gault, F. de Geuser, L. T. Stephenson, M. P. Moody, B. C. Muddle and S. P. Ringer, Microsc. Microanal. **14**, 296 (2008).

4) B. Gault, a. Menand, F. De Geuser, B. Deconihout and R. Danoix, Appl. Phys. Lett. **88** [2006], 12 (2006).

5) T. F. Kelly and D. J. Larson, Annu. Rev. Mater. Res. **42** [1], 1 (2012).

6) D. N. Seidman, Annu. Rev. Mater. Res. **37** [1], 127 (2007).

7) D. J. Larson, T. J. Prosa, B. P. Geiser and W. F. Egelhoff, Ultramicroscopy **111** [6], 506 (2011).

8) H. A. DAYNES and M.Sc, Proc. R. Soc. London. Ser. A, Contain. Pap. a Math. Phys. Character **97** [685], 286 (1920).

9) S. W. Rutherford and D. D. Do, Adsorption **3** [4], 283 (1997).

10) G. L. Graff, R. E. Williford and P. E. Burrows, J. Appl. Phys. **96** [4], 1840 (2004).

11) G. A. Choudalakis and A. D. Gotsis, in *Materials Research Society Symposium Proceedings* (Pergamon, 2011) Vol. 1312 pp. 397.

12) E. E. Nuxoll, R. A. Siegel and E. L. Cussler, J. Memb. Sci. **252** [1–2], 29 (2005).

13) S. W. Seo, E. Jung, C. Lim, H. Chae and S. M. Cho, Thin Solid Films **520** [21], 6690 (2012).

14) M. Al-Ismaily, J. G. Wijmans and B. Kruczek, J. Memb. Sci. **423**–**424**, 165 (2012).

15) H. Wu, N. Al-Qasas, B. Kruczek and J. Thibault, J. Fluid Flow, Heat Mass Transf. [DOI:10.11159/jffhmt.2015.003].

16) S. Majee, M. F. Cerqueira, D. Tondelier, B. Geffroy, Y. Bonnassieux, P. Alpuim and J. E. Bourée, Surf. Coatings Technol. **235**, 361 (2013).

17) T. Nishizawa and K. Ishida, Bull. Alloy Phase Diagrams **5** [2], 161 (1984).

18) J. Y. Kwon, T. S. Yoon, K. B. Kim and S. H. Min, J. Appl. Phys. **93** [6], 3270 (2003).

19) O. van der Straten, Y. Zhu, J. Rullan, K. Dunn and A. E. Kaloyeros, J. Mater. Res. **21** [01], 255 (2006).

20) K. Shima, H. Shimizu, T. Momose and Y. Shimogaki, ECS J. Solid State Sci. Technol. **4** [2], P20 (2014).

21) K. Shima, H. Shimizu, T. Momose and Y. Shimogaki, ECS Solid State Lett. **3** [2], P20 (2014).

22) H. Kim and Y. Shimogaki, J. Electrochem. Soc. **154** [1], G13 (2007).

23) S. P. Murarka and S. W. Hymes, Crit. Rev. Solid State Mater. Sci. **20** [2], 87 (1995).

24) M. Delalande, M. J. F. Guinel, L. F. Allard, A. Delattre, R. Le Bris, Y. Samson, P. Bayle-Guillemaud and P. Reiss, J. Phys. Chem. C **116** [12], 6866 (2012).

25) C. S. Bonifacio, S. Carenco, C. H. Wu, S. D. House, H. Bluhm and J. C. Yang, Chem. Mater. **27** [20], 6960 (2015).

26) M. Oezaslan, F. Hasché and P. Strasser, Chem. Mater. **23** [8], 2159 (2011).

27) J. D. McBrayer, J. Electrochem. Soc. **133** [6], 1242 (1986).

28) K. C. H. Kumar, I. Ansara, P. Wollants and L. Delaey, Int. J. Mater. Res. **87** [8], 666 (1996).

29) P. Walker, W. H. Tarn, B. Raton, B. London and N. Y. Washington, .

30) J. W. Olesik, Anal. Chem. **63** [1], 12 (1991).

31) T. W. Barnard/', M. I. Crockett, J. C. Ivaldi, P. L. Lundberg, D. A. Yates, P. A. Levine and D. J. Sauer, Anal. Chem **65**, 1231 (1993).

32) Agilent Technologies, *Agilent 5100 ICP-OES DUAL VIEW ICP-OES* (2014).

33) X. H. Dai, L. Zhang, Z. D. Feng, X. H. Li, J. X. Guo, Y. J. Fu, Y. Zhou, Q. X. Zhao, J. Z. Lou, L. X. Ma, X. Y. Zhang and B. T. Liu, Mater. Lett. **159**, 94 (2015).

34) J. S. Reid, E. Kolawa, R. P. Ruiz and M. A. Nicolet, Thin Solid Films **236** [1–2], 319 (1993).

35) G. S. Chen, P. Y. Lee and S. T. Chen, Thin Solid Films **353** [1], 264 (1999).

Chapter 4

Investigation of the thickness dependence of the barrier properties and crystallinity

The overall goal of my research is a quantitative evaluation of barrier properties. In Chapter 2, I proposed a method to quantitatively evaluate the barrier properties by calculating the diffusion coefficient (D) from the concentration profile of Cu diffused in 20-nm-thick Co(W). In Chapter 3, for the thinner 10-nm-thick Co(W) barrier layer, I first applied the time-lag method to Cu interconnects and established the measurement method. At this time, a modified time-lag method was developed for the first time, and D was calculated using this method to quantitatively evaluate the barrier properties. In this chapter, I used modified time-lag method to investigate how the barrier properties vary with respect to the thickness of the liner/barrier layer. The barrier properties were quantitatively evaluated by experimentally estimating the D of Cu for 8, 10, 12-nm-thick PVD-Co(W) single liner/barrier layer. At this time, the activation energy (E_a) for diffusion in the 780, 830, and 855°C was also obtained to explain the diffusion behavior from the nanostructure point of view.

The thickness dependence of the barrier properties is important for all diffusion field, including gas diffusion and solid diffusion[1),2)]. It would be desirable if the barrier properties are improved as the thickness of the barrier layer became thinner. On the contrary, if the barrier properties decrease as the thickness of the barrier layer becomes thinner, the cause should be investigated, and countermeasures should be established. This is important because the starting point of the miniaturization of Cu interconnects is the dependence of the thickness of the barrier layer. For an ultra-thin barrier layer of 10 nm or less, quantitative evaluation of the barrier properties according to the change in the thickness of the barrier layer has rarely been performed. Therefore, in this chapter, I discussed the thickness dependence of the barrier properties of PVD-Co(W) using the modified time-lag method. Additionally, it deals with crystallinity and adhesion properties of PVD-Co(W) thin film. The preparation and measurement process of the sample for evaluating barrier properties used in this chapter are described in Chapter 3.3, so they are omitted here.

4.1 Preparation: Composition and crystallinity of barrier layer

4.1.1 Check whether the composition of Co and W is changed

Before evaluating the barrier properties, it is necessary to confirm that the composition of Co and W does not change according to the change in the thickness of the barrier layer. If the composition of Co and W varies according to the PVD-Co(W) thickness, consistent discussion is difficult. Table 1 shows the measurement results of the composition of Co and W for PVD-Co(W) having a thickness of 1, 3, 5, 8, 10, and 12 nm obtained using ICP-OES. The composition of Co and W was obtained from the standard solution of Co and W in the same manner as the method of obtaining the concentration of Cu. At the interface with SiO_2, the substrate of Co(W), W is segregated and the W concentration is slightly increased. This is thought to be due to the difference in the sticking probability of Co and W to SiO_2. In the continuous growth stage after the thin film is sufficiently thick, the sticking probability of Co and W to Co(W) becomes constant. As a result, a Co(W) thin film with a constant composition in the film thickness direction is formed. In the manufacturing process of a bulk material, atoms move due to energetic instability at the interface, as a result, there may be a concentration change at the interface. However, since the manufacturing process of a thin film material is a metastable state, the concentration of an interface is determined by sticking probability etc. That is, although the composition of Co(W) may be slightly different at the SiO_2 interface, segregation will not occur at least during thin film production. Therefore, it is considered that there is no change in the composition of Co and W. Through this, it was found that the composition of Co and W according to the thickness of PVD-Co(W) was constant.

Table 1. The ratio of Co and W using ICP-OES for various Co(W) thickness.

	Co(W) thickness					
	1 nm	3 nm	5 nm	8 nm	10 nm	12 nm
W/(Co+W)	0.25	0.20	0.16	0.15	0.14	0.13

4.1.2 Confirmation of the relationship between the crystallinity and barrier properties

The crystal structure has a great influence on the barrier properties. In general, structures with low crystallinity tend to have excellent barrier properties because they do not have the fast diffusion path such as a grain boundary or a dislocation. Figure 1 shows the XRD measurement results before and after 780°C annealing with 8, 10, 12-nm-thick PVD-Co(W) samples. In these results, it can be seen that Ti was oxidized to Rutile TiO_2 by using oxygen of SiO_2 after annealing. Cu has a (111) plane before annealing, and a new (021) plane appeared by annealing. However, crystallization of Co and W, which we are concerned about, did not occur. Through these results, it can be seen that the excellent barrier properties of the current PVD-Co(W) layer are due to the material properties of Co(W) that are not crystallized even at high temperatures.

The sample used for crystallinity evaluation is the same as the sample used for barrier property evaluation of the thinned PVD-Co(W) layer. In addition, the XRD used for crystallinity evaluation is also the same equipment as the XRD used in Chapter 2. The measurement conditions of XRD are also completely the same.

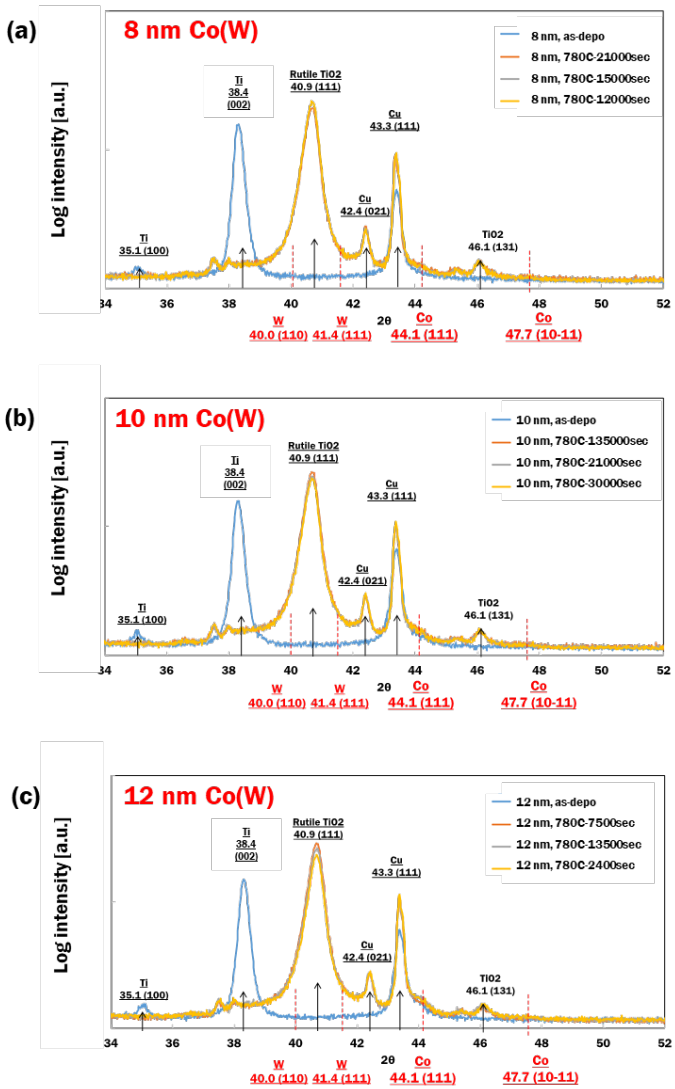

Fig 1. XRD pattern before and after annealing.

4.2 *D* with various Co(W) thickness and annealing temperature

Figure 2 is the results of applying the modified time-lag method to 8, 10, 12-nm-thick PVD-Co(W) layers at an annealing temperature of 780°C. The x-axis represents annealing time (t), and the y-axis represents the number of diffused Cu moles per unit area (Q). In the region above the detection limit, it was confirmed that the diffused Cu moles per unit area is proportional to the annealing time. The change in time-lag (x-intercept) according to the change in PVD-Co(W) thickness is large (5111 s at 8 nm, 7778 s at 10 nm, and 6222 s at 12 nm). However, the time-lag decreased at 12 nm. This means that the thickness of the PVD-Co(W) has an absolute influence on the amount of diffused Cu. In general, as the PVD-Co(W) became thicker, the time-lag also showed a tendency to increase. There is no change in the slope according to the change in the thickness of the PVD-Co(W) (4.5×10^{-14} mol/cm^2/s at 8 nm, 4.5×10^{-14} mol/cm^2/s at 10 nm, and 4.5×10^{-14} mol/cm^2/s at 12 nm).

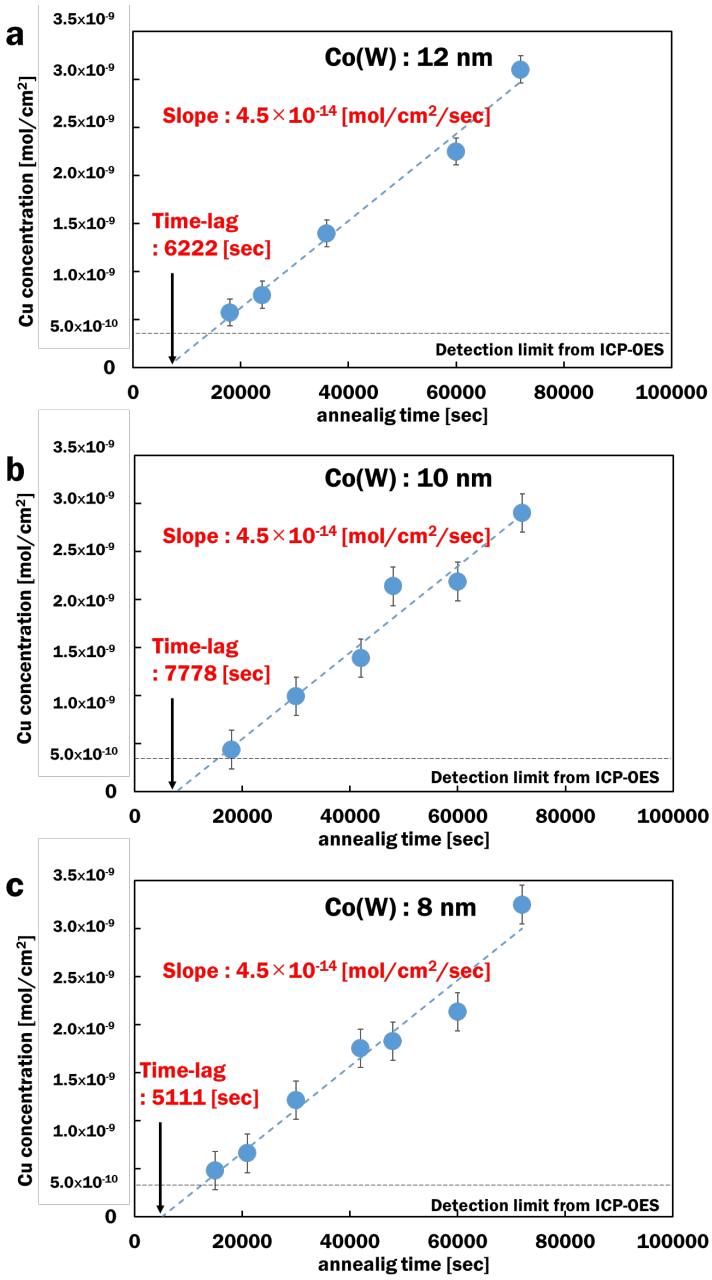

Fig 2. Q-t plot of modified time-lag method at 780°C.

Figure 3 is the results of applying the modified time-lag method to 8, 10, 12-nm-thick PVD-Co(W) layers at an annealing temperature of 830°C. Except for 12-nm-thick PVD-Co(W), the time-lag still increases as PVD-Co(W) gets thicker (1222 s at 8 nm, 2273 s at 10 nm, and 1314 s at 12 nm). That is, even at 830°C, it was confirmed that the thickness is still an important factor in determining the barrier properties. In addition, a change in the slope according to the change in the thickness of PVD-Co(W) was observed (3.6 x 10^{-13}

mol/cm^2/s at 8 nm, 4.4 x 10^{-13} mol/cm^2/s at 10 nm, and 3.5 x 10^{-13} mol/cm^2/s at 12 nm). This is probably due to the increase of the annealing temperature, which caused more diffusion than at 780°C, and the result also affected the change in slope.

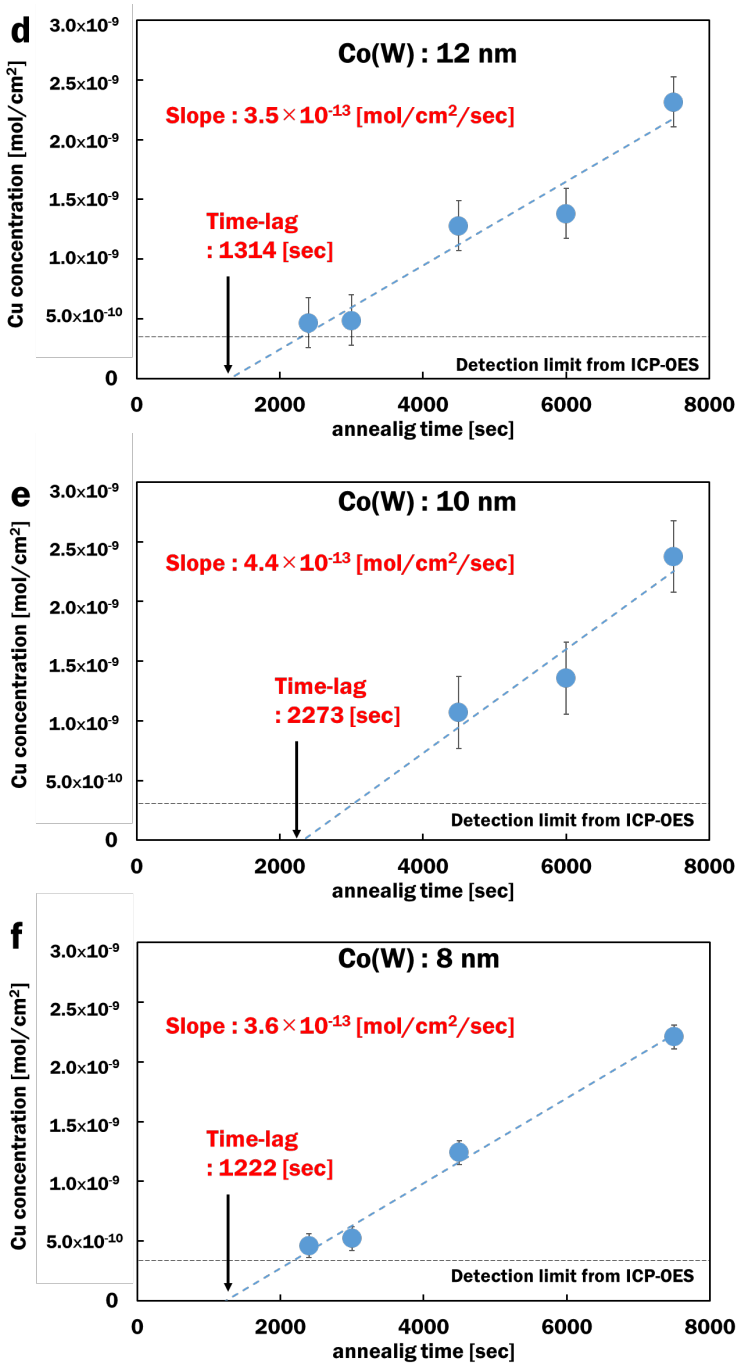

Fig 3. Q-t plot of modified time-lag method at 830°C.

Figure 4 is the results of applying the modified time-lag method to 8, 10, 12-nm-thick PVD-Co(W) layers at an annealing temperature of 855°C. Except for 12-nm-thick PVD-Co(W), it can be seen that the time-lag increases as the PVD-Co(W) gets thicker (500 s at 8 nm, 691 s at 10 nm, and 630 s at 12 nm). In addition, a change in the slope according to the change in the thickness of PVD-Co(W) was observed (8.2 x 10^{-13} mol/cm^2/s at 8 nm, 1.1 x 10^{-12} mol/cm^2/s at 10 nm, and 1.0 x 10^{-12} mol/cm^2/s at 12 nm). The results of the three annealing temperatures are summarized as follows. At all three temperatures, as the PVD-Co(W) became thicker, the time-lag (x-intercept) showed a tendency to increase. However, the time-lag decreased at 12 nm. This indicates that during the growth of PVD-Co(W) from 10 nm to 12 nm, certain factors that influence the barrier properties may have changed. The change in the slope according to the change in the thickness of PVD-Co(W) was not large, whereas the change in the slope according to the annealing temperature change was evident. As the temperature increases, the slope becomes steeper.

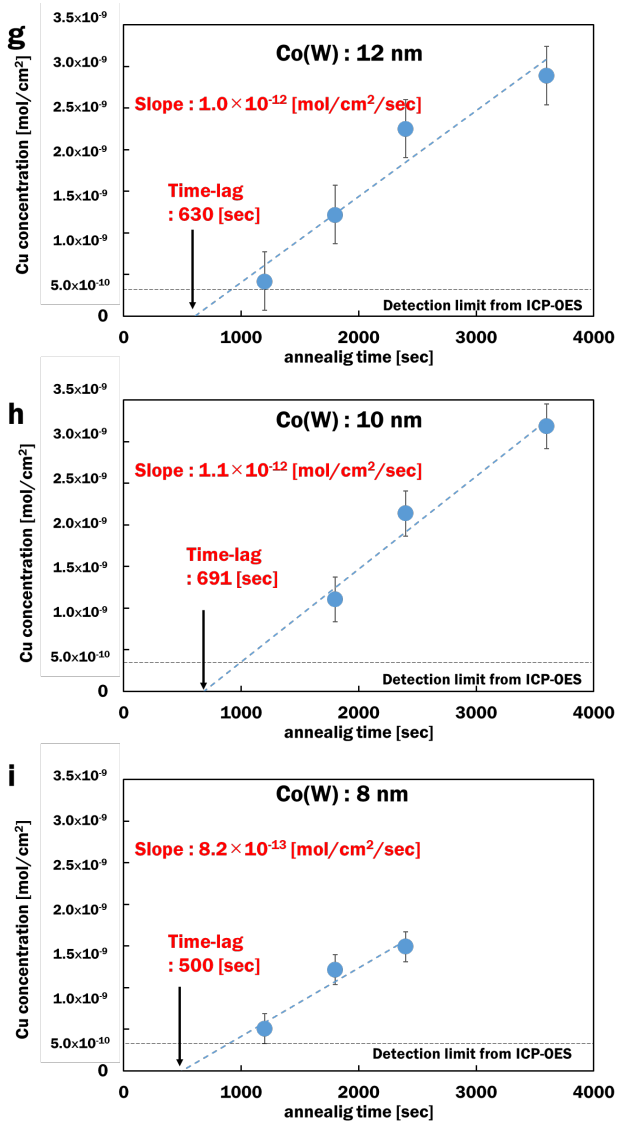

Fig 4. Q-t plot of modified time-lag method at 855°C.

The barrier properties are quantitatively evaluated by obtaining *D* using the x-intercept and slope of the Q-t plot for 8, 10, 12-nm-thick PVD-Co(W) with three temperatures (780, 830, and 855°C). The relationship between slope, C_0, L, and *D* in the modified time-lag method is as follows.

$$\text{slope} = \frac{DC_0}{L} \qquad (1),$$

where L is the thickness of Co(W) and *D* is the diffusion coefficient. C_0 is the concentration of Cu at the interface between Cu and Co(W), and we predicted C_0 from the Co-Cu phase diagram [3]. Since Cu does not dissolve in W, Co-Cu binary phase diagram was used. Therefore, the C_0 is determined only by Cu in Co. According to the Co-Cu phase diagram, the solubility of Cu to Co at each temperature is different (2.2 at. %

at 780°C, 2.9 at. % at 830°C, and 3.3 at. % at 855°C). Since the quantity of dissolved Cu is exceedingly small, the volume increase of Co(W) could be neglected. To determine the C_0, I start with Cu molar concentration (mol/cm^3).

(1) The Cu molar concentration in pure Co (mol/cm^3) is calculated using the Co density (g/cm^3) and the Co molar mass (g/mol). Note that as the solubility of Cu in Co is small, molar density of Cu-Co mixture was approximated to be that of Co.

(2) Cu molar concentration in pure Co after applying the Cu solubility (mol/cm^3) is then calculated multiplying the Cu molar concentration in pure Co (mol/cm^3) by Cu solubility (at. %).

(3) Finally, C_0 (mol/cm^3) is obtained by applying the ratio of Co in Co(W). It is difficult to obtain the volume ratio, so the atomic ratio of Co and W was used in this paper. C_0 calculated based on the phase diagram is summarized in Table 2.

Table 2. C_0 obtained at various temperatures and thicknesses.

Annealing temperature	**C_0 (mol/cm^3)**		
	8 nm	**10 nm**	**12 nm**
855°C	4.3×10^{-3}	4.3×10^{-3}	4.4×10^{-3}
830°C	3.8×10^{-3}	3.8×10^{-3}	3.9×10^{-3}
780°C	2.9×10^{-3}	2.9×10^{-3}	2.9×10^{-3}

Figure 5 shows the *D* of Cu for 8, 10, 12-nm-thick PVD-Co(W) obtained by the slope and x-intercept (time-lag) and the *D* of Cu for 20-nm-thick PVD-Co(W) obtained by the depth profile method at three annealing temperatures. *D* increases as the annealing temperature increases. In addition, at the same annealing temperature, it shows an almost constant *D* regardless of the thickness of the barrier. In addition, the change in *D* according to the thickness change from 8 to 12 nm stays within about 2 times. According to

another study examining *D*, an error of up to 42% is accepted even in the same measurement of *D* [4)5)]. Therefore, it can be seen that the decrease in *D* according to the decrease in the thickness of the barrier layer is not so large. From the thickness-dependent trend, excellent barrier properties are maintained even when PVD-Co(W) is thinned.

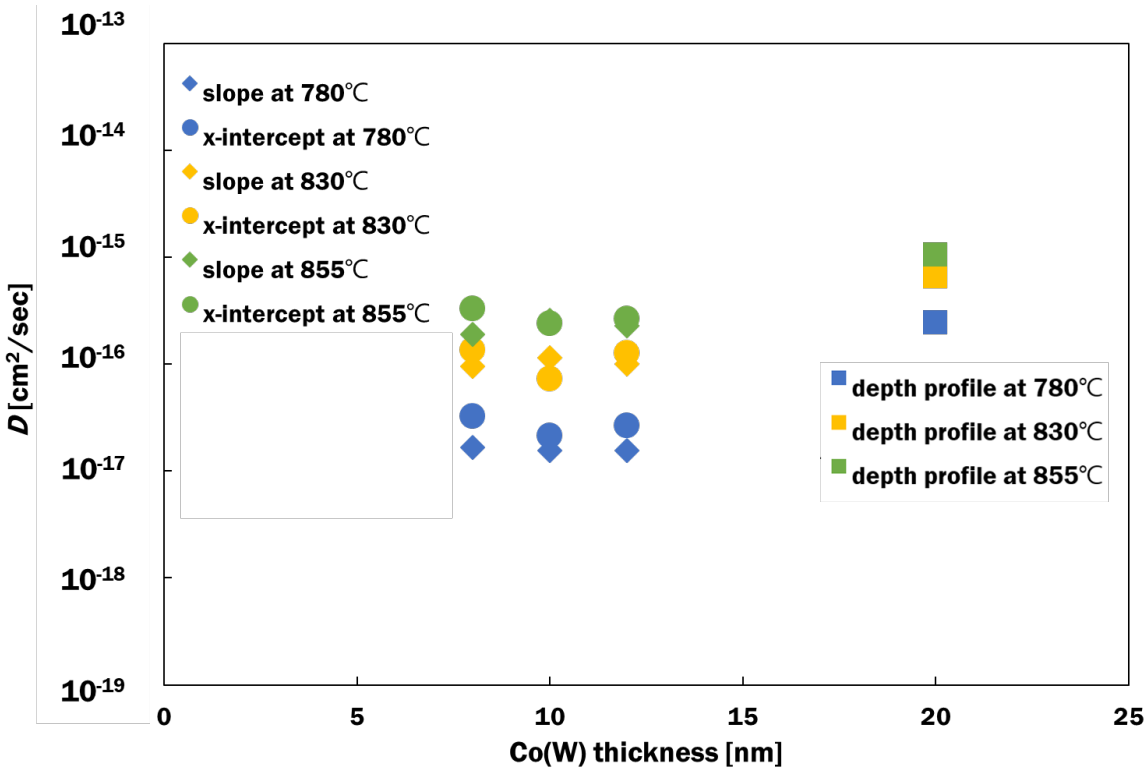

Fig 5. *D* obtained by using the slope and x-intercept at three annealing temperatures.

4.3 Confirmation of change of diffusion mechanism according to PVD-Co(W) thickness

The diffusion mechanism describes how diffusion atoms move and depends on activation energy (E_a). Most diffusion studies predict the diffusion mechanism by comparing the value of E_a. In general, if E_a is known, the diffusion mechanism can be discussed. This means that the diffusion path can be predicted from the value of E_a. This is because the diffusion path is determined by diffusion mechanism. Diffusion mechanism is largely divided into vacancy diffusion and interstitial diffusion. In vacancy diffusion, diffusion occurs through the exchange of positions between atoms and vacancies. The vacancy diffusion is largely determined by the following two. First, the greater the number of adjacent vacancies, the greater the probability of diffusion. The smaller E_a required for the exchange of atoms and vacancies, the greater the probability of diffusion. E_a of self-diffusion through vacancy of well-known materials is as follows. Cu-2.2 eV [6], Ag-1.8 eV [7], Ni-2.9 eV [8], and Pt- 2.6 eV [9]. It can be seen that diffusion through vacancy occurs around 2 eV. If a fast diffusion path of two-dimensional vacancy, such as dislocation or grain boundary, is generated, diffusion may occur with an E_a smaller than 2 eV described above. For interstitial diffusion, diffusion occurs as interstitial atoms of much smaller size move to interstitial sites between matrix atoms. That is, since vacancy for diffusion is not required, the diffusion rate is faster than vacancy diffusion. Therefore, E_a required for diffusion is also much smaller than vacancy diffusion. Interstitial diffusion is used to describe the diffusion of H, C, N, and O into the metal. As explained in Chapter 1, the diffusing atoms try to be in the lowest energy state. In other words, if there is a path that can be moved with low energy, diffusion will occur through that path. Therefore, if I know the diffusion mechanism, I know how the atom diffuses.

The diffusion mechanism of metal is the best studied area of solid-state diffusion. In the case of self-diffusion of most fcc metal, it has the following characteristics. The D near the melting point is between about 10^{-8} cm^2/s and 10^{-9} cm^2/s, and D_0 is between about 10^{-2} cm^2/s and 1 cm^2/s. On the other hand, in the case of self-diffusion of bcc metal, the D near the melting point is between about 10^{-7} cm^2/s and 10^{-8} cm^2/s, which is about one order greater than that of fcc metal. For the self-diffusion of the hcp metal, the D near the melting point is about 10^{-8} cm^2/s, similar to that of the fcc metal. This is because fcc and hcp are both close-

packed. It is possible to predict how *D* is affected by the crystal structure through the result of the phase transition of Ti in Figure 6 [10)11)12)]. At the transition temperature of 1155K, the crystal structure changes from hcp Ti to bcc Ti. At this time, the *D* increases by about three times during the transformation from hcp to bcc. This indicates that the diffusion in the high-density hcp structure is relatively slow, while the diffusion of the bcc metal having a relatively low density is relatively fast. The same trend is shown in terms of E_a. The E_a of hcp Ti was about 1.6 eV, which is greater than that of bcc Ti, about 1.4 eV. From this result, it can be seen that a higher density crystal structure is more effective as a diffusion barrier.

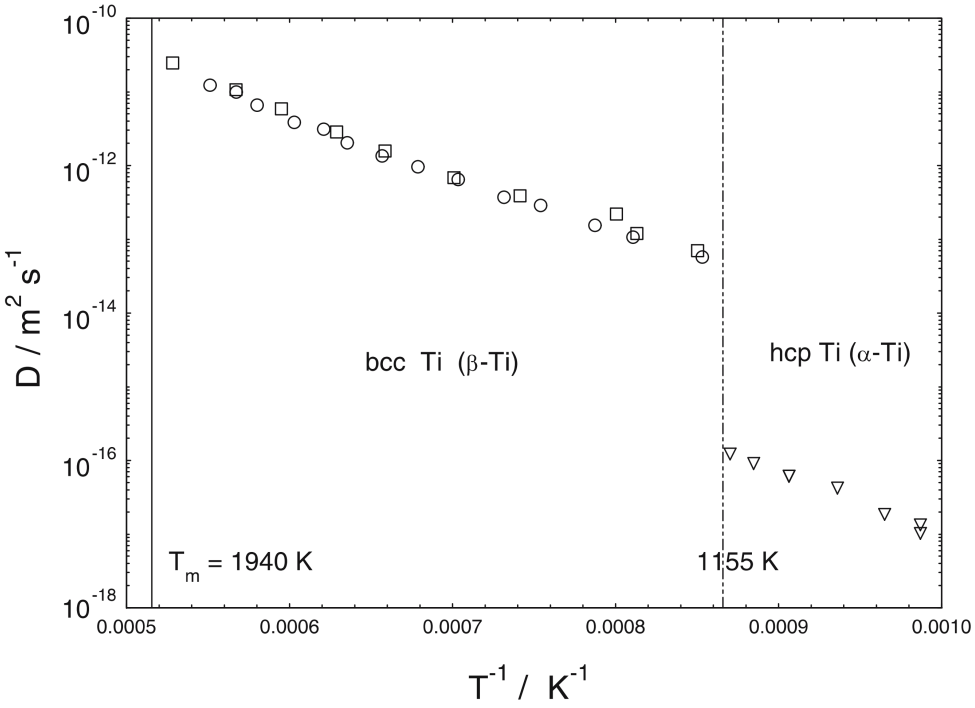

Fig 6. Relationship between Ti phase transition results and *D* [10)11)].

Figure 7 is the Arrhenius plot of *D* from the modified time-lag method using x-intercept and slope. For comparing, it also shows the Arrhenius plot of *D* from the depth profile method. First of all, as the graph maintains a straight line in the measurement temperature range (780-855°C), it means that there is no change in the diffusion mechanism in this temperature range. Compared with the 20-nm-thick PVD-Co(W), 8, 10, 12-nm-thick PVD-Co(W) has a relatively higher E_a and lower *D*. Also, there seems to be no significant

difference between the results of figure 7(a) using the x-intercept and figure 7(b) using the slope. Therefore, reliable results could be obtained by using both the x-intercept and the slope.

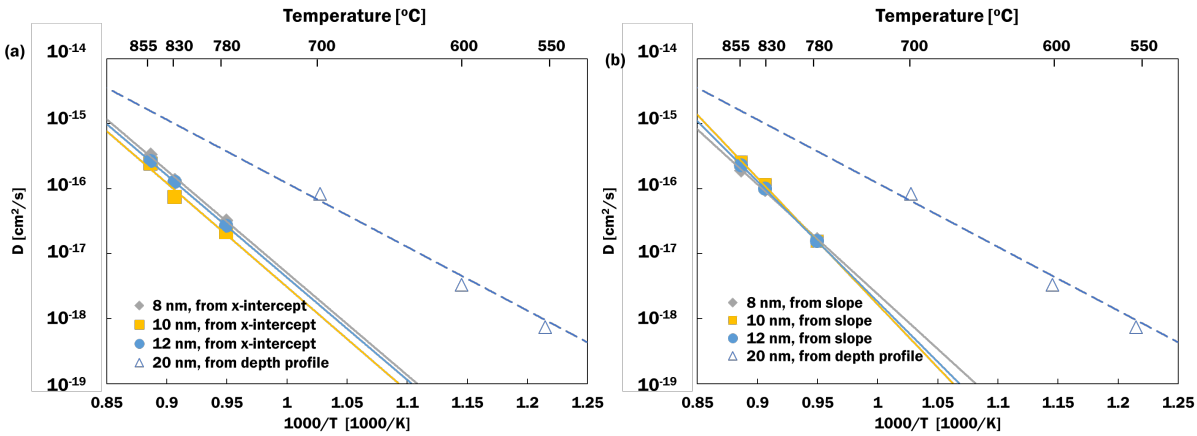

Fig 7. Arrhenius plot of D obtained by the (a) x-intercept and (b) slope at three annealing temperatures.

From the slope and y-intercept obtained from the Arrhenius plot, E_a and D_0 are calculated and compared. Figure 8 shows the change of E_a and D_0 according to the change of PVD-Co(W) thickness. From the results of the modified time-lag method for 8, 10, 12-nm-thick PVD-Co(W), it was confirmed that the barrier properties were still excellent even when the thickness of Co(W) was reduced from 20 nm to 8, 10, and 12 nm. Basically, high E_a indicates the absence of fast diffusion paths such as grain boundaries. All E_a in figure 8 has a high E_a near 3 eV. In general, reported E_a values for amorphous alloy for various metals are about 1-3 eV. [13] From these results, we predict that the current thinned PVD-Co(W) will have an amorphous structure. According to the results of chapter 2, in the case of 20-nm-thick PVD-Co(W), it was an amorphous-like structure in which a small amount of Cobalt existed in a partially crystallized state in the amorphous structure of Co(W).

I compare the experimental results of the XPS depth profile method for 20-nm-thick PVD-Co(W) and the modified time-lag method for 8, 10, 12-nm-thick PVD-Co(W). When the thin film was changed from 20 nm to 12nm, E_a increased about 2.0 eV. The cause of the increased E_a can be found in the relationship between the thickness of the thin film and the crystallinity. In a sandwich structure such as Cu/Co(W)/low-

k, the influence of the interface on both sides makes it difficult for atoms near the interface to move, and crystallization becomes difficult near the interface. On the other hand, since the central part of the thin film is not affected by the interface, the crystalline clusters surrounded by the amorphous material freely gather and crystallize. In other words, the thinner the film, the greater the influence of the interface, making crystallization difficult. The retardation of crystallization due to the presence of such an interface has been introduced in several previous studies [14),15)16)]. Thus, the thinner the thin film, the less likely nucleation will occur and, accordingly, the lower the probability of crystallization. As a result, 8, 10, 12-nm-thick PVD-Co(W) maintained the amorphous structure more firmly than 20-nm-thick PVD-Co(W) and E_a is predicted to increase. According to the results of related studies on the thickness and crystallization of the thin film, the thinner the thin film, the more inhibited the crystallization [17)18)19)20)]. As a result, we can predict that the thinner the thin film, the better the barrier properties.

Through the comparison of E_a in figure 8(a) and 8(b), I investigated which of the results obtained from the x-intercept and the slope is more valid. E_a obtained from the slope of figure 8(b) (3.4, 3.9, and 3.7eV) was about 0.5 eV larger than E_a obtained from the x-intercept of figure 8(a) (3.1, 3.2, and 3.1eV). There is a difference of about 15 % between the x-intercept and the slope, but, considering the first challenge of the modified time-lag method, the difference between the two is considered small.

The thickness dependence of PVD-Co(W) is also tried to analyze from the viewpoint of D_0. However, it is not easy to simply explain the physical interpretation of D_0. This is because D_0 is affected not only by the diffusion mechanism, but also by various nanostructure changes such as impurities, grain boundaries, and dislocations. So far, there have been no studies discussing the effect of D_0 in principle.

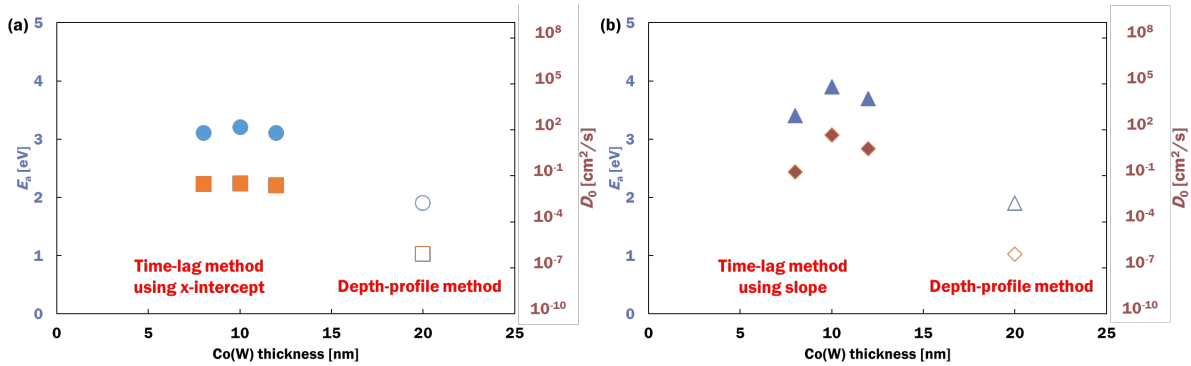

Fig 8. E_a and D_0 according to the change of PVD-Co(W) thickness obtained from the (a) x-intercept and (b) slope.

4.4 The effect of selection of data near the lower detection limit

All of the Q-t plots discussed above were used by simply employing data exceeding the lower detection limit. However, since data near the lower detection limit are greatly affected by experimental error, it is necessary to investigate how much the x-intercept (ie, *D*) will change depending on whether the data is selected or not. Therefore, when the error bar of the measurement data is smaller than the lower detection limit, we investigated how the result would change if the corresponding data was excluded.

The nine Q-t plots in figure 9 are the results before and after the selection of the corresponding data. The x-intercept and slope were obtained by using the measured data of the Q-t plot as a linear approximate straight line of the method of least squares. The blue point is the original data, and the orange point is the result after excluding the corresponding data. In some Q-t plots, as the data was excluded, the number of measurements decreased and the x-intercept shortened. However, the effect was limited and the change in *D* was about 10%. However, with respect to the result of 855°C-12nm sample, except for the data of 1200 seconds, the value of *D* was significantly changed as the standard deviation of the remaining experimental data increased. However, this is not due to excluding the corresponding data, but because there was no data with a long annealing time.

It can be seen from the above results as follows. (1) If the error bar of the data is lower than the detection limit, it is excluded. (2) The standard deviation of the data should be minimized by acquiring a sufficient number of experimental data. (3) From the viewpoint of data reliability, it is necessary to minimize the decrease in the value of coefficient of determination (R^2) even when data near the detection lower limit is omitted. For example, it is necessary to establish a rule such as "when data near the lower detection limit is omitted, it is not excluded if R^2 is 0.9 or less".

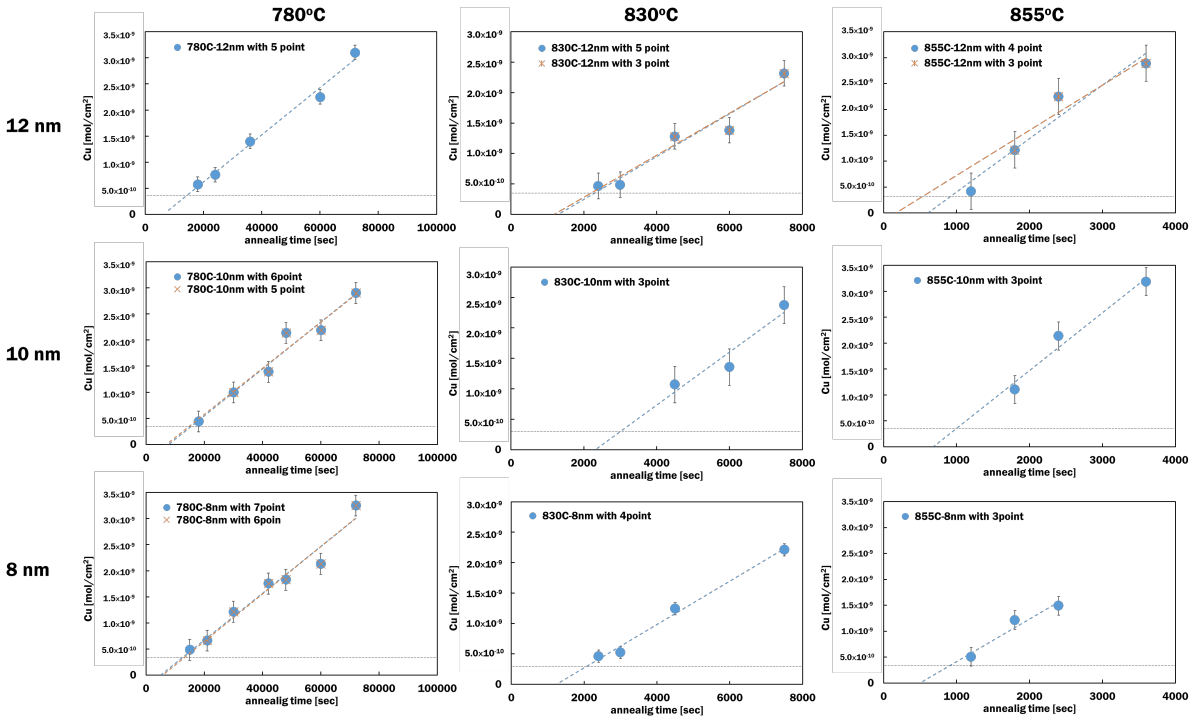

Fig 9. The nine Q-t plots before and after the selection of the data near the lower detection limit.

Figure 10 shows four types of Arrhenius plots. (a) is an Arrhenius plot of *D* obtained from the x-intercept before excluding data near the lower detection limit, (b) is an Arrhenius plot of D obtained from the slope before excluding data near the lower detection limit, (c) is an Arrhenius plot of D obtained from the x-intercept after excluding data near the lower detection limit, (d) is an Arrhenius plot of D obtained from the slope after excluding data near the lower detection limit. As the data near the lower detection limit was excluded, the activation energy was changed, but the degree of the change was different according to the thickness of the barrier film. In the case of the 8-nm-thick barrier (3.1 eV → 3.3 eV) and the 10-nm-thick barrier (3.2 eV → 3.0 eV), the change in activation energy is very small, 0.2 eV, which is 10% or less. In the 12-nm-thick barrier (3.1 eV → 4.7 eV), there was a relatively large change due to the lack of data where the annealing time was long. In addition, 4.7 eV is an impossibly high activation energy, and a value of this level is not physically possible. In other words, the result of the 12-nm-thick barrier is simply an error due to lack of data, and I think that the activation energy of the 12-nm-thick barrier is 3.1eV.

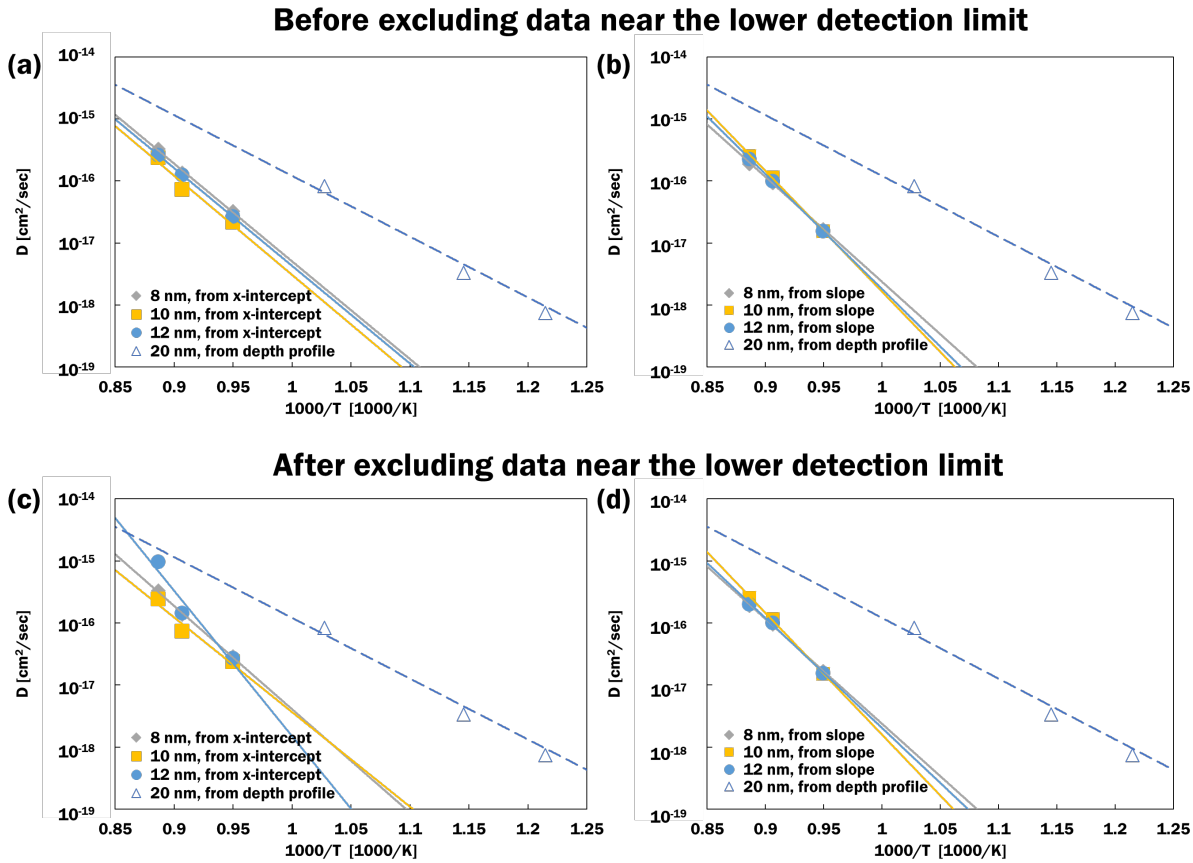

Fig 10. The four types of Arrhenius plots.

4.5 Conclusion

This chapter mainly deals with the quantitative evaluation of the barrier properties of thinned PVD-Co(W). The modified time-lag method established in Chapter 3 was applied to PVD-Co(W) with various thickness to investigate the thickness dependence of barrier properties. Evaluating the thickness dependence of barrier properties with a modified time-lag method is also a new achievement of my study. From my experimental results, even with the thinned barrier, D remained almost constant. Rather, as it became thinner, D showed a tendency to decrease slightly. By deriving E_a and D_0, the nanostructure of PVD-Co(W) is estimated. From the result, it was confirmed that the thinned PVD-Co(W) has excellent barrier properties. In addition, since similar results were obtained using both the slope and the x-intercept, my modified time-lag method proved to be a useful method again. In addition to the barrier properties, crystallinity was additionally examined. From the result of XRD, it was confirmed that crystallization of Co and W did not occur. The reason for the superiority of the barrier properties was proved by combining the crystallinity results and the barrier properties results.

Reference

1) J. Noguchi, T. Saito, N. Ohashi, H. Ashihara, H. Maruyama, M. Kubo, H. Yamaguchi, D. Ryuzaki, K. I. Takeda and K. Hinode, IEEE Int. Reliab. Phys. Symp. Proc. **2001-Janua**, 355 (2001).

2) H. Chatham, *Surf. Coatings Technol.*, 1996, 78, 1–9.

3) T. Nishizawa and K. Ishida, Bull. Alloy Phase Diagrams **5** [2], 161 (1984).

4) H. Wang, A. Tiwari, X. Zhang, A. Kvit and J. Narayan, Appl. Phys. Lett. **81** [8], 1453 (2002).

5) S. Herth, M. Eggersmann, P. D. Eversheim and R. Würschum, J. Appl. Phys. **95** [9], 5075 (2004).

6) S. J. Rothman and N. L. Peterson, Phys. status solidi **35** [1], 305 (1969).

7) N. Q. Lam, S. J. Rothman, H. Mehrer and L. J. Nowicki, Phys. status solidi **57** [1], 225 (1973).

8) K. Maier, H. Mehrer, E. Lessmann and W. Schüle, Phys. status solidi **78** [2], 689 (1976).

9) G. Rein, H. Mehrer and K. Maier, Phys. status solidi **45** [1], 253 (1978).

10) J. F. Murdock, T. S. Lundy and E. E. Stansbury, Acta Metall. **12** [9], 1033 (1964).

11) U. Köhler and C. Herzig, Phys. status solidi **144** [1], 243 (1987).

12) F. Dyment, Titan. ’80, Sci. Technol. Proc. Fourth Int. Conf. Titanium, Kyoto, Japan, 519 (1980).

13) F. Faupel, W. Frank, M. P. Macht, H. Mehrer, V. Naundorf, K. Rätzke, H. R. Schober, S. K. Sharma and H. Teichler, *Rev. Mod. Phys.*, 2003, 75, 237–280.

14) G. V. M. Williams, A. Bittar and H. J. Trodahl, J. Appl. Phys. **67** [4], 1874 (1990).

15) M. Zacharias, J. Bläsing, P. Veit, L. Tsybeskov, K. Hirschman and P. M. Fauchet, Appl. Phys. Lett. **74** [18], 2614 (1999).

16) M. Zacharias and P. Streitenberger, Phys. Rev. B - Condens. Matter Mater. Phys. **62** [12], 8391 (2000).

17) Z. H. Lu, D. J. Lockwood and J. M. Baribeau, Solid. State. Electron. **40** [1–8], 197 (1996).

18) S. Miyazaki, Y. Ihara and M. Hirose, J. Non. Cryst. Solids **97**–**98** [PART 2], 887 (1987).

19) M. Zacharias, J. Bläsing, P. Veit, L. Tsybeskov, K. Hirschman and P. M. Fauchet, Appl. Phys. Lett. **74** [18], 2614 (1999).

20) J. Gonzalez-Hernandez and R. Tsu, Appl. Phys. Lett. **42** [1], 90 (1998).

Chapter 5 Conclusion

This dissertation focused on the development of a new method for the quantitative evaluation of barrier properties for continuously miniaturized Cu interconnect in ULSI devices. Quantitative evaluation of barrier properties is essential to make an excellent barrier layer in Cu interconnects and will help us understand the diffusion phenomenon of continuously miniaturized Cu interconnects.

In chapter 1, I summarized the issues arising from the miniaturized Cu interconnects so far and discussed the solution. Cu generally diffuses into Si in the semiconductor manufacturing process, creating an active deep level. Therefore, the development of effective diffusion barriers for Cu interconnects is the most important issue. Cu interconnects generally have Cu/liner/barrier/low-k structures. The latest ULSI device needs to have a thinner liner/barrier layer in order to maintain the cross-sectional area of Cu. However, there are some difficulties when manufacturing technology is extremely miniaturized; (1) resistance-capacitive (RC) signal delay, (2) electro-migration (EM) and stress-induced voiding (SIV). Subsequently, specific requirements to solve the issues were summarized from the viewpoints of material, structural, and manufacturing; (1) diffusion barrier should not to react chemically with Cu, (2) diffusion barrier should not dissolve in Cu. In order to satisfy these requirements, I proposed amorphous Co(W) single layer made by Physical Vapor Deposition (PVD). The methods of evaluating barrier properties for Cu diffusion also have been systematically organized; (1) qualitative, (2) semi-quantitative, and (3) quantitative evaluation. (1) The method in which any numerical discussion cannot be made from the measurement results is called a qualitative evaluation method. The qualitative evaluation method only evaluates whether the barrier layer prevents diffusion or whether the barrier layer has lost its barrier properties due to diffusion. (2) The semi-quantitative evaluation method can numerically evaluate the change in barrier properties. In this method, the superiority and inferiority of the barrier properties are determined by comparing the experimental results caused by the change of the experimental conditions. However, since only the experimental results such as sheet resistance, leakage current, and RMS by diffusion are compared, the intrinsic barrier properties of the barrier layer are unknown. (3) A method capable of directly measuring the quantity of diffused Cu is called

a quantitative evaluation method. Since the quantity of diffused Cu is directly used, the barrier properties can be evaluated most accurately. Finally, the importance of quantitative evaluation of Cu diffusion represented by diffusion coefficient (*D*) was explained.

In Chapter 2, the quantitative evaluation of the barrier properties of 20-nm-thick PVD-Co(W) for Cu was covered. Its principles and experimental methods were also explained. Samples of the stacked structure [100-nm-thick Cu / 20-nm-thick PVD-Co(W) / 100-nm-thick SiO_2 / Si wafer] were annealed by rapid thermal anneal (RTA). After annealing, the concentration profile of Cu diffused into PVD-Co(W) was obtained by X-ray Photoelectron Spectroscopy (XPS). At this time, for the first time, the back-side depth profile method, which measures from the rear of the sample, was applied. The experimental concentration profile of Cu obtained by XPS was then fitted to a theoretical profile based on Fick's second law and *D* was determined. For the Arrhenius plot of *D* of Cu in PVD-Co(W) film with six different W concentrations, the logarithm of *D* varied linearly against reciprocal of temperature in the range of 500 to 700ºC. This means that the diffusion mechanism of Cu in Co(W) was unchanged in this temperature range. At low W concentrations (23, 35, 43 at. %), the E_a slightly increased with the W concentration, while E_a fluctuated at higher W concentrations. *D* at 500°C was compared with ALD-Co(W) with W 20 at. % and PVD-TaN, because it was the closest to the temperature used in the back end of line (BEOL) manufacturing. Of the W concentrations tested, PVD-Co(W) with W 43 at. % showed the lowest *D*, and thus expecting better Cu diffusion barrier properties than PVD-Ta/TaN and ALD-Co(W). Therefore, PVD-Co(W) with W 43 at. % was considered to be optimal for BEOL manufacturing. Crystallinity and resistivity results were also measured to find the optimal composition of PVD-Co(W) single layer. The significance of this chapter is that it is a starting point for quantitative evaluation of the barrier properties of PVD-Co(W) single layer. If quantitative evaluation is successfully introduced, it will be possible to predict what will happen in the initial stage of thin film growth.

Chapter 3 deals with the process of establishing a quantitative evaluation method of barrier properties for thinned PVD-Co(W). A quantitative evaluation of the barrier properties using the depth profile

method has already been completed in chapter 2. However, the depth profile method is difficult to apply to ultra-thin films such as 1 or 2 nm. This is because, in the depth profile method, a barrier layer having a certain thickness is essential for the concentration profile of diffused Cu. Therefore, it is essential to develop a method capable of quantitative evaluation of ultra-thin films. First of all, quantitative evaluation using atomic probe tomography (APT) was attempted. Then, considering the reason why the APT measurement failed, I could obtain the experimental results using Wavelength Dispersive X-ray Fluorescence (WDXRF) and Inductively coupled plasma-optical emission spectrometry (ICP-OES). For this, I developed the modified time-lag method to measure the trace quantity of Cu passing through the Co(W) barrier layer. The structure for the modified time-lag method was [100-nm-thick Cu/10-nm-thick Co(W)/1000-nm-thick sputtered SiO_2/100-nm-thick Ti/150-nm-thick Co(W)/100-nm-thick thermal SiO_2/Si substrate]. The whole procedure of the modified time-lag method after annealing was as follows. (1) [100-nm-thick Cu and 10-nm-thick Co(W) structure] were etched by $FeCl_3$ solution. (2) The diffused Cu in the [1000-nm-thick SiO_2/100-nm-thick Ti/150-nm-thick Co(W) structure] was dissolved with 1HF (5%) + 1HNO_3 (5%) mixed solution. (3) The Cu concentration (ppb) in the mixed solution was measured using ICP-OES. (4) It was converted Cu concentration (ppb) into the quantity of Cu atoms per unit area passing through the barrier layer (mol/cm^2). By repeating these procedures at various annealing temperatures, *D* was obtained. I can obtain Q-t plot from the x-axis represents annealing time (t) and the y-axis represents the number of diffused Cu moles per unit area (Q). The slope in Q-t plot denotes a flux of the substance passing through the barrier. The x-intercept in Q-t plot is called "time-lag". According to the analytical solution of the diffusion equation, relations between *D* and x-intercept or slope are given by,

$$\text{(x intercept, i.e. time-lag)} = \frac{L^2}{6D} \qquad (1),$$

$$\text{(slope, i.e. flux)} = \frac{DC_0}{L} \qquad (2),$$

where C_0 is the concentration of diffused substance at the upstream interface of the barrier, and *L* is a thickness of the barrier. *D* is, therefore, obtained from the time-lag using equation (1), since *L* is known in general prior to the measurement. *D* is also obtained from the slope using equation (2), since C_0 is the experimental

condition. To prove the validity of the modified time-lag method, two *D* values obtained using the x-intercept and slope from the Q-t plot were compared. It was confirmed that the results obtained from the modified time-lag method are valid. Through comparison with the result of 20-nm-thick PVD-Co(W), it was possible to predict the change in barrier properties according to the change in the thickness of the thin film. The barrier properties of PVD-Co(W) were quantitatively evaluated using the modified time-lag method, and the reliability of the results was also secured.

Chapter 4 mainly deals with the quantitative evaluation of the barrier properties of thinned PVD-Co(W). The modified time-lag method established in Chapter 3 was used to discuss the thickness dependence and temperature dependence of the barrier properties of PVD-Co(W) layer. The thickness dependence of barrier properties is important because the starting point for miniaturization of Cu interconnects is the thickness dependence of the barrier layer. The barrier properties were quantitatively evaluated by experimentally estimating the *D* of Cu for 8, 10, 12-nm-thick PVD-Co(W) layer in the 780, 830, and 855°C. *D* increases as the annealing temperature increases. At the same annealing temperature, *D* tends to decrease slightly as the PVD-Co(W) barrier becomes thinner. Basically, as the thin film becomes thinner, the probability of nucleation required for crystallization decreases. Therefore, the thinner the thin film, the more improved the amorphous state could exist. At this time, the activation energy (E_a) for Cu diffusion in the 780, 830, and 855°C was obtained to explain the diffusion behavior from the nanostructure point of view. From the results, it was confirmed that the thinned PVD-Co(W) has excellent barrier properties. In addition, since similar results were obtained using both the slope and the x-intercept in Q-t plot, modified time-lag method proved to be a useful method again. I also discussed crystallinity. From the result of XRD, it was confirmed that crystallization of Co and W did not occur. The reason for the superiority of the barrier properties was proved by combining the crystallinity results and the barrier properties results. The adhesion was also additionally discussed. To evaluate adhesion, the contact angle of the cross-sectional image of SEM was used. From the results, the dependence of the adhesion on the change of the W concentration was investigated. The excellent adhesion of PVD-Co(W) was confirmed through comparison with the results of ALD-Co(W).

5.1 Achievement through my research

(1) The quantitative barrier properties of PVD-Co(W) were evaluated using the back-side depth profile method to avoid knock-on phenomenon.

In my group's previous work, quantitative evaluation of barrier properties using the depth profile method for CVD-Co(W) was completed. However, unlike CVD-Co(W), PVD-Co(W) is greatly affected by the substrate. When PVD-Co(W) was deposited on Cu, evaluation of the original barrier properties of PVD-Co(W) was impossible due to the influence of substrate Cu. So, on the contrary, after depositing Cu on PVD-Co(W), quantitative evaluation of the barrier properties was performed for the first time using the depth profile method in the opposite direction. From this result, it was possible to quantitatively obtain the correct barrier properties of PVD-Co(W) in the actual Cu interconnects structure.

(2) For the first time, time-lag method for Cu interconnects has established to quantitatively measure the barrier properties of the thinned barrier layer.

There are various methods for evaluating barrier properties, but most of the barrier property evaluation methods so far have been qualitative evaluation with laboratory-level as described in Chapter 1. Therefore, it is meaningful if the barrier properties of ultra-thin films can be quantitatively evaluated in the actual manufacturing process. There are quantitative evaluation methods such as the depth profile method and the BTS-TVS method, but there is no method to evaluate the D of an ultra-thin film. In an actual semiconductor manufacturing process, it is known that barrier properties are mainly evaluated through only TDDB measurement. However, it is not possible to know why the barrier is deteriorated by this method. Since only the time at which the barrier is deteriorated can be known, this result alone cannot be used to develop barrier materials. However, if the modified time-lag method is used, not only D can be calculated, but also the diffusion path can be specified through the investigation of the temperature dependence of diffusion. Using this result, it is possible to explain how to better prevent the diffusion from the principle. Then, material development will be possible more efficiently and more quickly. The modified time-lag method will be the first method to properly evaluate the barrier properties of a 1-nm-thick barrier layer. The

thinner the thin film, the greater the influence of the initial stage of growth, so the composition and crystallinity may be different from those of the thick film. Therefore, if the barrier properties can be quantitatively evaluated even in ultra-thin films, it is possible to predict what will happen in the initial stage of thin film growth. Also, since the methodology has been established, it is necessary to apply the modified time-lag method to various barrier materials. At this time, the barrier material is limited to a material that does not form a compound with Cu, but a material that forms a compound with Cu cannot be a barrier candidate material from the beginning. Therefore, material selection does not limit the scope of application of the modified time-lag method.

(3) The time-lag method was used for the first time to find out whether the barrier properties change according to the thickness of the barrier layer.

It is important to investigate whether the barrier properties change as the thickness of the barrier layer becomes thinner. The miniaturization of Cu interconnects is an irresistible trend. Thinning the film is the most important priority. Under this premise, it is really important to know if the barrier properties of the thinned barrier layer are maintained. By using modified time-lag method, it is theoretically possible to evaluate the barrier properties, no matter how thin the barrier layer is.

In the case of the PVD-Co(W) of 10 nm or less discussed here, it was possible to quantitatively evaluate the barrier properties successfully. As a result of comparing the D and E_a values obtained at this time, it was confirmed that it had better barrier properties than that of 20nm PVD-Co(W). From this result, the possibility of thinned PVD-Co(W) was confirmed.

5.2 My proposal from the results of this study

This chapter deals with the proposal from results of my study. In particular, these contents are expected to help increase the efficiency of the manufacturing process of Cu interconnects. First of all, I deal with the optimal conditions for using PVD-Co(W) as a liner/barrier layer. With the barrier properties as the main, I propose what conditions PVD-Co(W) is best to use. Finally, it deals with the possibilities of PVD in making ultra-thin films.

5.2.1 An evaluation method that uses both the x-intercept and slope.

When determining D using the x-intercept ($D_{\text{x-intercept}}$), the x-intercept can be directly converted to D (Equation 1). On the other hand, when determining D using the slope (D_{slope}), C_0 is required to transform D from the slope (Equation 2). In this study, since the D_{slope} and the $D_{\text{x-intercept}}$ are not significantly different, it is sufficient to use only the x-intercept. However, when measuring the 1-nm-thick barrier in the future, it will be difficult to use only the x-intercept because the x-intercept becomes very small. Therefore, it is necessary to use C_0 and the slope at that time.

From the Arrhenius equation for 8-nm-thick PVD-Co(W) obtained in Chapter 4, $D_{\text{x-intercept}}$ can be obtained as follows.

$$D = 2.8 \times 10^{-2} exp\left(\frac{3.1}{kT}\right)[cm^2/s] \qquad (3),$$

Using this formula, the thickness dependence and temperature dependence of Co(W) were predicted. Figure 1 shows how the x-intercept and slope of Q-t plot change according to the change in the thickness of the Co(W) barrier and the change in the annealing temperature based on the results obtained from the 8-nm-thick PVD-Co(W). The left side of figure 1 is the prediction of the change in Q-t plot when the thickness of the thin film is changed using D at 780ºC. The solid line is the experimental result, and the dotted line is the predicted result. The thinner the barrier film, the shorter the x-intercept. The right side of figure 1 is a prediction of the change in Q-t plot when the annealing temperature is changed using E_a of 8 nm. The solid line is the experimental result, and the dotted line is the predicted result. The x-intercept gets longer when the temperature is lowered. According to the calculation using the measurement result of 780ºC-8nm, the x-

intercept becomes 896 s (700°C) and 63,879 s (600°C) when the film thickness is reduced to 1 nm.

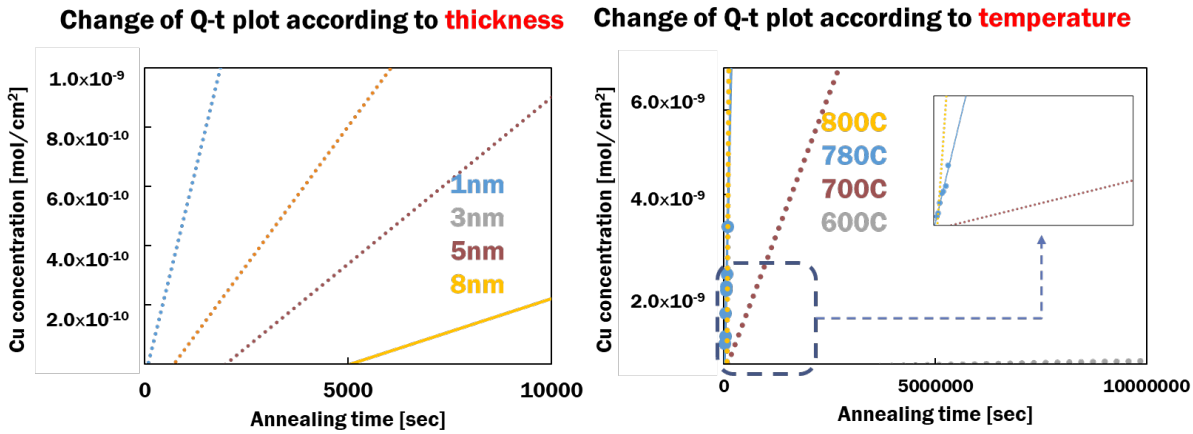

Fig 1. The x-intercept and slope change according to the change in the thickness of the barrier and the change in the annealing temperature.

Figure 2 is a Q-t plot of 690°C-1nm, 700°C-1nm, and 710°C-1nm samples predicted using the result of equation (3). The time-lag of 690°C-1nm, 700°C-1nm, and 710°C-1nm is 1304, 882, and 612s, respectively, and the difference is not significant. These are the prediction results when the annealing time is approximately 24 times (6 hours), 28 times (7 hours), 32 times (8 hours), 36 times (9 hours), and 40 times (10 hours) of the time-lag. Since D can be measured at both the x-intercept and the slope with a total of 40 hours of annealing, C_0 can also be obtained from these two results. If D for three temperatures is obtained, it is also possible to evaluate the temperature dependence. Temperature dependence can be evaluated by annealing for 120 hours. This is a sufficiently realistic experimental condition. When measuring 1-nm-thick barrier, it is necessary to evaluate the barrier properties from the Arrhenius plot in the temperature range where both the x-intercept and the slope are well measured.

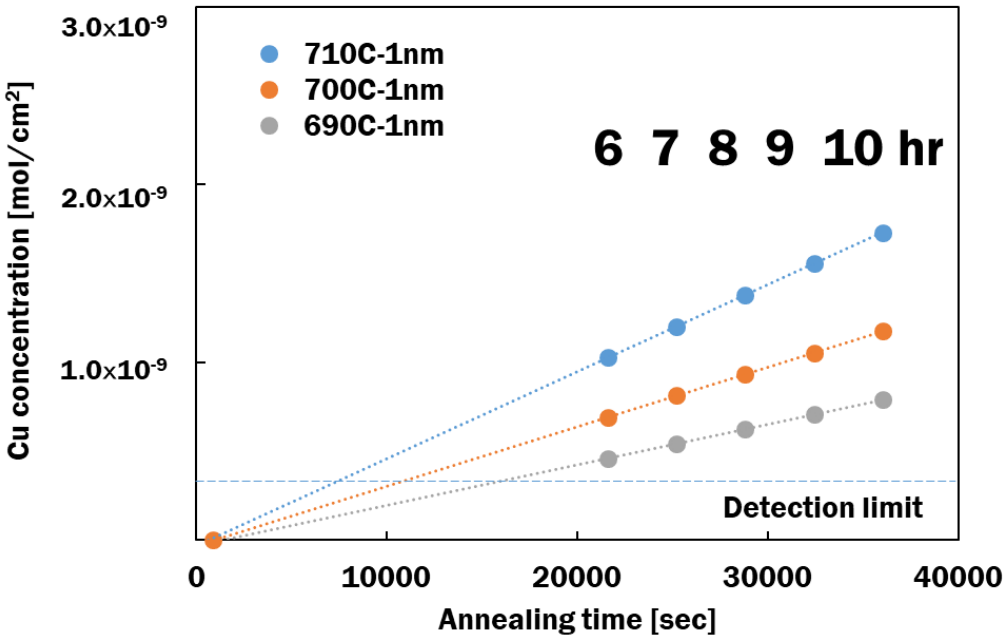

Fig 2. Q-t plot of 690°C-1nm, 700°C-1nm, and 710°C-1nm samples.

It may not be realistic to find the x-intercept in a 1-nm-thick barrier. For example, in the case of 600°C-1nm, it is necessary to perform annealing for about 420 hours in order to diffuse to the detection limit. Conversely, in the case of 800°C-1nm, since the expected time-lag of 200 seconds is too short, it can be greatly affected by errors during measurement. Therefore, in that case, it is necessary to obtain D from the slope using the correct C_0 at 1-nm-thick barrier. There are two ways to obtain C_0 here.

(1) After finding the temperature at which stable $D_{\text{x-intercept}}$ and D_{slope} can be obtained through Q-t plot, C_0 is calculated using the two D values.

(2) C_0 is calculated from the phase diagram data.

When the temperature dependence of C_0 is small, the method (1) is used, and when the temperature dependence of C_0 is large, the method (2) can be used to obtain D from the slope.

5.2.2 Optimal thin film conditions for using PVD-Co(W) as a liner/barrier layer

First, I tried to find the thickness of PVD-Co(W) that has optimal barrier properties. Naturally, the thicker PVD-Co(W), the less Cu diffusion. What I am discussing here is the inherent barrier properties of a

barrier layer (I.e., the ability to prevent diffusion). Using the depth profile method and modified time-lag method, the thickness of PVD-Co(W) was changed from 20 nm to 8 nm, and the change of barrier properties was verified from the quantitative evaluation results. As a result, excellent barrier properties were maintained in all thicknesses of PVD-Co(W), and it was confirmed that the barrier properties improved as the thickness became thinner. The W composition at this time was 23 [W/Co+W].

Subsequently, using PVD-Co(W) having 6 different W concentrations, an optimal composition with the best barrier properties was found. At this time, the thickness of PVD-Co(W) was maintained at 20 nm. From the result of the concentration dependence of 20-nm-thick PVD-Co(W), it was confirmed that PVD-Co(W) of W 43 at. % had the largest activation energy for Cu diffusion. Through this, it was confirmed that PVD-Co (W) of W 43 at% has the excellent barrier properties. In addition, the cause of excellent barrier properties was predicted through crystallinity evaluation using XRD. In 20-nm-thick Co(W), a very small Co peak appeared at low W concentration, but the Co peak disappeared as the Co(W) thin film became thinner to 12, 10, and 8 nm. As the thickness of the thin film decreased, the possibility of nucleation decreased, and Co(W) was no longer crystallized. As a result, the thinned Co(W) exhibits a completely amorphous structure, which is considered to have improved barrier properties.

5.2.3 A single layer incorporating barrier properties and adhesion properties

Co(W), the material chosen in my research, plays a role as a liner layer as well as a barrier layer. The top priority in the ULSI field is miniaturization. However, even with miniaturization, barrier layer and liner layer are required. Therefore, an alloy material that exhibits both properties is needed. A pioneering study by Shimizu et al. has already confirmed the possibility of Co(W). Through the evaluation of the adhesion of my research, I found the following facts. First, as the W concentration increased (Co concentration decrease), the adhesion decreased. This is valid from a lattice misfit perspective. From the point of view of the crystal structure, Co has an hcp structure and has excellent compatibility at the interface with Cu, which is an fcc structure. And even with the same Co(W), it was confirmed that the adhesion was

also different if the deposition method was different. As a result of comparing the adhesion of ALD-Co(W) of Shima et al. to that of my PVD-Co(W), the change of adhesion began at a temperature of 200ºC higher for PVD-Co(W). This means that PVD-Co(W) has much better absolute adhesion than ALD-Co(W). This result is thought to be due to the high bond energy between PVD-Co(W) and Cu.

The use of a single layer incorporating such barrier properties and adhesion properties will improve the following points in Cu interconnects. (1) It is very advantageous to make ultra-thin films. (2) A single layer is also effective in lowering the overall resistance of Cu interconnects. Conventional metal compound barriers such as TaN and alloy barriers such as Co(W) have higher resistivity than pure Cu. Therefore, increasing the cross-sectional area of Cu rather than lowering the resistivity of the barrier layer itself is effective in lowering the overall resistance of the Cu wiring, and can be realized using a single layer. (3) Since the deposition process can be reduced by one step, the cost of manufacturing Cu interconnects can be lowered.

5.2.4 The need for a metal liner/barrier layer

The liner/barrier layer of Cu interconnects must be a conductor. From the point of view of R/C delay, while Cu interconnects is miniaturized, the resistance of Cu interconnects should not increase at the same time. It looks like a contradiction. As a solution, the cross-sectional area of the liner/barrier single layer explained in the previous chapter has to be reduced to maintain the cross-sectional area of Cu. At this time, two options are available. The first is to choose an insulator material that is as thin as a monolayer and has excellent barrier properties but is not electrically conductive. The second is to select a conductor material with excellent electrical conductivity, although a certain thickness is required to express excellent barrier properties. Conductor barriers are more preferred than insulator barriers. If the liner/barrier layer is applied only to the side walls of Cu interconnects, the insulator liner/barrier layer will not have any problem. However, in the case of via hole of Cu interconnects, a liner/barrier layer is also deposited at the bottom, but if it is deposited as an insulator, the via hole will not work. If an insulator is to be used on this bottom part, only the

bottom part needs to be selectively etched after in the next process. This is very inefficient and difficult.

In terms of resistivity, a metal liner/barrier layer is required. The thinner the thin film, the greater the influence of the surface oxide layer, so it is difficult to measure the resistivity of pure Co(W). However, it is possible to predict the resistivity of Cu, Co, and W of an ultra-thin film based on the FM (Fuchs-Sondheimer)-MS (Mayadas-Shatzkes) model. In the FS-MS model, the phenomenon of increasing resistivity as the thin film becomes thinner is explained by surface scattering and grain boundary scattering. Figure 3 shows the results of predicting the resistivity of Cu, Co, and W according to the thickness using the FS-MS model. In this case, P factor: 0.52 and R factor: 0.43, which are frequently used for sputtering Cu, were used. Since there is no data on the P factor and R factor for Co and W, Cu data was inevitably used, but the trend can be predicted. First, for all thin films, the resistivity increases rapidly at 5 nm or less due to the thin film effect. According to the FS-MS model, the resistivity of the thin film is proportional to $\rho_0 \times {}^{\lambda}/_{d}$. where ρ_0 is the resistivity of the bulk material, λ is the electron mean free path of the bulk material, and d is the wiring width. Since, the λ to Co (7.8 nm) is significantly smaller than the λ to Cu (39.9 nm), the resistivity is reversed below wiring with of 5 nm. Accordingly, at 1 nm, the advantage of Cu wiring is lost, and in this case, it is necessary to use a material having a short λ such as Co as the wiring material. In the case of W, the λ (19.1 nm) is smaller than that of Cu, but the difference is not as large as that of Co, so the resistivity is still higher than that of Cu at 1 nm.

In general, since alloys are made by substituting other metals as impurities in the crystal structure of a pure metal, the movement of free electrons is hindered by distortion of the crystal structure. Therefore, when a pure metal becomes an alloy, ρ_0 increases. Unlike ρ_0, information on λ is limited, and moreover, it cannot be known because few studies on λ of alloys have been conducted. If the λ becomes intermediate between the λ of Co and W due to the alloying of Co(W), the resistivity of Co(W) at 1 nm can be similar to that of Cu. Therefore, I propose that in this study, a Co(W) liner/barrier layer of conductors is required.

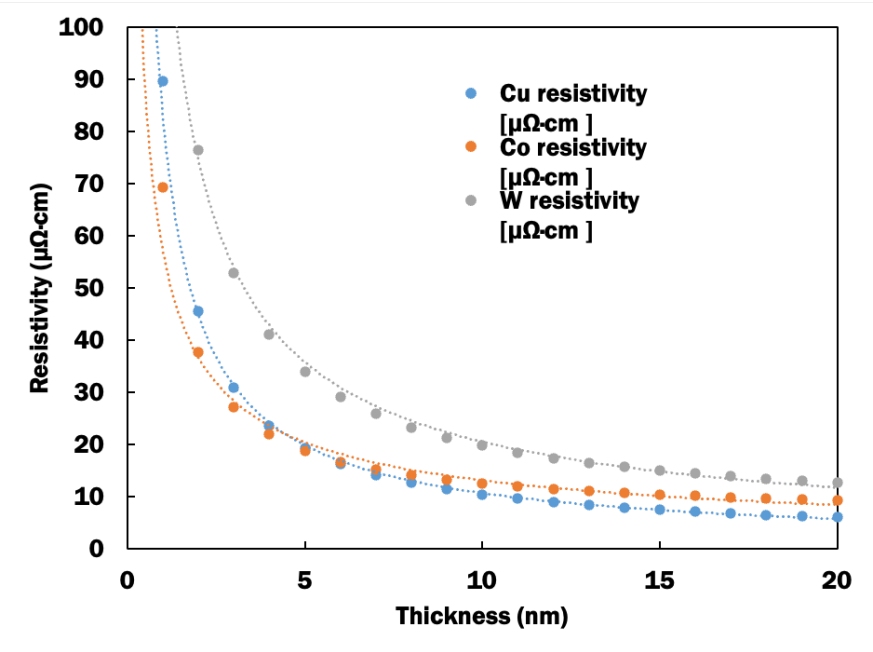

Fig 3. The predicting resistivity of Cu, Co, and W according to the thickness using the FS-MS model.

5.2.5 The possibility of PVD for extremely thin barrier layer such as 1 nm

When Shimizu et al. first quantitatively evaluated the barrier properties using Co(W), they deposited a Co(W) layer using ALD and CVD. As a result of their study, the excellent barrier properties of ALD/CVD-Co(W) were demonstrated. However, there were also some limitations. The most serious problem was that the film was not flat. This fact can be confirmed in the TEM cross-sectional picture of 20-nm-thick ALD/CVD-Co(W). It was uneven around the grain boundary. This is probably because the thin film was grown in the form of Volmer-Weber growth due to the low nucleation density of ALD/CVD. If 1-nm-thick ALD/CVD-Co(W) is made under these conditions, the thin film will be discontinuous due to the low nucleation density. On the other hand, PVD is much more suitable for making ultra-thin films like 1 nm thanks to its high nucleation density. So, I succeeded in quantitatively evaluating the barrier properties for PVD-Co(W) for the first time considering the excellent barrier properties of Co(W) and the superiority of producing ultra-thin films of PVD.

If a thin film using PVD is used for the barrier layer of Cu interconnects, improvements can be found from the following viewpoints. (1) It is possible to manufacture a thin and continuous barrier thin film.

Thanks to the high nucleation density mentioned above, it is possible to produce a continuous thin film of 1 nm. Then, it is possible to manufacture a continuous and flat thin film even on a Cu interconnects whose width is further reduced due to miniaturization. (2) Manufacturing process efficiency can be expected. Currently, most of the existing Cu interconnects deposition processes are based on PVD. The introduction of ALD was considered because of the need for a thin film of the atomic layer, but since PVD can be used continuously for Cu interconnects where the aspect ratio is not large, additional equipment is not required.

5.3 Future studies

(1) Possibility for quantitative evaluation of barrier properties even for 1 nm barrier layers

Several challenges remain to apply the time-lag method to a thin film of about 1 nm, which is much thinner than now. First of all, process error should be lowered. The thinner the barrier layer, the shorter the time-lag. Since the process error that occurs during measurement is not change, the error of time-lag becomes relatively large as the barrier layer becomes thinner. Therefore, it is necessary to increase the accuracy. For this, it is necessary to increase the performance of measurement using the more precise equipment such as ICP-MS which can measure a finer amount than ICP-OES.

(2) Investigating how the D and E_a vary according to the change in the composition of Co(W)

It is important to find the optimum composition with the best barrier properties. Therefore, it is necessary to investigate the composition dependence of Co and W of PVD-Co(W). According to previous research results, in 20-nm-thick PVD-Co(W), the barrier property tends to be improved with the increase of the W composition. However, no one knows whether the same results will be achieved for ultra-thin films such as 1 nm. In particular, since 1 nm is the initial stage of thin film growth, different results may appear from 20 nm in which the thin film was grown.

(3) Applicability to quantitative evaluation of barrier properties of oxygen or moisture barrier

Barrier layer should actually prevent the diffusion of moisture and oxygen as well as Cu. Modified time-lag method will be able to measure not only the barrier properties for Cu, but also the barrier properties for the SiO_2 (or low-k materials) on the opposite side. Diffusion occurs not only between Cu and the barrier layer but also between the barrier layer and SiO_2 in the [Cu/barrier layer/SiO_2 (or low-k) structure] due to interdiffusion. At this time, the diffusion of oxygen plays an important role in the barrier properties of the barrier layer. If the modified time-lag method is conducted based on oxygen, the barrier properties can be quantitatively evaluated by obtaining the D of the barrier layer for oxygen.

(4) Applicability to trench structures

The state of the thin film deposited on the planar structure and the state of the thin film deposited

on the trench structure are likely to be different. According to the latest IRDS, the aspect ratio of future Cu interconnects is between 1.5 and 2.5. Although the aspect ratio is not large, it is necessary to know whether the state of the thin film deposited on the top of the trench and the state of the thin film deposited on the bottom are the same or not. At this time, the important thing is the thickness and composition. It should be deposited with a uniform thickness. In addition, it is necessary to investigate whether the composition of the barrier layer deposited at the top of the trench is the same as that of the barrier layer deposited at the bottom of the trench. Through this investigation, it will be possible to distinguish a part with excellent barrier properties and a part with weak barrier properties in the trench structure.

Acknowledgment

I would like to express my sincere thanks to Professor Yukihiro Shimogaki for guiding my entire PhD program. Thanks to his advice, I have developed the power to constantly think to solve problems. Without his guidance, the entire structure of this dissertation could never have been completed. Also, when faced with numerous problems, his advice based on scientific insight allowed me to move forward with my research. I would also like to thank all the committee members who took time out of their busy schedules to review my dissertation. I would also like to express my sincere thanks to Professor Takeshi Momose for refining the details of the dissertation. His numerous advices contributed greatly to the completion of this dissertation.

I would like to thank all members of the former and current Shimogaki/Momose Group. In particular, Yubin Deng, a good friend of mine, helped me a lot in completing my dissertation.

Lastly, I love my whole family, and I dedicate this thesis to them all.

Taewoong Kim